Forecast-based Energy Management Systems

by

AMEENA AL-SOROUR

A thesis submitted to

SWANSEA UNIVERSITY

In fulfilment of the requirements for the Degree of

DOCTOR OF PHILOSOPHY

College of Engineering

SWANSEA UNIVERSITY 2023

Prifysgol Abertawe
Swansea University

DECALARATION

Statement 1

This work has not previously been accepted in substance for any degree and is not being concurrently submitted in candidature for any degree.

Signed …..AMEENA AL-SOROUR……..

Date ……17/4/2023…….

Statement 2

This thesis is the result of my own investigations, except where otherwise stated. Other sources are acknowledged by footnotes giving explicit references. A bibliography is appended.

Signed …..AMEENA AL-SOROUR……..

Date ……17/4/2023…….

Statement 3

I hereby give consent for my thesis, if accepted, to be available for photocopying and for inter-library loan, and for the title and summary to be made available to outside organisations.

Signed …..AMEENA AL-SOROUR……..

Date ……17/4/2023……

Statement 4

The University's ethical procedures have been followed and, where appropriate, that ethical approval has been granted.

Signed …..AMEENA AL-SOROUR……..

Date ……17/4/2023……

ABSTRACT

The high integration of distributed energy resources into the domestic level has led to an increase in the number of consumers becoming prosumers (producer + customer), which creates several challenges for network operators, such as controlling renewable energy sources over-generation. Recently, self-consumption as a new approach is encouraged by several countries to reduce the dependency on the national grid. This work presents two different Energy Management System (EMS) algorithms for a domestic Photovoltaic (PV) system: (a) real-time Fuzzy Logic-based EMS (FL-EMS) and (b) day-ahead Mixed Integer Linear Programming-based EMS (MILP-EMS). Both methods are tested using the data from the Active Office Building (AOB) located in Swansea University, Bay Campus, UK, as a case study to demonstrate the developed EMSs. AOB comprises a PV system and a Li-ion Battery Storage System (BSS) connected to the grid. The MILP-EMS is used to develop a Community Energy Management System (CEMS) to facilitate local energy exchange. CEMS is tested using the data from six houses located in London, UK, to form a community. Each household comprises a PV system and BSS connected to the grid. It is assumed that all six households use an EV and are equipped with a bidirectional charger to facilitate the Vehicle to House (V2H) mode. In addition, two shiftable appliances are considered to shift the demand to the times when PV generation is maximum to maximise community local consumption. MATLAB software is used to code the proposed systems.

The FL-EMS exploits day-ahead energy forecast (assumed it is available from a third party) to control the BSS with the aim of reducing the net energy exchange with the grid by enhancing PV self-consumption. The FL-EMS determines the optimal settings for the BSS, taking into consideration the BSS's state of health to maximise its lifetime. The results are compared with recently published works to demonstrate the effectiveness of the proposed method. The proposed FL-EMS saves 18% on total energy costs in six months compared to a similar system that utilises a day-ahead energy forecast. In addition, the method shows a considerable reduction in the net energy exchanged between the AOB and the grid.

The main objective of the MILP-EMS is to reduce the net energy exchange with the grid by including a two days-ahead energy forecast in the optimisation process. The proposed method reduces the total operating costs (energy cost + BSS degradation cost) by up to 35% over six months and reduces net energy exchanged with the grid compared to similar energy optimisation technique. The proposed cost function in MILP-EMS shows that it can outperform the performance of alternative cost function that directly reduce the net energy exchange.

CEMS uses two days-ahead energy forecast to reduce the net energy exchange with the grid by coordinating the distributed BSSs. The proposed CEMS reduces the total operating costs (energy costs + BSSs degradation costs) of the community by 7.6% when compared to the six houses being operated individually. In addition, the proposed CEMS enhances community self-consumption by reducing the net energy exchange with the grid by 25.3% over four months compared to similar community energy optimisation technique. A further reduction in operating costs is achieved using V2H

mode and including shiftable appliances. Results show that introducing the V2H mode reduces both the total operating costs of the community and the net energy exchange with the grid.

TABLE OF CONTENTS

DEDICATION

I am grateful to God and the number of people who supported me to carry out this work.

First and foremost, my deepest gratitude goes out to my supervisors Dr. M. Fazeli and Dr. M. Monfared for their enormous support, motivation and continuous guidance from the beginning to the end of my PhD journey. Their important feedback made several works (publications) achievable. My deep appreciation also goes to Dr. A. Fahmy for his invaluable guidance and encouragement.

Very special thanks to my friends who have listened to me and supported me during my studies at Swansea University. I would like to take this opportunity to thank my father who has been always my most incredible role model and my mother for her continuous engorgement and love. Thank you so much for making me the person I am today. Also, I would gratitude my sister and brothers for their advice and support.

Warm thanks to my lovely daughter Maryam for her love, patience and her smiles that motivated me to keep moving forward, thanks for being there for me.

Finally, I would like to also express my sincere gratitude to the Qatar National Research Fund (a member of the Qatar Foundation) for funding my PhD study at Swansea University. I am hopeful that I can reattribute to my country everything that it has given to me and take part in developing my country.

LIST OF PUBLICATIONS

1. A. Al-Sorour, M. Fazeli, M. Monfared, and A. A. Fahmy, “Investigation of Electric Vehicles Contributions in an Optimized Peer-to-Peer Energy Trading System,” *IEEE Access*, vol. 11, pp. 12489-12503, 2023, doi: 10.1109/ACCESS.2023.3242052.

2. A. Al-Sorour, M. Fazeli, M. Monfared, A. Fahmy, J. R. Searle, and R. P. Lewis, “Enhancing PV Self-Consumption Within an Energy Community Using MILP-Based P2P Trading,” *IEEE Access*, vol. 10, pp. 93760-93772, 2022, doi: 10.1109/ACCESS.2022.3202649.

3. A. Sorour, M. Fazeli, M. Monfared, A. A. Fahmy, J. R. Searle, and R. P. Lewis, “MILP Optimized Management of Domestic PV-Battery Using Two Days-Ahead Forecasts,” *IEEE Access*, vol. 10, pp. 29357-29366, 2022, doi: 10.1109/ACCESS.2022.3158303.

4. A. Sorour, M. Fazeli, M. Monfared, A. A. Fahmy, J. R. Searle, and R. P. Lewis, “Forecast-Based Energy Management for Domestic PV-Battery Systems: A U.K. Case Study,” *IEEE Access*, vol. 9, pp. 58953-58965, 2021, doi: 10.1109/ACCESS.2021.3072961.

5. A. Sorour, M. Fazeli, M. Monfared, A. Fahmy, J. Searle, and R. Lewis, “Enhancing Self-consumption of PV-battery Systems Using a Predictive Rule-based Energy Management,” *IEEE PES Innovative Smart Grid Technologies Europe (ISGT Europe)*, Finland, 2021, pp. 1-6, doi: 10.1109/ISGTEurope52324.2021.9640051.

LIST OF FIGURES

LIST OF TABLES

ABBREVIATIONS

PV	Photovoltaic
RESs	Renewable Energy Sources
EVs	Electric Vehicles
SGs	Smart Grids
BSSs	Battery Storage Systems
EMSs	Energy Management Systems
SEG	Smart Export Guarantee
FL	Fuzzy Logic
HEMS	House Energy Management System
MILP	Mixed Integer Linear Programming
AOB	Active Office Building
FL-EMS	Fuzzy Logic-based Energy Management System
MILP-EMS	Mixed Integer Linear Programming-based Energy Management System
DERs	Distributed Energy Resources
CEMS	Community Energy Management System
DSM	Demand-side Management
MGs	Microgrids
FIT	Feed-in Tariff
E7	Economy 7
TOU	Time of Use
RTP	Real-Time Pricing
DR	Demand Response
DE	Differential Evolution
PSO	Particle Swarm Optimization
ACO	Ant Colony Optimisation
AI	Artificial Intelligence
ANFIS	Adaptive Neural Fuzzy Inference System
ANN	Artificial Neural Network
Li-ion	Lithium-ion
SOH	State-of-Health

DOD	Depth of Discharge
GA	Genetic Algorithm
LP	Linear Programming
NLP	Non-linear Programming
ML	Machine Learning
P2P	Peer-to-Peer
V2G	Vehicle to Grid
V2H	Vehicle to House
H2G	House to Grid
MFs	Membership Functions
GHG	Greenhouse Gases
AI	Artificial Intelligence

NOMENCLATURE

n	The n^{th} house
$E_{Day\text{-}f}{}^{n}$	Next day energy forecast (kWh)
ΔT	Sample time (hr)
$SOC_B{}^{n}(t)$	House battery state of charge (%)
$SOC_{B\text{-}max}{}^{n}$	Maximum limit of the house battery state of charge (%)
$SOC_{B\text{-}min}{}^{n}$	Minimum limit of the house battery state of charge (%)
$P_B{}^{n}(t)$	House battery discharge/charge power (kW)
$P_{B\text{-}rating}{}^{n}$	Maximum house battery discharge/charge power (kW)
$P_{B\text{-}disch}{}^{n}(t)$	House battery discharge power (kW)
$P_{B\text{-}charg}{}^{n}(t)$	House battery charge power (kW)
$B_{capacity}{}^{n}(t)$	Estimated house battery capacity (kWh)
$SOC_B{}^{n}(t_\alpha)$	House battery state of charge at initial time t_α (%)
$SOC_B{}^{n}(t_\beta)$	House battery state of charge at final time t_β (%)
$N_{Bcycle}{}^{n}$	House battery life cycle
P_{base}	Base power (kW)
$SOH(t)$	Battery state-of-health (%)
B_{nom}	Nominal house battery capacity (kWh)
$E_B{}^{n}(t)$	Energy stored in the house battery at time t (kWh)
$E_B{}^{n}(t\text{-}1)$	Energy stored in the house battery at time t-1 (kWh)
$I_B{}^{n}(\tau)$	House battery charge/discharge current (A)
E_{import}	Imported energy from the grid (kWh)
E_{export}	Exported energy to the grid (kWh)
N_{houses}	Number of houses in the community
C_{bill}	Energy bill
C_F	Optimisation cost function (£)
$Pair_{no.}$	Number of available pair
$SOC_{EV}{}^{n}(t)$	State of charge of EV battery (%)

$SOC_{EV\text{-}max}^{n}$	Maximum limit of the EV state of charge (%)
$SOC_{EV\text{-}min}^{n}$	Minimum limit of the EV state of charge (%)
$P_{EV}^{n}(t)$	EV battery discharge/charge power (kW)
$P_{EV\text{-}rating}^{n}$	Maximum EV battery discharge/charge power (kW)
$P_{EV\text{-}disch}^{n}(t)$	EV battery discharge power (kW)
$P_{EV\text{-}charg}^{n}(t)$	EV battery charge power (kW)
$EV_{capacity}^{n}(t)$	Estimated EV battery capacity (kWh)
$N_{EVcycle}^{n}$	EV battery life cycle
$E_{EV}^{n}(t)$	EV energy at time t (kWh)
$E_{EV}^{n}(t\text{-}1)$	EV energy at time t-1 (kWh)
$I_{EV}^{n}(\tau)$	EV battery charge/discharge current (A)
$P_{L}^{n}(t)$	Recorded historical data of load power (kW)
$P_{PV}^{n}(t)$	Recorded historical data of PV power (kW)
$P_{PV\text{-}1}^{n}(t)$	Forecasted PV generation for day-1 (kW)
$P_{L\text{-}1}^{n}(t)$	Forecasted load demand for day-1 (kW)
$P_{PV\text{-}2}^{n}(t)$	Forecasted PV generation for day-2 (kW)
$P_{L\text{-}2}^{n}(t)$	Forecasted load demand for day-2 (kW)
$P_{G}^{n}(t)$	Power exchange between the house and the grid (kW)
$P_{Gmax\text{-}export}^{n}$	Maximum allowed exported power to the grid (kW)
$P_{Gmax\text{-}import}^{n}$	Maximum allowed imported power from the grid (kW)
$P_{G\text{-}export}^{n}(t)$	Exported power to the grid (kW)
$P_{G\text{-}import}^{n}(t)$	Imported power from the grid (kW)
$\Phi_{export}^{n}(t)$	Binary variable to indicate the house is exporting energy to the grid
$\Phi_{import}^{n}(t)$	Binary variable to indicate the house is importing energy from the grid
$\Phi_{B\text{-}disch}^{n}(t)$	Binary variable to indicate the house battery is discharging
$\Phi_{B\text{-}charg}^{n}(t)$	Binary variable to indicate the house battery is charging
$\Phi_{EV\text{-}disch}^{n}(t)$	Binary variable to indicate the EV battery is discharging
$\Phi_{EV\text{-}charg}^{n}(t)$	Binary variable to indicate the EV battery is charging

CC_B^n	Capital cost of the house battery (£)
CC_{EV}^n	Capital cost of the EV battery (£)
C_{BSS}^n	House battery degradation cost (£)
C_{EV}^n	EV battery degradation cost (£)
C_{buy}^n	Price of imported energy from the grid (£/kWh)
C_{sell}^n	Price of exported energy to the grid (£/kWh)
$f_{sell}(t)$	Tariff for selling energy to the grid (£/kWh)
$f_{buy}(t)$	Tariff for buying energy from the grid (£/kWh)
C_{house}^n	Optimisation cost function for the individual house (£)
$C_{sum\text{-}P2P}$	Optimisation cost function for the paired houses (£)
C_{P2P}^n	Cost of energy exchanged between the paired houses (£)
$f_{P2P\text{-}exp}^n(t)$	Export exchange tariff between the paired houses (£/kWh)
$f_{P2P\text{-}imp}^n(t)$	Import exchange tariff between the paired houses (£/kWh)
$P_{P2P}^{A\leftrightarrow B}(t)$	The power exchanged between the paired houses (kW)
$P_{P2P,max}^n(t)$	Maximum power exchanged between the houses (kW)
$\sigma_{export}^n(t)$	Binary variable to indicate the house (n) is exporting energy to the neighbour
$\sigma_{import}^n(t)$	Binary variable to indicate the house (n) is importing energy from the neighbour
$C_{house\text{-}cost}^{individual(n)}$	Operational cost per day when a house is operating individually (£)
$C_{house\text{-}cost}^{P2P(\mathrm{n})}$	Operational cost per day when a house is operating as paired (£)
t_0	The time of the day starts at 12 AM (hr)
T	The time of the day ends after 24 hours (hr)
t	Current time (hr)
η_{conv}^n	House battery DC/DC converter efficiency (%)
η_c^n	House battery charging efficiency (%)
η_d^n	House battery discharging efficiency (%)
η_{EVd}^n	EV battery discharging efficiency (%)
η_{EVc}^n	EV battery charging efficiency (%)

η_{EV}^{n}	EV converter efficiency (%)
T_D^{n}	EV travel distance (Km)
EV_A^{n}	EV arrival time (hr)
EV_D^{n}	EV departure time (hr)
$SOC_{EV\text{-}desired}^{n}$	Desired SOC of the EV for the second trip (%)
E_{reduce}^{n}	Estimated energy reduced during the journey (kWh)
E_{cons}^{n}	Energy consumption per km (kWh/km)
$I_{EV}^{n}(t)$	EV battery charge/discharge current (A)
$T_{start}^{n}(i)$	Appliance start time (hr)
$T_{wait}^{n}(i)$	Appliance maximum waiting time (hr)
$P_{L\text{-}sh}^{n}(i, t)$	Power of the shiftable appliance i at time t (kW)
$\sigma_L^{n}(i,t)$	Binary variable that indicates the operation status of a shiftable appliance i
$\sigma_{startup}^{n}(i,t)$	Binary variable that indicates the starting up of an appliance i
$T_{cycle}^{n}(i)$	Operation time needed for an appliance i (hr)
$T_{end}^{n}(i)$	Finishing time of the appliance operation (hr)
$P_{rate\text{-}L}^{n}(i)$	Rated power of the appliance i (kW)

1 INTRODUCTION

1.1 Background

The measures taken to reduce Greenhouse Gases (GHG) emissions have dramatically increased the use of Renewable Energy Sources (RESs) and Electric Vehicles (EVs) at consumption and distribution levels [1]. As a result, national electrical network systems are transitioning from conventional power systems to sustainable energy systems, often called Smart Grids (SGs) [2]. This transition requires significant investments in both EV charging stations and RESs infrastructure [3]. In addition, new policies and incentives must be implemented to encourage RESs adoption and EV use [4].

The intermittent nature of RESs necessitates the inclusion of Battery Storage Systems (BSSs) to maintain a balance between generation and demand which, in turn, requires the use of Energy Management Systems (EMSs) [5]. In this context, countries with a high penetration of RESs, such as the UK and Germany, are encouraging a self-consumption approach to be utilised in the EMS, with the aim of reducing the burden on the network operators [6, 7]. In addition, since the Smart Export Guarantee (SEG) scheme was introduced in the UK in 2020, the household are no longer receive payments for their energy generation by ceasing the generation tariff, and the export tariff has been progressively reduced [8]. As a result, it is more cost-effective for households to use their RESs locally to maximise self-consumption [8, 9]. One of the main challenges inherent in increasing self-consumption is to reduce the net energy exchanged between the house/community and the grid [10].

1.2 Toward Sustainability

The worldwide preoccupation with reducing GHG emissions have led to consequent changes in countries' energy policies. For example, in 2019, the UK government committed to achieving net-zero carbon emissions by 2050 [8]. Hence, the UK is undergoing an infrastructure modernisation initiative that replaces traditional electricity meters with smart meters, which offers numerous benefits, such as

enabling consumers to monitor their energy usage and facilitating the integration of EVs with RESs in a cost-effective manner. It is estimated that around 42% of domestic households had smart meters in 2020, and smart meter implementation is continuing [11].

Fig. 1.1 shows GHG emissions by sector. In 2020, the transportation sector was the most significant source of GHG emissions, representing 24% of the total emission. On the other hand, the residential sector contributes 16% of the total emissions [12]. The continuous growth in the use of EVs and integration of RESs into power systems can help to reduce GHG emissions [13]. In the UK, RESs contributed about 43.1% of the total electricity generated in 2020, which was 6% more than in 2019 [11].

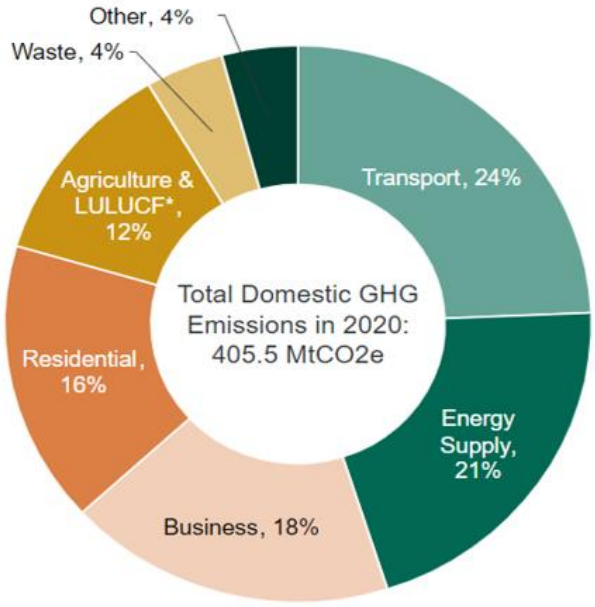

Fig. 1.1. UK greenhouse gas emissions by sector in 2020 [12].

1.3 Photovoltaic (PV) System

Among different RESs, the Photovoltaic (PV) system is the most attractive energy source [14]. The PV system is based on cells made of semiconductor p-n junction, which convert sunlight into electrical energy [15]. PV system costs have declined

rapidly over the last decade, making it an increasingly affordable and attractive choice for many households and businesses. Globally, PV's cost dropped by 82% between 2010 and 2019 [14].

1.4 Data Processing

Fig. 1.2 shows the steps taken for data processing. The data from the AOB and community (six houses) were obtained to be used as a case study and prepared before coding the proposed systems. It was found that the original measured PV and load data for AOB and the community had missing measurements (due to measurement problems). Therefore, the missing data was compensated for by using the previous available data. Additionally, the data were sampled every 1 minute, while the proposed algorithms require a sample time of 10 minutes. Hence, the data were averaged in 10 minutes intervals to be used as input. The proposed system was coded in MATLAB software, where the uncertainties of PV generation and demand (assumed it is available from a third party) are considered when optimisation is carried out.

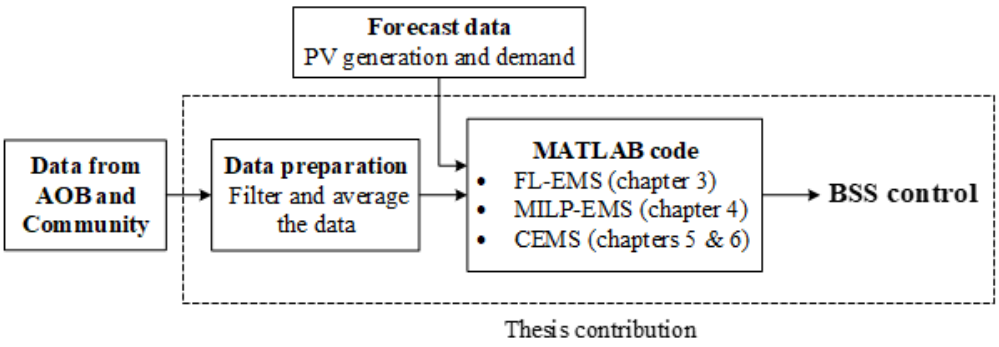

Fig. 1.2. Data processing.

1.5 Research Objectives and Contributions

Most recent studies on EMS have mainly focused on minimising operating costs. However, this work introduces a new approach that aims to minimise the net energy exchange between households/communities and the grid. In addition, numerous studies have focused on proposing various forecasting algorithms [7], however, there is a significant gap in the literature regarding the optimal utilisation of forecasted

data in an EMS. Therefore, in this work, the optimisation process takes into account a one/two-day ahead energy forecast and BSS health to reduce the net energy exchange with the grid, while extending the lifetime of the BSS.

This work proposed two different EMS algorithms for a domestic PV system: (a) real-time Fuzzy Logic-based EMS (FL-EMS) and (b) day-ahead Mixed Integer Linear Programming-based EMS (MILP-EMS). Both algorithms aims to maximise the PV self-consumption by reducing the net energy exchange between AOB and the grid. Then the problem is expanded into how a community energy management controller can be more effective when collectively controlling the BSSs, EVs, and shiftable appliances, of a community of houses, rather than the houses operating individually, confirming the importance of controlling EVs battery charging/ discharging cycles and shiftable appliances to reduce the burden on the national grid.

The main contributions of this work are:

1. To demonstrate that a real-time residential EMS:

    - can extend the lifetime of a household BSS by including SOH in a rule-based algorithm combined with a Fuzzy Logic (FL) controller.
    - can exploit the day-ahead energy forecast in the proposed algorithm, which reduces unnecessary BSS charging/discharging cycles, contributing to an extended life for the BSS.
    - facilitates a self-consumption approach that minimises the net exchanged energy between a house and the grid, which reduces transmission losses and load on the grid.

2. To demonstrate that the day-ahead residential EMS:

    - can optimise BSS operation using Mixed Integer Liner Programming (MILP) and including the cost of degradation of the household BSS in the cost function.

- uses the two days-ahead energy forecasts to eliminate unnecessary BSS charging/discharging cycles.
- enhances self-consumption approach into the optimisation process to reduce transmission losses and burdens on the grid.

3. Demonstrate that the Community Energy Management System (CEMS):

- enhances the energy independence of the community.
- facilitates the self-consumption approach by minimising the net energy exchange between the community and the grid.
- can include EVs, despite the uncertainty relating to their availability, as an alternative energy storage which enhances self-consumption of PV energy and reduces the need for new charging station infrastructure.
- optimises the use of EV batteries and BSSs by including degradation costs in the cost function.
- considers shiftable appliances in demand-side management to change appliance operation time to times when the energy cost is low or when the PV system produces surplus energy, which reduces peak load and net energy exchanged between the community and the grid.

1.6 Thesis Outline

This thesis consists of seven chapters, including the introduction. The following chapters are briefly summarised as follows:

Chapter 2 presents a literature review which discusses the power system revolution. This chapter also addresses the main challenges and possible solutions for integrating RESs and EVs into the consumption and distribution levels. In addition, it reviews the state-of-the-art of different approaches related to residential EMSs and CEMSs. The advantages and drawbacks of previous approaches are comprehensively detailed.

Chapter 3 presents a real-time residential EMS based on a FL (FL-EMS) controller. The proposed method is tested using measured data obtained from the Active Office Building (AOB) located at Swansea University, Bay Campus, UK. The proposed

algorithm is compared with three recently published state-of-the-art algorithms and with the current EMS installed in the AOB, to demonstrate the effectiveness of the proposed strategy. In addition, this chapter investigates the impact of different sizes of PV system and BSS capacity on the net amount of energy exchanged with the grid.

Chapter 4 presents a day-ahead residential EMS based on MILP (MILP-EMS). The proposed method is tested using measured data and compared with recent state-of-the-art and with the current EMS utilised in the AOB to show the effectiveness of the proposed method. In addition, different cost functions are investigated to show the effectiveness of the proposed cost function in reducing net energy exchanged with the grid.

Chapter 5 presents a day-ahead CEMS based on MILP. The proposed CEMS is tested using real data from six houses located in London, UK. A comparison between a house operating individually and as a community member is investigated.

Chapter 6 presents an extended version of the CEMS presented in Chapter 5 to investigate the impact of using EVs as alternative energy storage by enabling the Vehicle to House (V2H) mode and considering shiftable appliances in the system.

Chapter 7 presents the general conclusion of the work and suggests possible future work.

2 LITERATURE REVIEW

2.1 Introduction

Distributed Energy Resources (DERs) refer to small-scale power generation technologies such as Photovoltaic (PV) system panels, wind turbines, and Battery Storage Systems (BSSs) installed close to the consumers [16]. Their rapidly increasing use during the last decades has fundamentally changed the design and operation of electrical power systems. As a result, electrical systems are moving from a unidirectional (centralised) market to a bidirectional (decentralised) market which allows consumers to become prosumers, both producers and consumers [17]. These changes necessitate the electrical system's operators to include local Energy Management Systems (EMSs) to allow conventional prosumers to exchange excess energy not only with the grid but within a local community, enhancing self-consumption. According to a European Renewable Energies Federation study, the number of clean energy prosumers in the UK could reach 24 million by 2050 [18]. However, due to the intermittent nature of Renewable Energy Sources (RESs), more Battery Storage Systems (BSSs) and advanced control/management methods are essential to balance generation with demand.

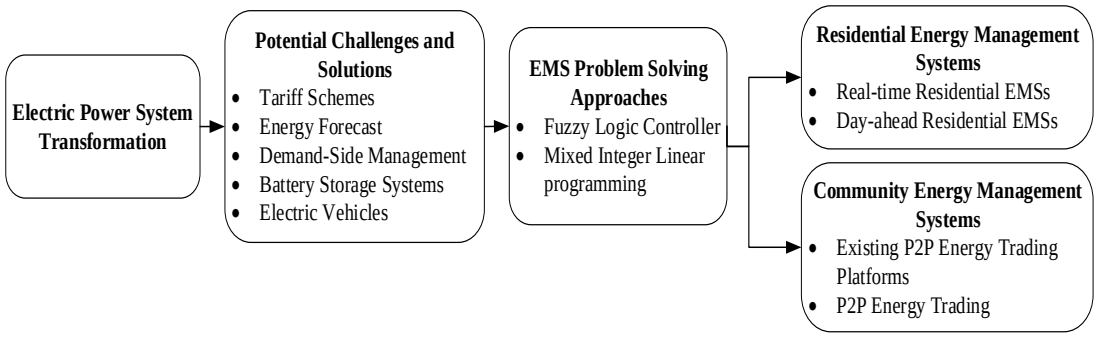

Fig. 2.1. Schematic of the literature review areas.

This chapter explores the main challenges and issues facing prosumers and the grid by providing a comprehensive literature review of EMSs. Fig. 2.1 presents the topics addressed in the literature review, and this is followed by a brief description of the electric power system transformation in Section 2.2. Next, Section 2.3 presents some

challenges and possible solutions facing prosumers and the grid. Then, Section 2.4 presents EMS problem-solving approaches. An overview of recent publications concerning state-of-the-art residential EMSs and Community Energy Management System (CEMS) is provided in Sections 2.5 and 2.6, respectively. Finally, Section 2.7 presents the conclusion of Chapter 2.

2.2 Electric Power System Transformation

The electric power sector is going through a transition, with new technologies being introduced on both the customer and network sides. Traditional electricity grid structures are being transformed into Smart Grids (SGs). Fig. 2.2. shows the electric power network transitions. The transitions can be summarised as following three phases:

- Past generation: As shown in Fig. 2.2 (A), the electric power system flow was unidirectional, where electricity flows from large-scale fuel based generators to consumers over long distances via transmission and distribution lines [19]. Transformers increase the voltage for transmission and then reduce the voltage prior to the electricity being delivered to the consumers. It is worth mentioning that around 8% to 15% of the total energy transmitted can be dissipated during transmission, depending on the line resistance and distance [20].
- Present generation: As shown in Fig. 2.2 (B), the electric power system is a bidirectional power flow that allows customers to become prosumers by utilising RES generation and Electric Vehicles (EVs). Households can purchase/sell their electrical energy from/to a single supplier by adopting a control system and so reduce operating costs (requires monitoring of consumption through a smart meter) [4].
- Future generation: As shown in Fig. 2.2 (C), the electric power system will have a complex bidirectional power flow, which enables prosumers to trade their surplus energy with different peers within one community, the grid and, eventually, other communities. This will require the adoption of RESs and

use of EVs to achieve the government's vision of net-zero carbon emissions by 2050 [12]. In this regard, Peer-to-Peer (P2P) energy trading is currently considered an efficient approach to DERs, which offers local market solutions [21]. Furthermore, P2P allows prosumers to trade surplus energy generation with their peers over short distances to lessen reliance on the grid, reduce transportation losses, and increase user and grid benefits. P2P energy trading is able to maximise self-consumption by the community by reducing energy exchange with the grid and enabling a more economic dispatch [5].

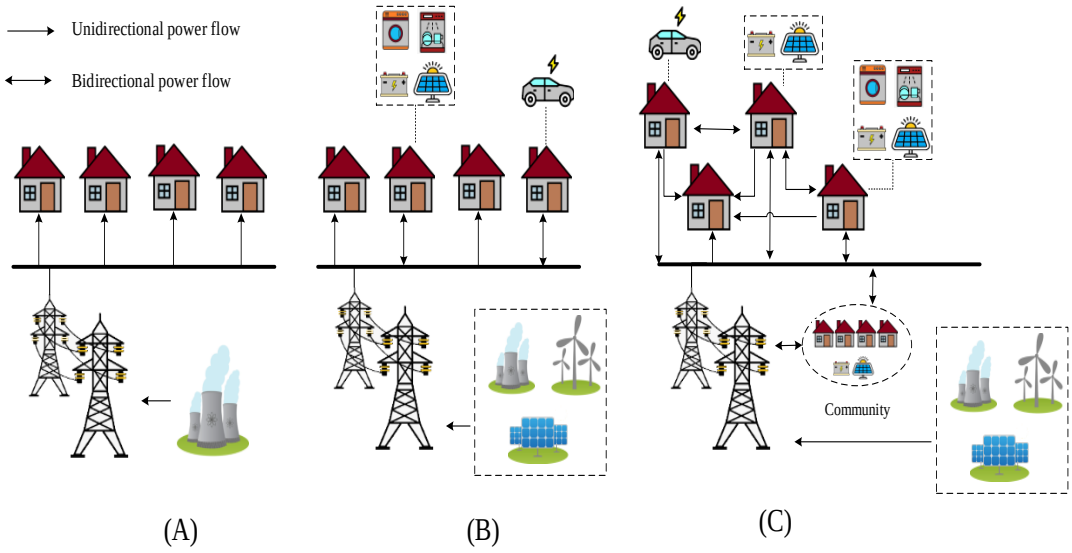

Fig. 2.2. Electric power network transitions: (A) past, (B) present, and (C) future network structures.

2.3 Potential Challenges and Solutions

The increasing penetration of DERs poses significant challenges for network operators due to their intermittent nature [22]. Fig. 2.3 shows some examples of the challenges facing both the prosumers and the grid when implementing DERs, with associated solutions. One of the main challenges is controlling RES over-generation [7]. For example, In 2019, Germany and UK exceeded the expected RES generation limit [23, 24]. As a result, the power generation was higher than demand and the capacity of their electricity networks. In the UK, this resulted in the utility paying

customers to use the excess energy generated from wind turbines [24], and in Germany, consumers and neighbouring countries were paid to consume the surplus energy [23]. However, the quantity of surplus power was so great it overwhelmed the capacity of Germany's neighbours' systems. According to [25], "Germany's negative electricity price rules have caused an estimated €50 million in losses for offshore wind projects in February 2020 alone". Another example is, in 2017, California paid Arizona to take surplus PV energy to avoid overloading its own network [26].

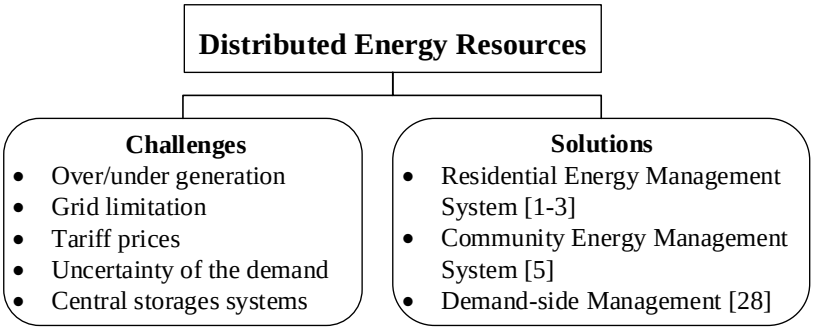

Fig. 2.3. DERs challenges and solutions.

Since the uncontrolled nature of RESs export can significantly affect grid stability, several countries have already limited the export of RESs energy to the grid. For example, in Germany, the export is limited to 50% of the peak power of the PV panels [7]. To prevent the need for greater transmission and distribution capacity, self-consumption, as a new trend, is encouraged by several countries such as the UK [7]. In 2020, the SEG was proposed, which is similar to a net metering program [8]. However, the "generation tariff" has now ended for newly fitted household PV installations [27]. Such changes encourage a move towards more advanced local EMSs to reduce the prosumers' dependency on the grid by reducing the net energy exchanged with the grid.

To control excess generation on the prosumer side, one or a combination of the measures below can be used:

i) Installing suitable BSS capacity in house to store the excess power to use later instead of exporting to the grid. In addition, EV can be used, if

available, as extra storage. However, the cost, size, efficiency, and battery management must all be considered in the EMS [1-3, 28].

ii) Forming communities and trading excess energy within the community rather than with the grid [5].

iii) Implementing Demand-side Management (DSM), to control appliances (e.g., water heaters, dishwashers, and air conditioners). However, this approach may not be preferred by all customers as it would control their daily routine [29].

Other alternatives for controlling the over-production of RESs are: (i) limiting the local RESs, which means more centralised generation is required to supply demand, and/or (ii) employing (more) centralised storage to store the excess energy from the RES. However, both alternatives imply that the grid must have a higher transmission and distribution capacity to handle the exchanged power [28].

2.3.1 Tariff Schemes

In the UK, the Feed-in Tariff (FIT) was launched in April 2010 to encourage householders to install PV systems and get paid for energy exported to the grid. As a result, PV generation capacity has increased from 95 MW in 2010 to 13,800 MW in 2021 [30]. The rapid increase of PV integration into Microgrids (MGs) led to a reduction in generation tariffs from 54.17 p/kWh in 2010 to 3.79 p/kWh in 2019, as shown in Fig. 2.4 [31]. In 2020, the FIT was replaced with the Smart Export Guarantee (SEG) scheme, whereby the householders receive payback only for the energy exported to the grid [8]. Currently, the export tariff has been reduced to almost half of the off-peak energy price and one-third of the peak time energy price, making it more cost-effective for new installations using local RESs to maximise self-consumption [8, 9].

Different tariff schemes are proposed by utilities in the UK, including:

- Economy 7 (E7) (also known as the multi-rate plan) was launched in the 1970s, proposing different tariff prices for peak and off-peak times to

incentivise consumers to use the electricity generated from nuclear power stations during off-peak hours [32].

- Time of Use (TOU) is similar to E7 but offers multiple levels throughout the day (i.e., peak, mid-peak, and off-peak tariffs) to allow households to have more flexibility in controlling their consumption [33].
- Real-Time Pricing (RTP), also known as dynamic pricing; the prices in RTP are varied and updated almost every 30 mins [24]. A smart meter is required to receive information about the consumption and electricity cost [34]. This tariff is usually used in real-time energy control as a fast control decision is required [35].

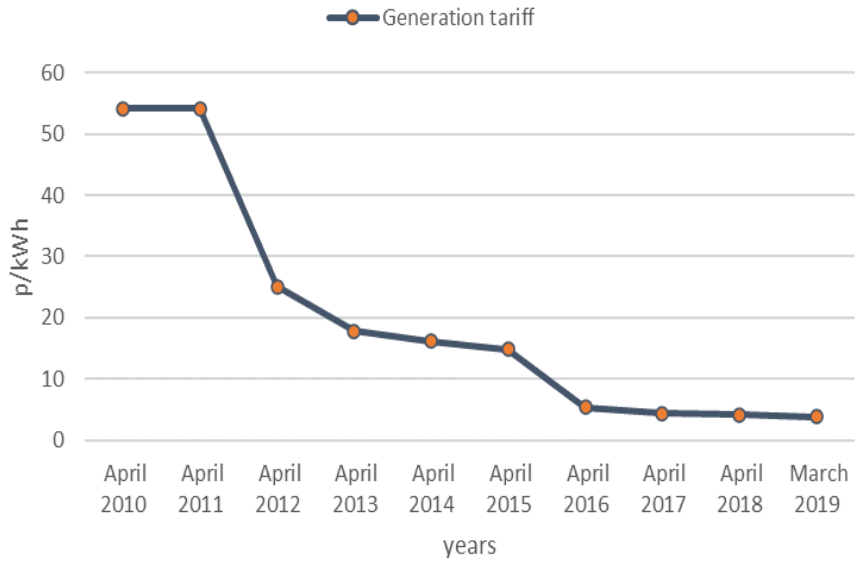

Fig. 2.4. Feed in Tariff rates from 2010 to 2019 [31].

There are two main types of SEG tariffs in the UK [8]:

- Fixed-rate, where a fixed amount is paid to prosumers per kilowatt hour of electricity exported to the grid, regardless of the time.
- Flexible rate, where the export price varies depending on when the energy is exported to the grid.

2.3.2 Energy Forecast

Generation and demand forecasting are critical for load planning, next day trade and BSS operation for both prosumers and network operators [36]. Several approaches have been introduced in the literature to forecast generation and demand, such as Differential Evolution (DE), Particle Swarm Optimisation (PSO) [37], Fuzzy Logic (FL) [38], and Artificial Neural Networks (ANNs) [39].

In recent years, several companies are available to provide forecast data, which can be fed into the customers' EMSs, these include DNV [40], VAISALA [41], and AleaSoft [42]. Since a forecaster company can provide the forecast data, several EMS researchers assumed that developing a forecast methodology is beyond the scope of their studies [43]. Alternatively, researchers use historical PV and demand data and impose error percentage by using Weibull [44] or Normal (or Gaussian) distributions to represent the forecasted data [9, 45, 46].

2.3.3 Demand-Side Management (DSM)

During past years Demand Response (DR) has gained attention for its ability to reduce the reliance on the grid by shedding or shifting energy consumption based on users' comfort and grid requirements [29]. Several companies worldwide have designed EMSs incorporating DR to control user energy consumption. For example, the British Gas in the UK has designed an EMS that controls house appliances through smartphones [47].

House appliances can be classified as controlled, semi-controlled, and uncontrolled. The start times of appliances such as EVs, washing machines, and dishwashers can be controlled/scheduled based on user comfort and grid requirements. Other semi-controlled appliances such as heaters, fans, and air conditioning units can adjust their operating mode to low or high power. Uncontrolled appliance which cannot be shifted or have their operational modes adjusted include TVs, refrigerators, and lights [48].

Installing a smart meter is essential to enable the exchange of information between the customer and the utility. Based on the literature, there are two main approaches to DR [49]:

1. Incentive-based: The scheme aims to reduce and/or shift consumption to off-peak times to reduce peak demand. Customers get a discount on energy rates or bill credit [29]. The schemes included the following programs:
    - Direct load control program: Based on the contract between the utility and the customer, the utility can directly turn on/off a user's electric equipment at short notice [49].
    - Interruptible/curtailable program: The program aims to stabilise the grid during emergencies by switching off or shifting the loads to the off-peak periods [29].
    - Demand bidding (also known as buyback program): Consumers can bid on specific load reductions in the wholesale electricity market a day in advance. Customers will be rewarded if they achieve the target and will not be penalised if they do not reduce their energy consumption as required [29].
2. Price-based: The scheme includes different tariff programs, where customers can receive financial rewards for reducing their electricity consumption based on electricity tariff time [49], such as:
    - Peak time rebate: Consumers obtain a rebate when reducing their consumption during peak time [29].
    - Critical peak pricing: A reward is given to customers willing to reduce or shift their demand to off-peak hours. However, short notice is given to the customer to respond as the price can change at any time. This program is usually proposed a few times during the year, especially in seasons when the demand increases significantly [29].
    - TOU and RTP are described in Subsection 2.3.1.

Several researchers encourage householders to schedule their daily electrical consumption and increase self-consumption by shifting their appliance loads to the times when the RESs are at maximum or when the electricity is at its lowest tariff [29].

It should be noted that shifting appliance on times means that the users' overall energy consumption during the day remains the same, only the shape of the load curve changes.

Various scheduling algorithms have been reported in the literature, including rule-based, optimisation techniques, and Artificial Intelligence (AI). For example, authors of [50] proposed an EMS based on FL and PSO to optimise household energy consumption by scheduling the appliances. Similarly, authors of [1, 48] proposed an FL rule-based method to control electrical appliances by considering load priority. The implementation of a rule-based algorithm is simple as it is based on a set of inputs and if-then rules [51]. A FL controller can cope with non-linear and linear systems. In addition, it is simple to implement as it depends on linguistic rules, and no mathematical model is required [29]. However, rule-based algorithms have several shortcomings, such as a lack of ability to extend the system and difficulty dealing with extensive data, which makes controlling the appliances in real-time challenging [29].

On the other hand, AI techniques, such as PSO, ANN, and Adaptive Neural Fuzzy Inference Systems (ANFISs), require extensive data for training and learning [29].

2.3.4 Battery Storage Systems (BSSs)

BSSs are widely employed in power systems to supply loads, support peak shaving, and regulate frequency and voltage. Self-consumption as a new approach necessitates utilising BSSs to make the most of the installed RESs. For example, BSSs were installed in about 50% of new PV installations in Germany in 2018 [7]. It has been shown that a BSS with a capacity of between 0.5-1.0 kWh for each 1 kW_p of the installed PV system can increase self-consumption by between 13-24% [52]. Moreover, BSSs can reduce energy costs by storing the excess RES's power and discharging that power when required.

Presently, the manufacturing market for BSSs is extremely competitive. Comparing different types of BSSs, it was found that lithium-ion (Li-ion) has gained high popularity worldwide due to their low self-discharge rate, high energy density, and

acceptable usage cost [53]. BSS-based Li-ion prices are likely to be reduced further in the next few years [54]. As shown in Fig. 2.5, according to a BloombergNEF Survey, the average battery pack cost is expected to reach $94 per kWh in 2024 and $62 by 2030 [55].

Several tech brands in the UK, such as Tesla and Samsung, sell house BSSs-based PV systems. For example, Tesla sells the Powerwall BSSs of 6.4 kWh and 13.5 kWh for £3,000 and £6,300, respectively [5]. In addition, energy companies, such as EDF Energy, Eon, and OVO, are also currently selling BSS packages [56].

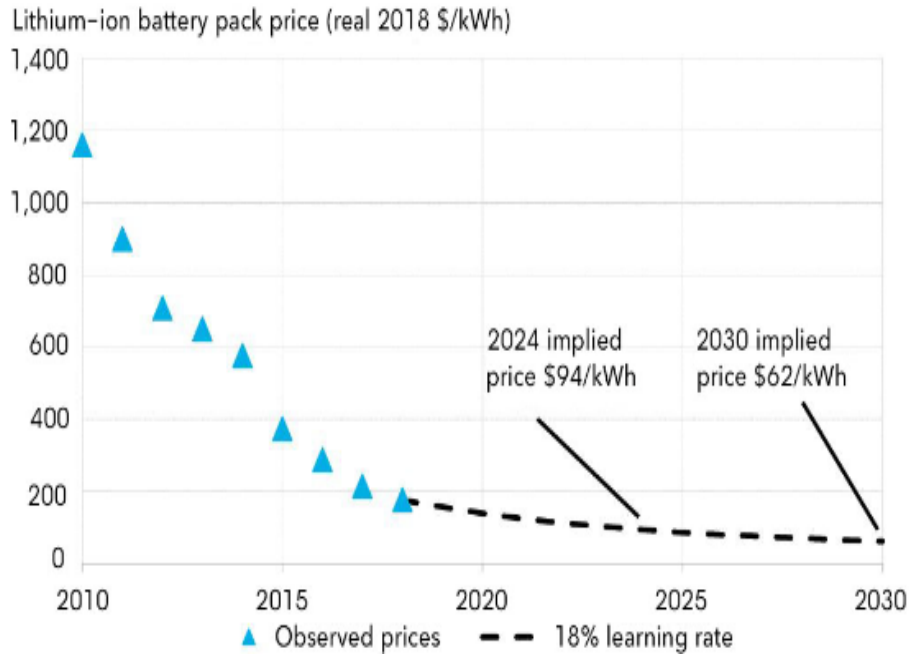

Fig. 2.5. Lithium-ion battery price from 2010 to 2030 [55].

From a financial perspective, the BSS replacement cost is the household's most significant maintenance expense [57]. Therefore, it is essential to include BSS lifetime when optimising the performance of a system. The BSS degradation directly affects its efficiency and operation [58]. The State-of-Health (SOH) measures the amount of energy that can be stored and delivered by estimating the current capacity percentage against the initial capacity, and most BSSs have to be replaced when the SOH drops to 80% [53].

The BSS lifetime is impacted by several factors, including temperature, over charge/discharge, the Depth of Discharge (DOD), and the number of charge and discharge cycles [59]. Based on the literature, there are two main ways to estimate BSS lifetime:

a) Performance-based models: Experiments are required to examine and measure the BSS degradation over time. For example, analytical models, equivalent electrical circuit models and ANN [60].
b) Cycle counting models: Count the number of charging and discharging cycles, such as the Rainflow counting algorithm [59].

There are several ways to include the BSS lifetime into EMSs, such as considering:

- BSS maintenance cost [61].
- BSS degradation cost [4, 62].
- SOH of the BSS [28].

2.3.5 Electric Vehicles (EVs)

The integration of EVs into the distribution level, aimed to decarbonise the transportation sector, has increased rapidly in the 21st century [63, 64]. Globally, the number of EVs had reached about 16.5 million and public chargers of 500 thousand in 2021 [65]. In the UK, the number of fully electric car sales increased to about 100,000 in the first five months of 2022, compared to less than 1,000 in 2011 [66].

In 2009, the UK government introduced an ultra-low emission vehicle strategy, which includes vehicles emitting less than 75 g/km of CO_2, to encourage use of pure electric and hybrid EVs [64]. Table 2.1 presents some incentives that are given by the UK government to EV users. These incentives increased the sales of fully electric cars to 100,000 in the first five months of 2022, compared to fewer than 1,000 in 2011 [66]. In addition, it is estimated that the total number of EVs on UK roads will reach about 10 million by 2030 [67]. Furthermore, the growth of EV popularity contributes to the rapid improvement in battery technology, greater efficiency, longer life and a greater number of life cycles, all at a lower price [68]. Thus, the price of

Li-ion battery packs has declined rapidly by about 89% in the last decade, from $1,100 per kWh to $137 per kWh, making EVs more affordable [69].

Table 2.1. UK governments' incentives for EV users

Incentives	Description
Discounts for EV buyers	Some discounts are given to brand new low-emissions car buyers [70].
Grant for EV charger installation	Up to 75% of the EV charger installation cost at UK domestic properties is covered by the EV ChargePoint grant [71].
Reduction in the congestion charge	EV users receive exemptions and discounts for the congestion charge [70].
Discounted parking	Free or discounted parking is given to EV users [72].
Reduction in charge battery tax	The EV users pay a tax of 5% when they charge EV batteries at house, lower than VAT on the fuel for cars, which is 20% [64, 70].
Reduction in road tax	Pure EVs are exempted from road tax, while the tax for hybrid EVs users varies depending on the level of CO_2 emission. Compared to fuel-based cars, the hybrid and EV's tax is much lower, usually between £0 - £135 [70].

2.3.5.1 EV Challenges and Solutions

From the grid's perspective, the integration of EVs into the distribution/domestic level can be seen as:

- Uncontrollable load: EV charging is uncontrolled and treated as a household load which means it possibly doubling a typical household's peak load [73], contributing to overloading transmission lines, damaging local distribution transformers [57, 74], and causing undervoltage [75].

- Controllable load: EV charging is controlled by the grid operator or local/household EMS. For example, authors of [35] proposed an EMS that controls the EV charging time to reduce peak demand and energy costs.
- Distributed energy resources: The bidirectional EV battery features allow EVs to operate as DERs which can be incorporated into several programs to mitigate some of the difficulties caused by the increase in the number of both RESs and EVs [76]. For example, EV batteries are capable of supporting grid frequency and voltage regulation by enabling the Vehicle to Grid (V2G) mode [13, 76-79], as in the commercial Project Sciurus in the UK [80]. In addition, when the Vehicle to House (V2H) mode is enabled it can reduce household electricity costs [81], reduce peak load [82], supply a house during outages [83], and improve household self-consumption [74, 84].

The growth in the number of EVs requires more charging stations with higher capacity; however, limited space is available to build new charging stations [68]. Thus, to reduce the burden of developing such a new infrastructure; (1) EV batteries can be charged using the surplus energy from local RESs [85], and (2) EV charging/discharging activities can be controlled as part of P2P energy trading [28, 62]. Furthermore, P2P trading can increase RESs self-consumption and reduce energy costs by using EVs as extra storage for the RESs surplus energy from households/neighbours and discharge that energy when required such as during high tariff periods [67].

Although EVs can be used for ancillary services and to balance power requirements in a similar manner to DR, their primary purpose is transportation. The random nature of driving patterns leads to the need to include EV uncertainty in system operation and planning. Several stochastic models, such as Markov-Chain models, have been proposed to estimate EV availability [75, 86]. In addition, it is essential to consider the lifetime of the EV battery when optimising the use of EVs to supply a house or the grid.

2.4 EMS Problem Solving Approaches

Different studies have considered different objectives for residential house and community operations, such as minimising energy costs, maximising self-consumption, and minimising CO_2 emissions [87, 88]. The decision-making at the energy management level can be accomplished by several approaches, as shown in Fig. 2.6.

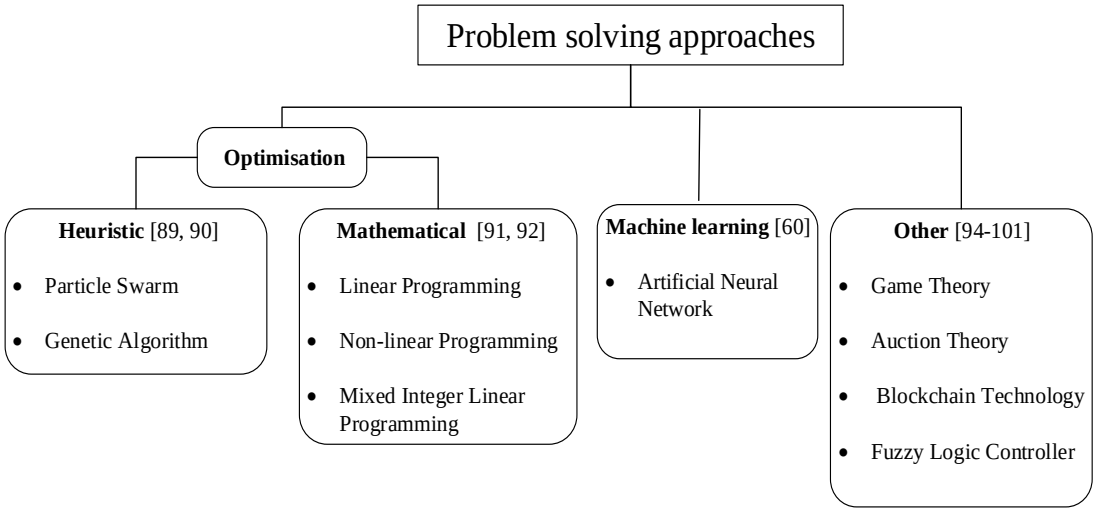

Fig. 2.6. Problem solving approaches used in EMSs.

Optimisation approaches include heuristic algorithms [89, 90] and mathematical formulation [91, 92]. The heuristic algorithms are usually built on pre-defined rules and do not require a detailed system model [93]. Consequently, decision-making is not computationally intensive and can achieve a satisfactory solution in a short time, such as with the Genetic Algorithm (GA) and PSO [90]. They usually solve non-linear programming problems by iteratively searching through all feasible solutions [61]. Whereas the mathematical method depends on having a model of the system. The mathematical approach is achieved by solving the optimisation problem and ensuring that the most favourable solution has been determined, such as Linear Programming (LP), Non-linear Programming (NLP), and Mixed integer linear programming (MILP) [91, 92]. In addition, it is possible to implicitly define the system behaviour via a cost function and make “the best” choice by resolving an optimisation problem [91].

In order to overcome the computational complexity faced by optimisation approaches, Machine Learning (ML), such as ANN can be preferred because it reduces computational complexity by using only historical data to extract general features. However, a large amount of data is required for the training to be reliable [60].

Other techniques used in recent P2P energy trading schemes in residential communities are:

1. Game theory: A set of models used to investigate interactions between the members of the P2P energy market [94-96].
2. Auction theory: A technique that allows sellers and buyers to cooperate and trade their electricity [97-99].
3. Blockchain technology: A decentralised distributed database allows the transactions/information to be shared between users securely [100, 101].

This study uses FL controller and MILP, which will be discussed in more details in the following subsections.

2.4.1 Fuzzy Logic Controller (FL)

The FL controller is a powerful tool that is modelled on the human expert for decision-making, where the system's complexity can be transformed into a crisp quantifiable parameter [1]. In addition, the human experience is translated into “IF-THEN” rules based on the given system inputs and outputs. The FL uses the truth value concept that varies between 0 and 1 [102]. Due to its simplicity, the FL controller has been widely used in energy system planning as it can provide pragmatic solutions. For example, the FL approach has been applied for PV forecast [7], PV maximum power point tracking [103], DSM and battery power control [1].

The FL operation comprises three main steps, as shown in Fig. 2.7 and listed below:

1. Fuzzifier: The crisp input or real input, such as either 0 or 1, is transformed into a linguistic variable (also called a classical set, where its value is between 0 and 1) to

represent fuzzy data through the Membership Function (MF). In this process, the input is normalised based on the MF's scale.

2. Inference process: A collection of "IF-THEN" statements is generated based on expert knowledge. In addition, the MFs are combined via sets of rules to generate the fuzzy output [104].

3. Defuzzifier: Converts the fuzzy output into the desired crisp value.

Based on previous literature, several types of MFs are used in energy systems modelling, such as 'Π' trapezoidal, 'Λ' triangular, 'Γ' function, 'L' function, 'S' function, and Gaussian fuzzy set [102].

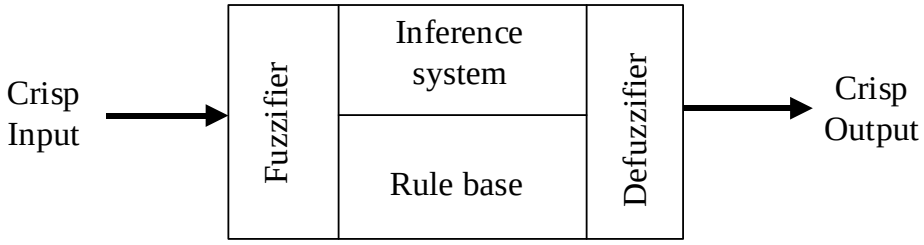

Fig. 2.7. FL controller.

2.4.2 Mixed Integer Linear Programming (MILP)

MILP is a mathematical modelling approach used for analysing and optimising large, complex systems. It provides insight into potential trade-offs between conflicting objectives, which can assist decision-makers in determining sustainable solutions for the optimised objective function [105, 106]. The associated variables and constraints can be integers and non-integers [107]. The MILP can be solved by three different approaches Cutting Plane, Branch and Bound, and Feasibility Pump [108]. The mathematical formulation of the MILP problem is as follows [3]:

$$\left.\begin{array}{c}\text{Objective: minimise} = \mathbf{C}x \\ \text{Constraints: } \mathbf{A}.\, x \le \mathbf{b} \\ x_{\min} \le x \le x_{\max}\end{array}\right\} \tag{2.1}$$

where $x \in Z^n$, **A** is a matrix, **b**, **C** are vectors, and Z is a set of integer numbers.

The optimum solution is a solution that attains the best value of the objective function. A feasible solution is a solution that satisfies all the constraints. Generally, MILP problems are usually solved via a Branch and Bound algorithm based on Linear Programming (LP) (also known as the Tree Search) [108].

A Branch and Bound algorithm begins with the original MILP without the limitations (i.e., the same objective and constraints as the original MILP but without integer constraints), which is called the ‘‘linear programming relaxation’’ of the original problem [108]. Three main steps are used to identify the solution [108, 109]:

1. Branching: The problem is recursively divided into two sub-problems by choosing a non-integer variable from the relaxed LP solution. On one branch, the variable is rounded down to the nearest integer, whereas on the other branch, it is rounded up to the nearest integer.
2. Bound: The best objective value for the node is determined using LP relaxation.
3. Prune: If the solution is not feasible, that tree branch is pruned, i.e., the tree will not be developed any further along this node.

MILP is used in chapters 4, 5, and 6, where different constraints are defined, such as BSS, EV, and grid limitations, to find optimal system operation by reducing the net energy exchanged with the grid.

2.5 Residential Energy Management Systems

The typical MG structure is presented in Fig. 2.8. MG can be defined as low-voltage distribution network, including BSSs, EVs, and RESs connected to local loads [110]. Local loads come in different scales, from residential houses to large buildings and communities (i.e., neighbourhood) [20]. A MG can operate in either island mode or grid-tied [111].

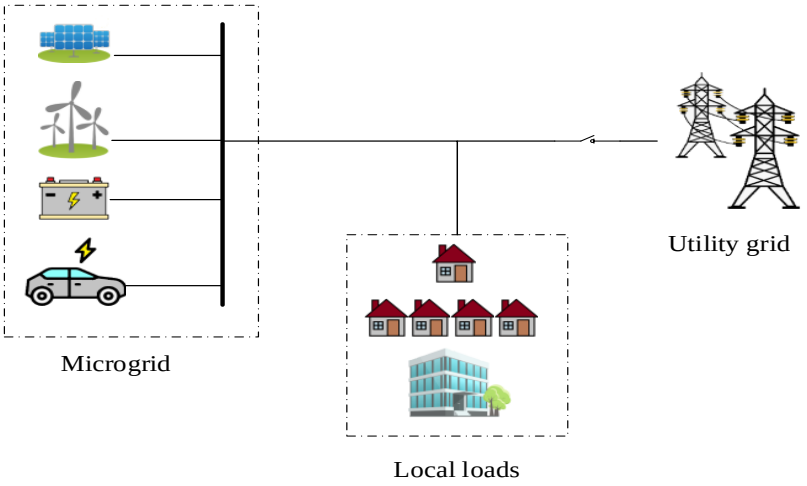

Fig. 2.8. Schematic of MG structure.

With the integration of RESs and EVs into EMSs at the domestic level, it is necessary to understand how to control these power sources while considering tariff prices to achieve optimal system operation. Different objectives can be defined for EMSs. For example, several studies have focused on reducing energy bills by scheduling the BSS operation [112], while other studies proposed scheduling domestic appliances based on tariff prices and load priority to maximise user comfort [113-115]. A residential EMS is essential for lowering energy costs, maximising RESs self-consumption, and enabling residents to participate in community energy schemes. Therefore, it is crucial to first understand the individual residential EMS operation before developing CEMS.

In terms of the implementation of EMS at the domestic level, the optimisation process can be carried out either in real-time (online) [1] or day-ahead (off-line) [4]. These two approaches will be discussed briefly in the following subsections.

2.5.1 Real-Time Residential EMSs

Numerous control techniques have already been proposed in the literature for real-time operations considering different tariff schemes. For example, an online rule-based RTP controller is proposed in [116]. Their work assessed the possibility of curtailing loads during interruptions and supplying energy from the EV by enabling the Vehicle to House (V2H) mode when required. The authors of [117] proposed a rule-based EMS

that maintains the MG's power balance while reducing energy costs. The impact of shiftable appliances and the charging and discharging of EVs on three individual houses is conducted in [57] without considering RESs or BSSs in their rule-based EMS. The aim target is to reduce the burden on the local distribution transformer by facilitating the V2H mode. However, their approach considered houses individually, and the possibility of mutually beneficial exchanges of excess energy between the three houses is ignored.

Among the rule-based EMS techniques, FL controllers are gaining popularity. Work in [88] used a variable price scheme in a FL rule-based controller to reduce energy costs and minimise CO_2 emissions. A FL-based EMS is proposed in [93] to minimise energy costs. The authors of [2] proposed a FL-based EMS to minimise operating costs for a residential MG. The main disadvantage of the proposed system in [2] is that FL's output acts mainly as a binary logic switch since the net power and output controller have no overlapping area in the MFs. In addition, the system limited the BSS capacity to 50%. The authors of [118] and [119] control the power switching signals of the BSS converter using an FL controller, but neither took into account different price tariffs. Additionally, the authors of [119] limit the battery SOC to 50%.

In [120] two different FL-based EMS algorithm are used to control an electric ship to reduce greenhouse gas emissions and operating costs. The first FL-based algorithm regulates the power exchanged between the generation and a BSS, and the other controls the inter-linking converters between the AC and the DC buses by modifying the duty cycle. However, the lifetime of the BSS is not considered. Authors of [1] proposed a real-time FL-based EMS to control power flows in a MG and show that the proposed EMS saves up to 5% of the energy cost.

Although rule-based and FL controllers can deal with the MG components' nonlinearities and avoid complex mathematical formulation, they rely on the designer's rules, which may not necessarily be comprehensive. Furthermore, extending the system when dealing with extensive data is challenging [29]. For example, the authors of [121] generated 25 FL rules based on two inputs, while [122] generated 50 FL

rules based on three inputs. A larger system can lead to a complex and computationally intensive programming process.

Other heuristic algorithms, such as PSO and Ant Colony Optimisation (ACO), are used in a real-time EMS [90]. Authors of [89] proposed an online EMS-based PSO for stand-alone hybrid wind and micro-turbine energy systems to achieve economic dispatch.

Alternatively, the ANN method can provide a fast solution to problem in real-time control [29]. For example, an ANN-based EMS developed in [123] to control house appliances is able to reduce energy consumption without affecting customer comfort. However, this approach requires training using historical data, which increases the computational time. In addition, a larger and more powerful central server may be required, leading to higher costs and inflexible systems. Although the online EMS does not require forecast data, it is challenging to deal with parameter uncertainty when the system becomes more extensive. Thus, for a larger system, prior planning is required (i.e., day-ahead scheduling).

2.5.2 Day-ahead Residential EMSs

Extensive research has been carried out on the forecasting methods to be utilised in EMSs, including intra-day [7] and day-ahead [124]. For instant, the authors of [125] proposed a rule-based EMS that optimises the day-ahead BSS charge/discharge power for peak shaving. In [84], a rule-based EMS controls MG energy flow and reduces energy costs using EVs as additional energy sources. Likewise, in [126], a rule-based House Energy Management System (HEMS) is proposed to reduce energy costs by enabling the V2H mode. However, the authors of [84, 125, 126] did not consider BSS and EV degradation in their EMS decision-making process. This omission is remedied in [61], where a MILP-based EMS is developed to optimise the EV battery use to extend its lifetime by including the maintenance costs of the EV battery.

An intra-day forecast-based EMS is designed for an islanded MG to reduce the BSS degradation and increase RESs self-consumption [127]. In [128], a day-ahead LP-based EMS is used for BSS scheduling to reduce greenhouse gas emissions and energy costs. The authors of [129] proposed day-ahead PSO-based EMS to reduce operational costs by including PV and BSS degradation costs in the objective function. A HEMS that exploits MILP to optimise the scheduling of shiftable appliances, EV, and BSS is introduced in [130], with the primary objective of compensating for reactive power while simultaneously reducing household energy costs. This is achieved by enabling V2H and House-to-Grid (H2G) modes. The authors of [130] assumed that energy sold to the grid is more expensive than energy purchased from the grid, which is not the case for most countries, such as the UK. Work in [131] facilitated V2H and V2G modes in a MILP-based HEMS to reduce peak power on the assumption that consumption behaviour is known. The authors of [132] proposed a hybrid algorithm comprising optimisation and rule-based prioritisation. The main target is to find optimal settings for EV and BSS to reduce energy costs.

The authors of [133] showed that a forecast-based EMS could extend the BSS lifetime by storing the following day's energy forecast. However, the export prices from the surplus PV energy are neglected. Likewise, authors of [3] state that the forecasted energy required for the next day is stored during off-peak times. However, their EMS did not use the surplus energy stored to supply load during the off-peak time, resulting in higher operating costs and increased net energy exchanged with the grid.

The main target of most EMSs reported in the literature is to reduce energy costs relative to existing tariffs. None of the above works considered two days-ahead energy forecast to increased self-consumption. It is noted that utilising the two days-ahead energy forecasts reduces unnecessary energy exchange with the grid and BSS charge/discharge cycles. For example, lack of knowledge of the day-2 energy forecast will invariably lead to the export of surplus RES energy during day-1 to the grid rather than storing it in the BSS and using it later during day-2.

The most common drawback of previous work reported in the literature is that the lifetime of a BSS, which requires avoiding unnecessary BSS discharging/charging cycles, is not considered as part of the decision-making process. To overcome this drawback, work reported in [2, 119, 134] restricted the battery SOC to charge/discharge to half its capacity (i.e., 50%). Similarly, the authors of [135] limited BSS capacity to between 35% and 60%. Although this method does extend BSS lifetime, it reduces the useable BSS capacity, which increases capital costs and undermines the self-consumption approach. An alternative solution is to include BSS degradation cost as an indication of the SOH of the BSS [4, 136, 137] or to include the BSS lifecycle in the optimisation process [28].

2.6 Community Energy Management Systems

P2P energy trading is becoming increasingly popular as it allows exchanging excess energy with neighbouring prosumers, communities, and organisations, not just with the main supplier (i.e., grid) [22]. The term "Peers" in P2P refers to individuals or groups of customers/prosumers where some can have their local generators, such as RESs and EVs.

The number of communities in the UK has gradually grown. Around 5,000 community groups have been formed since 2008 that used their RESs generation locally and produced more than 60 MW of generation capacity in 2013 [138].

2.6.1 Existing P2P Energy Trading Platforms

Several energy utilities in the UK have encouraged P2P energy trading. For example, EDF energy began a P2P energy trading trial at a social housing estate in south London using blockchain technology that allows participants to manage their energy usage through a P2P platform (accessible through an app) [67]. Similarly, Centrica (owner of British Gas) is also involved in P2P in a social housing scheme in Hackney, north-east London [67]. Another government-funded project called Project Piclo matches consumption with generation according to household preferences [139].

There are other existing P2P energy trading platforms worldwide, including PeerEnergyCloud in Germany [140], SOLshare in Bangladesh [141], and Enerchain, a blockchain-based initiative initially supported by over 40 European utility companies [142]. The major technological bases of these platforms are Auction theory [97, 98], Blockchain technology [96, 100, 143], Constrained optimisation algorithms [5, 144], and Game theory [94, 95].

2.6.2 P2P Energy Trading

P2P energy trading can be categorised into cooperative and non-cooperative models. Profits are shared equally among community members in cooperative models. In contrast, non-cooperative models, such as bidding, competition, and games, can result in unequal profit distributions among community members [145]. Based on recent studies, P2P energy trading can be roughly divided into three structures [146], as shown in Fig. 2.9.

1. Centralised: Peers trading with each other through a central controller, which can be an aggregator or utility. Customers' appliance requested start times and preferences are collected through smart meters to manage electricity usage within the neighbourhood and schedule the appliance operation and BSS in each house. Centralised control can be considered as cooperative model, as it provides cooperative scheduling to achieve optimal system setting considering the overall system parameters. Some of the limitations of this structure are:
    a) As the system becomes more complex and larger in scale, the server computing power must be upgraded.
    b) A failure in the central controller may lead to shutting down the entire system.

    In the centralised P2P power supply market, scalability, robustness, security and privacy issues are the primary concerns. To overcome the above backwords, networks are moving toward more intelligent network communication, from a centralised infrastructure to a decentralised system [111].

2. Decentralised: Peers trade excess energy with each other directly without a mediator [147]. All required information is distributed among community members, the control is used to manage energy transactions and coordinate energy exchange activities to achieve each house's target (e.g., minimising its electricity costs). This structure offers more autonomy than the central structure, allowing each household to make its own decisions. This structure can be used for auction-based P2P energy trading as it allows local energy markets to be fully decentralised. Pairing houses in a decentralised manner can avoid failure of the inter-system when one-unit collapses. In addition, it is more flexible and easier to add more nodes to the network. However, one limitation of a decentralised structure is that it may not effectively achieve the overall system target [148].
3. Hybrid: Combines both centralised and decentralised structures, where peers are allowed to trade directly with other peers or through a mediator.

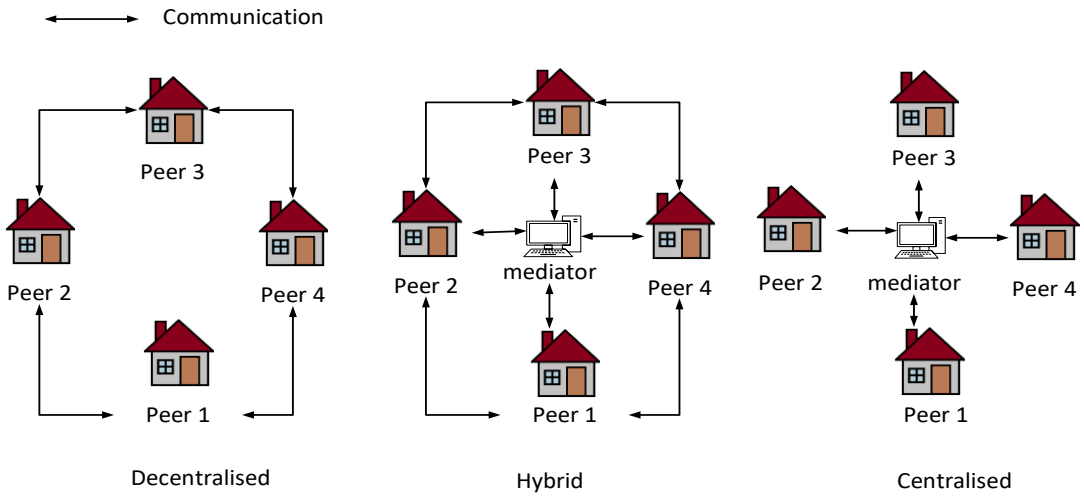

Fig. 2.9. Schematic of Peer-to-Peer structures.

This thesis uses hybrid coordination topology to minimise the overall energy exchange between the community and the grid. More details will be presented in Chapter 5.

As stated in Section 2.4, recent studies have identified four main techniques for P2P energy trading, which are Game theory, Auction theory, Blockchain technology, and

Constrained optimisation. This thesis focuses on P2P energy trading-based constrained optimisation approach. Thus, this section is concerned mainly with the state-of-the-art related to the mathematical formulation of the P2P problem. For example, a hierarchical MILP-based P2P EMS is proposed in [5] to reduce the operating costs of the four houses in the community. The import/export tariff for energy exchanged between the paired houses is set to zero, which may not be acceptable for some prosumers because it means they cannot profit. The authors of [149] used centralised P2P EMS to run a community consisting of four houses by feeding the required information into a central controller to make the optimal setting of each house. The main target is to reduce the operating costs of the whole community. The main drawback of their system is that profits are evenly distributed among houses in the community, resulting in the possibility of uneven profit distribution.

The authors of [150] proposed a centralised controller that reduces the neighbourhood's demand peaks and energy costs. The authors of [145] proposed rule-based P2P energy trading to choose the best pairs of houses. In [21], a P2P EMS is suggested to run a community of 5 prosumers to reduce energy bills. However, their system does not consider BSS lifetime, and the cost evaluation was only for one day. The authors of [151] proposed P2P energy sharing and a three-stage evaluation methodology to reduce the operating costs of 10 residential prosumers in a community. However, they did not consider BSSs in their system. Similarly, the authors of [9] proposed a P2P EMS for energy exchange between 5 buildings to minimise energy costs. Their system does not consider the BSS.

Several works consider EVs in the P2P EMS, focusing on controlling EV battery charging time. For example, the authors of [152] proposed a decentralised P2P EMS that controls the EV charging time and shares the excess energy between smart buildings to maximise social welfare. Similarly, a P2P EMS based on a bidding strategy to compensate for uncertainties associated with PV generation at the community level is proposed in [146]. However, neither [146, 152] consider using EV batteries as extra storage for the system; considering EVs as only flexible loads.

It has been demonstrated in [153] that P2P EMS can reduce community energy costs by up to 30% compared to conventional energy trading only with the grid. However, using EVs as extra storage can support grid frequency and voltage regulation by enabling the V2G mode, and enhancing self-consumption and lowering energy costs by enabling the V2H mode. For example, in [154], a centralised MILP-based EMS selects the best house pairs based on their consumption and locations. The main goal of [154] is to reduce the peak load and energy costs by supplying the neighbour with excess energy stored in EV and BSS. However, their system does not consider the BSS or EV lifetimes. The use of unidirectional EV chargers and bidirectional chargers that can discharge an EV battery to supply a house and/or grid are investigated in [22]. However, the EV use pattern remained constant throughout the year. In [155] a P2P EMS between buildings and EV charging stations is proposed to reduce energy costs and maximise the use of generated power from RESs. However, the SOC of the EVs' batteries are limited to 30%-85% to prolong their lifespan.

There are already initiatives across the world that limit the amount of energy a prosumer can inject into the grid. Most recent studies on P2P energy trading have focused on minimising operating costs rather than reducing net energy exchange between the community and the grid. However, minimising energy costs can lead to higher net energy exchange with the grid. Therefore, this thesis proposes a new approach that minimises net energy exchange between the community and the grid through P2P energy trading. Importantly, this thesis introduces the use of the two days-ahead energy forecast to reduce the energy exchange with the grid by storing the next-day energy forecast.

2.7 Conclusion

This chapter presented a literature review which addressed the main challenges and present solutions for integrating DERs into the consumption and distribution levels. In addition, it provides a review of the state-of-the-art approaches relevant to residential EMSs and CEMSs.

3 REAL-TIME RESIDENTIAL ENERGY MANAGEMENT SYSTEM

3.1 Introduction

The residential EMS can play a vital role in maximising self-consumption and reducing energy costs. This chapter proposes a real-time residential Fuzzy logic-based Energy Management System (FL-EMS). The proposed method has been tested using the Active Office Building (AOB) data located in Swansea, Bay Campus, UK, as a case study. The FL-EMS algorithm is compared with recently published state-of-the-art algorithms and with the current Energy Management System (EMS) utilised in the AOB to demonstrate the effectiveness of the proposed strategy. The analysis in this chapter has been performed by coding the previous state-of-the-art algorithms and the FL-EMS in MATLAB software.

Note that the results presented in this chapter have been published in IEEE Access journal:

A. Sorour, M. Fazeli, M. Monfared, A. A. Fahmy, J. R. Searle and R. P. Lewis, “Forecast-Based Energy Management for Domestic PV-Battery Systems: A U.K. Case Study,” *IEEE Access*, vol. 9, pp. 58953-58965, 2021, doi: 10.1109/ACCESS.2021.3072961.

This chapter is structured as follows. First, Section 3.2 describes the AOB system configuration. Section 3.3 describes the forecast data and tariff prices. The proposed FL-EMS is presented in Section 3.4. Section 3.5 discusses the results and demonstrates the impact of different Battery Storage System (BSS) capacities and Photovoltaic (PV) sizes on the energy exchange with the grid. Finally, Section 3.6 presents the conclusion of Chapter 3.

3.2 Active Office Building System Configuration

The AOB schematic diagram is presented in Fig. 3.1, comprises a PV system of 22.3 kW_p and a Li-ion BSS of 110 kWh connected to a 48 V-DC bus. Moreover, three single-phase inverters of 230 V-AC, 48 V-DC, and 15 kVA are used. The PV DC-DC converter rating and the maximum power load are 23.2 kW and 32.5 kW, respectively. The BSS rated charge/discharge power ($P_{B\text{-}rating}$) is 102.4 kW [156]. The minimum SOC ($SOC_{B\text{-}min}$) and the maximum SOC ($SOC_{B\text{-}max}$) limits are set to 20% and 98%, respectively [1]. The BSS's capital cost (CC_B) is assumed to be £273/kWh, though the costs are expected to reduce as BSS technology advances [157, 158]. The number of the BSS life cycles (N_{Bcycle}) is 6,000 [159].

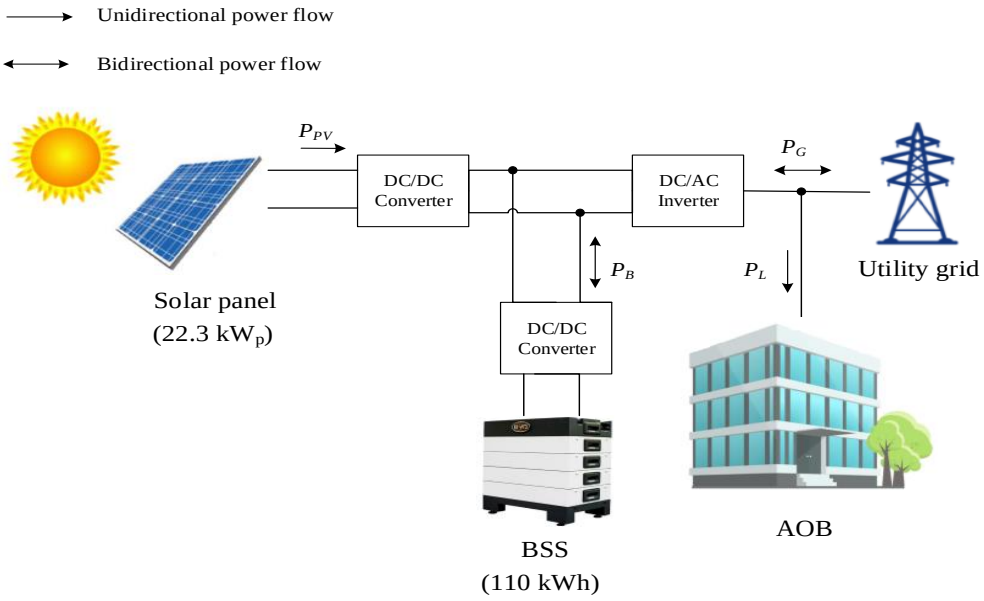

Fig. 3.1. Schematic diagram of the AOB configuration.

3.3 Forecast Data and Tariff Prices

In this study, two different rates are chosen for the peak and off-peak times, according to Economy 7 obtained from an electricity utility company in the UK. The peak and off-peak prices are £0.1666/kWh and £0.1104/kWh, respectively [160]. The peak and off-peak times are from 8:00 AM - 8:00 PM and 8:00 PM - 8:00 AM, respectively. The price of the PV power exported to the grid is £0.055/kWh [8].

The uncertainties of PV generation and demand are considered when optimisation is carried out. Several approaches are available in the literature for PV and demand forecast, as discussed in Chapter 2- Subsection 2.3.2. This study does not consider any specific forecast technique to avoid diverting attention from a forecast-based EMS to a forecasting method. Instead, as explained in [43, 45, 46], an error with a normal distribution is added to the recorded historical data of PV power (P_{PV}) and load power (P_L) to represent the one day-ahead forecasted PV power ($P_{PV\text{-}1}$) and load power ($P_{L\text{-}1}$). The accuracy of the forecast is measured using the Mean Absolute Percentage Error (MAPE) metric and calculated as [161]:

$$\text{MAPE} = \frac{100}{N}\sum_{\text{i=1}}^{N}\frac{|\,(P_{PV}(t) - P_L(t))\,dt - (P_{PV\text{-}1}(t) - P_{L\text{-}1}(t))\,dt\,|}{(P_{PV}(t) - P_L(t))\,dt}\,\% \tag{3.1}$$

where N is number of samples.

The MAPE is 30% over six months. It is worth noting that the choice of 30% energy forecast error is very pessimistic, as under most circumstances, the forecast methods are much more accurate, e.g., a 10% forecast error is reported in [7, 161]. Fig. 3.2 illustrates actual peak time energy (E_{Day}) against each day's forecasted peak time ($E_{Day\text{-}f}$). The forecasted peak time energy for each day is calculated as:

$$E_{Day\text{-}f} = \int_{t=8\text{ AM}}^{t=8\text{ PM}} (P_{PV\text{-}1}(\tau) - P_{L\text{-}1}(\tau))\,d\tau \tag{3.2}$$

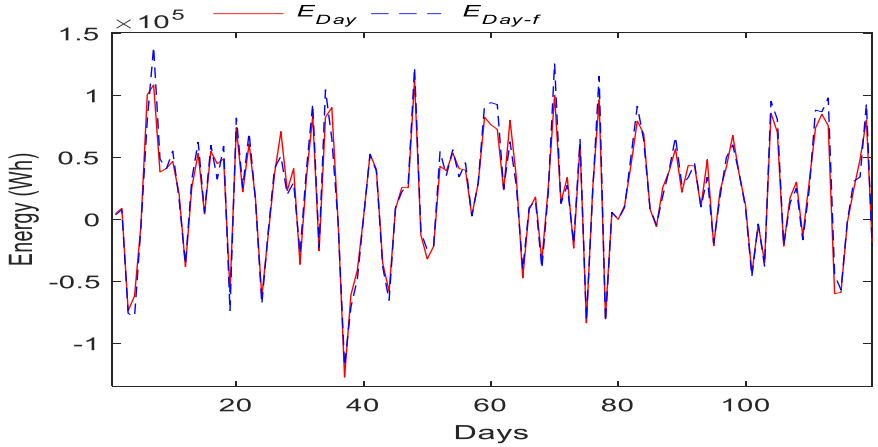

Fig. 3.2. Actual peak energies (E_{Day}) and forecasted peak energies ($E_{Day\text{-}f}$).

3.4 FL-based EMS

The FL-EMS has been designed to optimise the utilisation of the BSS, maximise PV self-consumption, and extend BSS life span. In addition, it regulates the difference between the demand and PV generation by determining the BSS charge/discharge power considering the one day-ahead peak time energy forecast. The proposed method is illustrated in Fig. 3.3 and follows the following procedures:

1- Input measured values and forecasted data for the one day-ahead (day-1) assuming that it is provided by a forecasting company: measured PV generation (P_{PV}), measured load demand (P_L), day-1 forecasted PV generation ($P_{PV\text{-}1}$), day-1 forecasted load demand ($P_{L\text{-}1}$).
2- Estimate the SOC and SOH of the BSS.
3- Calculate the peak period energy demand for the one day-ahead ($E_{Day\text{-}f}$) using (3.2).
4- Optimise the BSS operation using FL by considering $E_{Day\text{-}f}$.
5- Send the setting to the BSS.

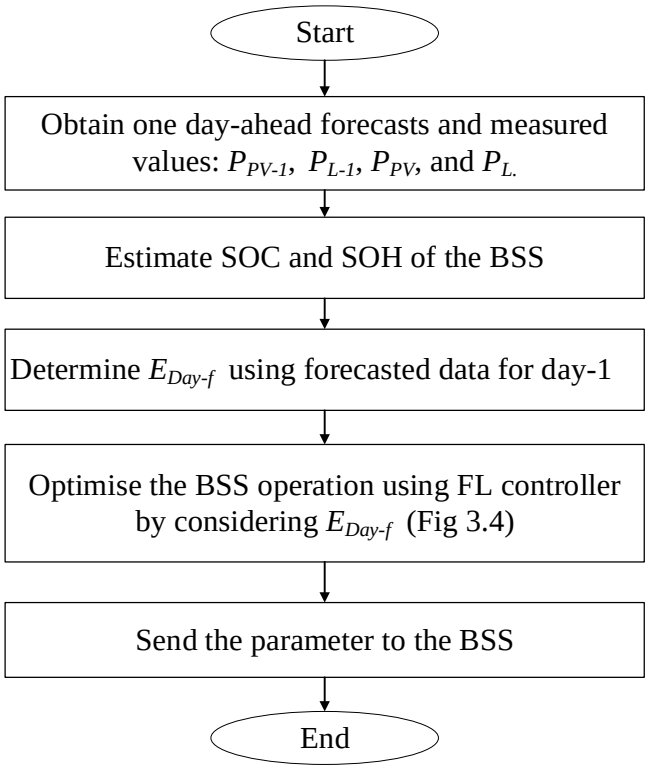

Fig. 3.3. Proposed FL-EMS.

3.4.1 SOC and SOH Battery Estimations

Accurate SOC and SOH estimations are necessary for EMS to deliver the optimum energy supply to customers while maintaining BSS health. SOH defines BSS aging, which is reflected in the capacity loss estimation [162]. Several studies during the past years have investigated SOC estimation using, for example, online parameter identification of Recursive Least Square algorithm [163-165], ANN [166-168], the Open-Circuit-Voltage method, the Kalman filter algorithm [169], and the Coulomb-counting method [1].

SOH is an important factor, as a longer BSS life has positive influences, such as less maintenance and fewer replacement. Several studies have proposed a degradation model based on incremental capacity analysis [170]. This study estimates the battery's SOC using the Coulomb-counting method [1]:

$$SOC_B(t)=SOC_B(0) - \frac{1}{B_{capacity}(t)} \int_0^t P_B(\tau)\, d\tau \tag{3.3}$$

And the SOH is estimated as [162]:

$$SOH(t) = \frac{B_{capacity}(t)}{B_{nom}} \tag{3.4}$$

where $SOC_B(0)$ is the initial value of SOC (%), $P_B(\tau)$ is the BSS charge/discharge power (kW), $B_{capacity}(t)$ is the estimated BSS capacity (kWh), and B_{nom} is nominal BSS capacity (kWh). The new capacity is estimated as [162]:

$$B_{capacity}(t)=\frac{1}{SOC_B(t_\alpha) - SOC_B(t_\beta)} \int_{t_\alpha}^{t_\beta} I_B(\tau)\, d\tau \tag{3.5}$$

where $I_B(\tau)$ is the BSS current (A). $SOC_B(t_\alpha)$ and $SOC_B(t_\beta)$ are the SOC of the BSS at initial time t_α and final time t_β (%), respectively. The new estimate of BSS capacity

is updated following each charge/discharge cycle (Δt=10 min) and is fed back into (3.3) to estimate the new SOC.

3.4.2 Proposed Fuzzy Logic Control Algorithm

The flowchart of the proposed FL-EMS algorithm is presented in Fig. 3.4, which is divided into two operating modes (a) peak time and (b) off-peak time.

a) Peak time:

As shown by the red solid lines in Fig. 3.4, if $P_{PV} > P_L$ and $SOC_B < 98\%$, the BSS is charged using the FL charging mode. Since the export price is considerably less than the grid purchase price, the BSS will be charged using PV surplus power regardless of the off-peak time forecast. Otherwise, if $P_{PV} > P_L$ and $SOC_B \geq 98\%$, the PV surplus power will be exported to the grid (hence $P_B = 0$). This process enables storage of excess energy from the PV and use of that energy during off-peak or during the next peak period. In addition, it will reduce emissions by reducing energy purchased from the grid.

As shown by the red dotted lines in Fig. 3.4, if $P_{PV} < P_L$ and $SOC_B > 20\%$, then the BSS is discharged using the FL discharging mode. Otherwise, if $P_{PV} < P_L$ and $SOC_B \leq 20\%$, any energy shortage will be purchased from the grid (hence $P_B = 0$).

b) Off-peak time:

As shown by the black solid lines in Fig. 3.4, if $P_{PV} > P_L$ and $SOC_B < 98\%$, the BSS will be charged using all the PV surplus power until it is fully charged using the FL charging mode. Otherwise, if $P_{PV} > P_L$ and $SOC_B \geq 98\%$, the PV surplus power will be fed into the grid (hence $P_B = 0$).

As shown by the blue solid lines in Fig. 3.4, if $P_{PV} < P_L$ and $SOC_B \leq 30\%$, the BSS will be charged up to 30% according to (3.6):

$$P_B = \frac{(30\% - SOC_B\,(t))\; B_{capacity}\;(t)}{\Delta T} \tag{3.6}$$

where ΔT is the sampling time of 10 minutes (i.e., the flowchart is re-executed every 10 min). This process ensures that SOC is at least 30% before the next peak period. A 10% safety margin is considered (from $SOC_{B\text{-}min}$ = 20%) to account for PV/load uncertainties during peak periods.

As shown in Fig. 3.4 in black dotted lines, if $P_{PV} < P_L$ and $SOC_B > 30\%$, the BSS will be discharged or charged based on the next day peak time energy forecast ($E_{Day\text{-}f}$). If $E_{Day\text{-}f} > 0$, this means generation is higher than demand during the peak period. Thus, the BSS will discharge to supply the load during the off-peak period using the FL discharging mode to avoid purchasing energy from the grid and to charge the BSS next day from PV surplus power. If $E_{Day\text{-}f} < 0$, this means the generation is less than the demand during peak period. Therefore, the system will check the BSS stored energy against the forecasted energy requirement, using (3.7) to calculate the required energy.

$$E_B = \left| E_{Day\text{-}f} \right| - (SOC_B\,(t) - 30\%)\; B_{capacity}\;(t) \tag{3.7}$$

where, E_B represents required BSS energy. If $E_B > 0$, this mean the available stored energy is not sufficient for the peak period. Therefore, the BSS will be charged according to (3.8).

$$P_B = \frac{E_B}{\text{Time}} \tag{3.8}$$

where the ‘‘Time’’ is the remaining time of the off-peak period at each cycle of the flowchart.

If $E_B < 0$, this means the BSS has sufficient energy to supply the loads during the peak period, and the FL discharge mode will be used to supply the load using the excess energy stored in the BSS. This process will guarantee that the predicted required energy needed for the peak period is stored in the BSS during the off-peak period. In addition, this process reduces energy exchange with the grid and the operational cost by purchasing only the estimated energy needed.

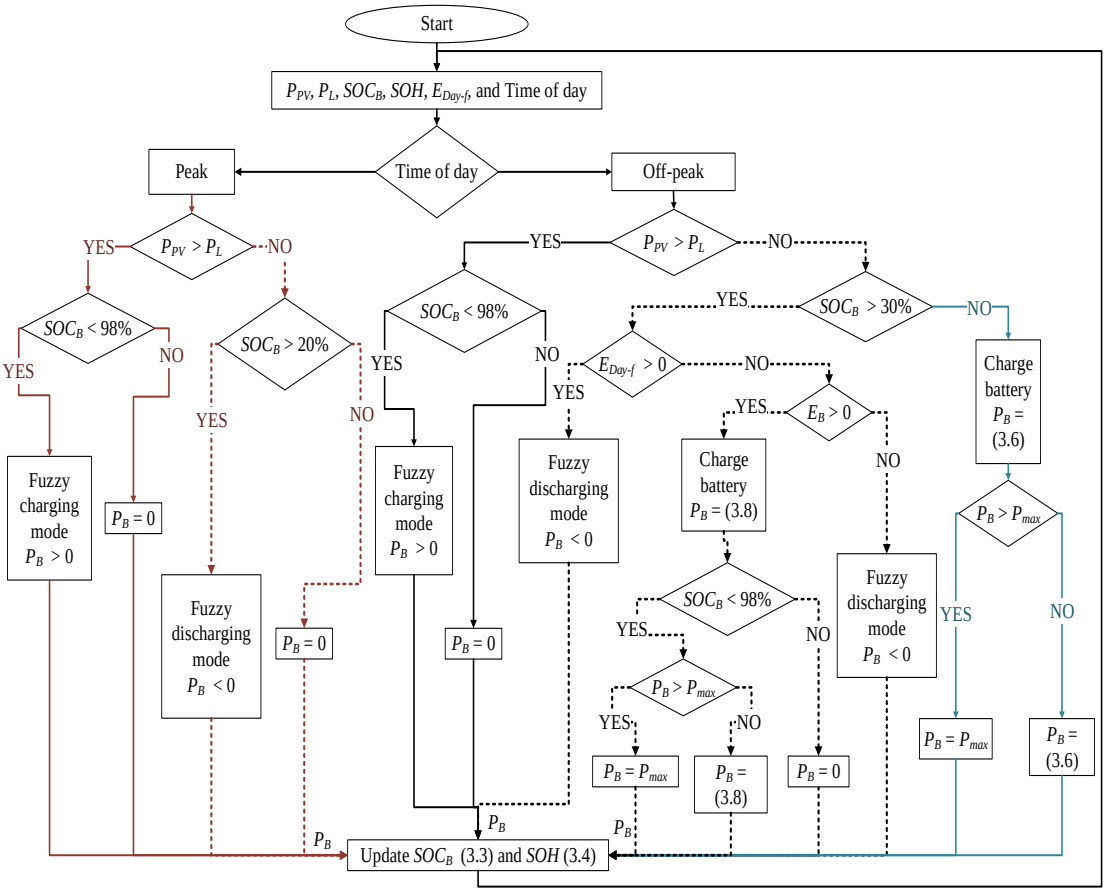

Fig. 3.4. Flowchart of the proposed FL-EMS algorithm.

3.4.3 Charging and Discharging FL Control Modes

The charge and discharge power of the BSS is controlled by the FL controller. To extend BSS lifetime the SOC and SOH contribute to charge/discharge decision making. Fig. 3.5 illustrates the charging mode of the BSS, where the inputs are P_{PV} - P_L, SOC_B, and SOH, and the output is BSS reference P_B. The inputs for discharging mode are P_L - P_{PV}, SOC_B, and SOH.

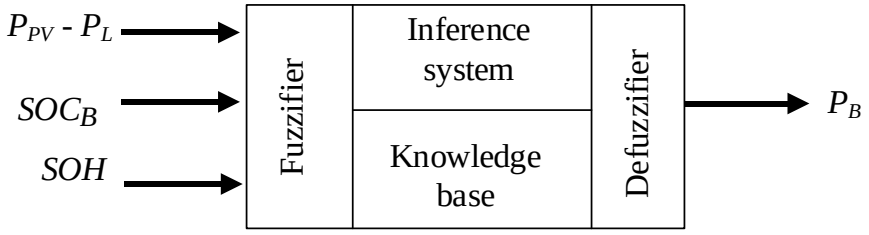

Fig. 3.5. FL structure for charging mode.

Figs. 3.6 (a) and (b) represent the fuzzy variable inputs, P_{PV} - P_L and P_L - P_{PV}, for charging and discharging modes, respectively. Figs. 3.6 (c) and (d) represent the Membership Functions (MFs) of SOC and SOH of the BSS, respectively, where both are used for charging and discharging modes.

As shown in Figs. 3.6 (a) and (b) the power is classified as power very low (PVL), power low (PL), power medium (PM), power high (PH), and power very high (PVH), where the values are in per unit (pu). The base power (P_{base}) is chosen to be the nominal load of the system, which is 32.5 kW.

Fig. 3.6 (c) shows the MFs of the SOC_B are between 0 and 1, where 1 represents the full capacity of the BSS (100%). The MFs of SOC, are classified as very low (VL), low (L), medium (M), high (H), and Full (F). Fig. 3.6 (d) shows the MFs of the SOH are divided into three ranges namely: low (L), medium (M), and healthy (H), where 1 represents a brand-new BSS. It is worth mentioning that most BSSs need to be replaced when the SOH drops to 70-80% depending on BSS type. In this study, a Li-ion BSS is used and this needs to be replaced when its SOH drops to 80% [162].

Fig. 3.7 shows MFs for the charging mode output variable, P_B, and is classified as very low (VL), low (L), medium (M), high (H), and maximum (MAX). The maximum limit for P_B MF is chosen as the $P_{B\text{-}rating}$. The output for the discharging mode is similar to the charging mode but with a negative sign ($P_B < 0$).

The FL inference rules are applied on the input MFs to infer the output. These rules were created based on SOC_B, SOH, and mismatched power between P_{PV} and P_L to maintain BSS lifetime while maximising PV self-consumption. There are 150 rules generated for BSS charge and discharge modes, with one half representing the charging mode and the other half representing the discharging mode.

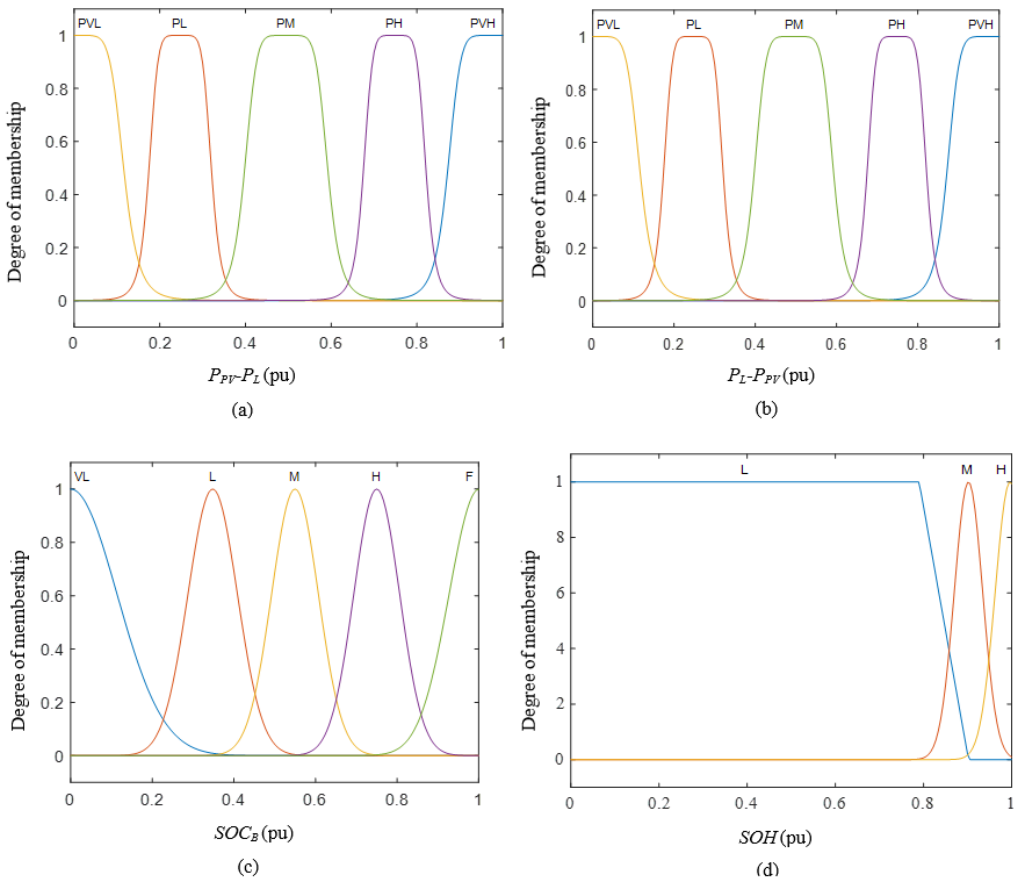

Figs. 3.6. (a), (b), (c), and (d) represent the MFs of P_{PV} - P_L, P_L - P_{PV}, SOC_B, and SOH, respectively.

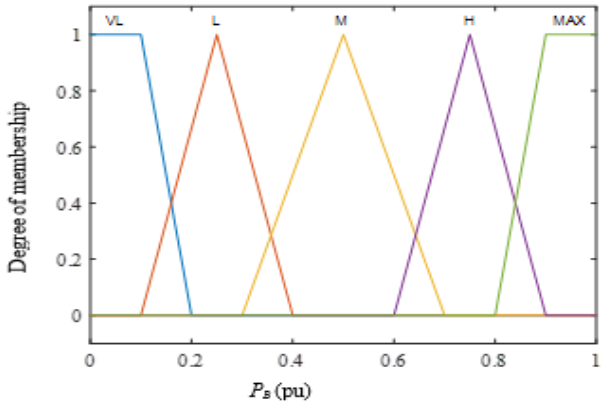

Fig. 3.7. MFs for the charging mode output battery reference P_B.

Table 3.1. Example of charging rules for healthy SOH.

Input/ output	MFs	1	2	3	4	5	6	7	8	9	10	11	12	13	14	15	16	17	18	19	20	21	22	23	24	25
$P_{PV}-P_L$	PVL	■	■	■	■	■																				
	PL						■	■	■	■	■															
	PM											■	■	■	■	■										
	PH																■	■	■	■	■					
	Pmax																					■	■	■	■	■
SOC_B	VL	■					■					■					■					■				
	L		■					■					■					■						■		
	M			■					■					■					■					■		
	H				■					■					■					■					■	
	F					■					■					■					■					■
SOH	H	■	■	■	■	■	■	■	■	■	■	■	■	■	■	■	■	■	■	■	■	■	■	■	■	■
	M																									
	L																									
P_B	VL	■	■	■	■	■					■					■					■					■
	L						■	■	■	■					■					■					■	
	M											■	■	■					■							
	H																■	■						■		
	Max																					■	■			

Table 3.2. Example of discharge rules for medium SOH.

Input/ output	MFs	1	2	3	4	5	6	7	8	9	10	11	12	13	14	15	16	17	18	19	20	21	22	23	24	25
P_L -P_{PV}	PVL	■	■	■	■	■																				
	PL						■	■	■	■	■															
	PM											■	■	■	■	■										
	PH																■	■	■	■	■					
	Pmax																					■	■	■	■	■
SOC_B	VL	■					■					■					■					■				
	L		■					■					■					■						■		
	M			■					■					■					■					■		
	H				■					■					■					■					■	
	F					■					■					■					■					■
SOH	H																									
	M	■	■	■	■	■	■	■	■	■	■	■	■	■	■	■	■	■	■	■	■	■	■	■	■	■
	L																									
P_B	VL	■	■	■	■	■	■					■					■					■				
	L							■	■	■	■		■					■						■		
	M													■	■	■			■					■		
	H																			■	■				■	■
	Max																									

Table 3.1 presents an example of the charging mode rules for a healthy BSS. As can be seen, when the BSS is in a healthy condition, it can be charged to a greater extent to reduce the energy exchange with the grid.

Table 3.2 presents an example of the discharging mode rules for medium SOH. As shown the BSS cannot be used to such a great extent as in Table 3.1 because the SOH of the BSS has deteriorated.

The FL controller prevents the BSS from being fully discharged. For example, during peak periods, $P_{PV} < P_L$, and SOC_B is just above $SOC_{B\text{-}min}$ (e.g., $SOC_B = 21\%$), the BSS will discharge (red dotted lines in Fig. 3.4). However, based on the rules in Table 3.2, the FL makes sure that the discharge rate is very low (VL), which prevents the BSS from being drastically discharged in one cycle (i.e., $\Delta t = 10$ min). As result, the BSS will not discharge further in the following cycle of the flowchart, since $SOC_B < 20\%$. As indicated by the solid blue lines in Fig. 3.4, the algorithm consistently maintains $SOC_B > 30\%$ during off-peak hours.

3.5 Case Studies

Comparisons of BSS performance and energy exchanged with the grid between the proposed FL-EMS, the commercial EMS system utilised in the AOB, and the EMSs proposed in recent publications [1], [2], and [3] are carried out in this section. The effects of different BSS capacities and PV system ratings on the net energy exchange with the grid are also investigated.

3.5.1 Performance Comparison

Figs. 3.8, 3.9, 3.10, and 3.11 present the system behaviour of the EMS proposed in [1], the FL-EMS proposed in this study, and the EMSs proposed in [2] and [3], for the two test days, 11th and 12th of May 2019, respectively. The red lines represent the SOC_B and the black lines represent the values of P_{PV} - P_L. It can be seen from the figures that on both days the PV generation exceeds demand most of the time ($P_{PV} > P_L$).

Fig. 3.8 shows the BSS is charged to full on day-1 during off-peak and peak periods from the grid and PV surplus, respectively. However, due to the lack of knowledge about the next day peak time energy forecast (on day-2), the BSS remains fully charged during the off-peak period. The main objective of the EMS in [1] is to keep the BSS fully charged during the off-peak period to avoid purchasing energy at a high cost. The main disadvantage of this system is that if the BSS is fully charged during the off-peak period, any PV surplus generated during the subsequent peak period will be fed into the grid rather than being used to charge the BSS. This can lead to higher energy costs because the grid will charge the BSS during off-peak time, eliminating the opportunity of charging BSS from the PV surplus. In addition, energy stored in the BSS is not used on the days when $P_{PV} > P_L$, as shown in Fig. 3.8, on day-2.

As shown in Fig. 3.9, unlike the EMS proposed in [1], the FL-EMS proposed in this work maintains the SOC at 30% because the following peak period does not require energy (i.e., $E_{Day\text{-}f} > 0$). During peak time, when the generation exceeds the demand ($P_{PV} > P_L$), the PV power will supply the load and charge the BSS. During off-peak period, the BSS can supply the load depending on the next day peak-time energy forecast ($E_{Day\text{-}f}$). These processes follow the black dotted, red solid, and blue solid lines in Fig. 3.4.

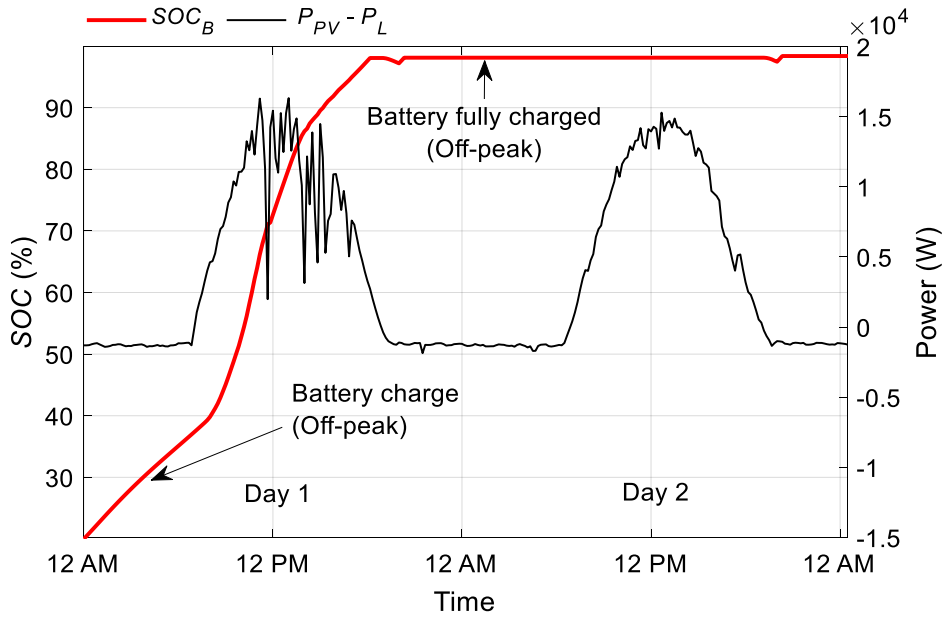

Fig. 3.8. System performance of EMS proposed in [1] for the two test days 11th and 12th of May 2019. The red line represents SOC_B, and the black line represents P_{PV} - P_L.

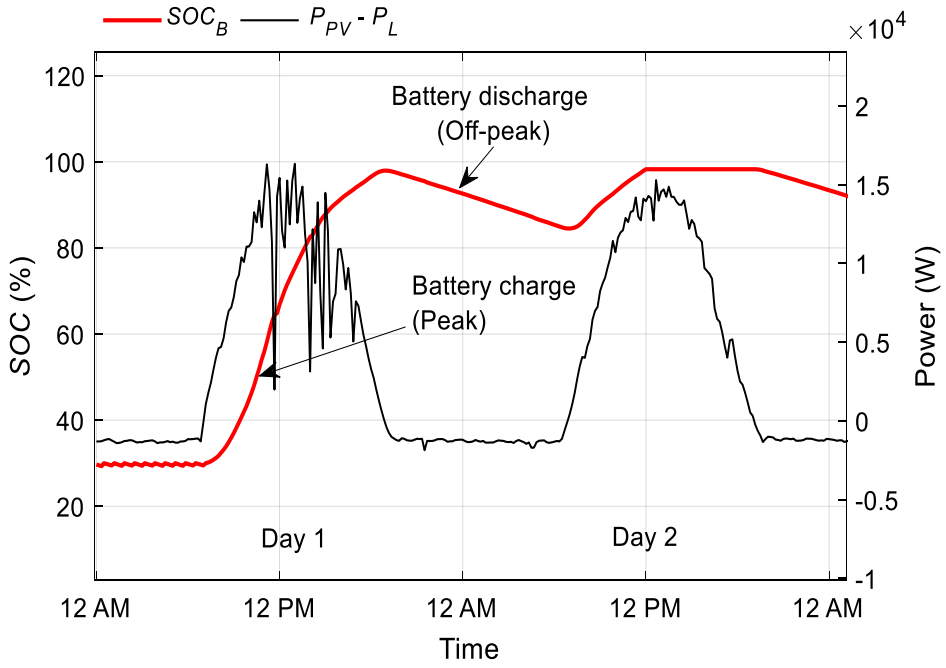

Fig. 3.9. System performance of the proposed FL-EMS for the two test days 11th and 12th of May 2019. The red line represents SOC_B, and the black line represents P_{PV} - P_L.

The system performance of the EMS proposed in [2] is presented in Fig. 3.10. Their system ensures that the SOC of the BSS always remains above 50% to maintain the BSS's health. Moreover, the system does not consider tariff prices and only charges the BSS from the PV surplus power, which may increase operating costs. The FL rules employed in [2] imply that if the SOC is between 85% and 100% (considered the full range) and the net power required is small, then the BSS is discharged, as shown in Fig. 3.10. During the off-peak period in day-2, the BSS discharged until the SOC fell to 85%. The BSS will be disconnected if the SOC is in the medium or low ranges and the power required is in the small range.

The system performance of the EMS proposed in [3] is presented in Fig. 3.11, which shows the PV surplus power is used to charge the BSS during day-1. However, the BSS stays fully charged throughout the off-peak period. The EMS proposed in [3] aims to ensure the BSS is charged during off-peak times according to the next day forecast $E_{Day\text{-}f}$. The main disadvantage of their system is that the excess energy stored in the BSS does

not contribute to the off-peak load, which undermines the PV self-consumption for the next day. It also increases energy exchanged with the grid and operational costs.

Fig. 3.12 presents the results obtained for the two days, 16th and 17th May 2019, for the proposed FL-EMS and the three EMSs proposed in [1], [2], and [3]. The blue, red, green, and purple dashed lines are the SOC_B of the proposed FL-EMS, EMSs in [1], [2], and [3], respectively. The black line represents P_{PV} - P_L. Unlike in Figs. 3.8, 3.9, 3.10, and 3.11, as shown in Fig. 3.12, the demand is higher than the generation most of the time ($P_{PV} < P_L$). Fig. 3.12 shows that during off-peak time, the proposed FL-EMS enables the BSS to store the energy required for the day-ahead peak period only, which follows the black dotted line in Fig. 3.4. As shown in Fig. 3.12, the SOC of the proposed FL-EMS is maintained at 70% during the off-peak period via continuous checking of the following day energy forecast ($E_{Day\text{-}f}$). However, in [1] (red line), the BSS is fully charged throughout the off-peak period, irrespective of the energy required for the next day. In [2] (green line), the BSS is charged only from PV power. This adversely affects purchasing energy from the grid during peak periods when the tariff is highest. The proposed EMS in [3] (dashed purple line), keeps the SOC at 95%, because the energy is not needed for the following peak period ($E_{Day\text{-}f} > 0$). However, surplus energy stored in the BSS is not used during the off-peak time.

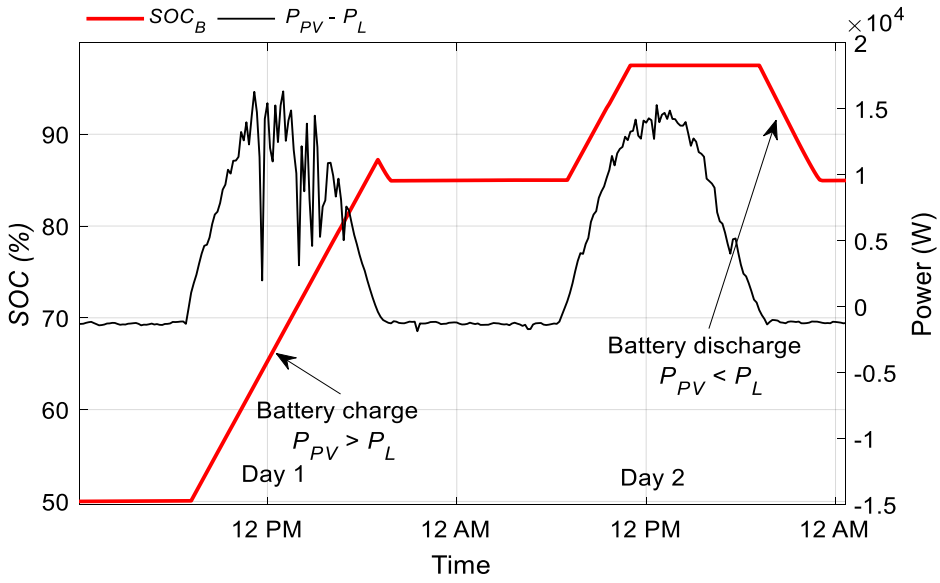

Fig. 3.10. System performance of EMS proposed in [2] for the two test days 11th and 12th of May 2019. The red line represents SOC_B, and the black line represents P_{PV} - P_L.

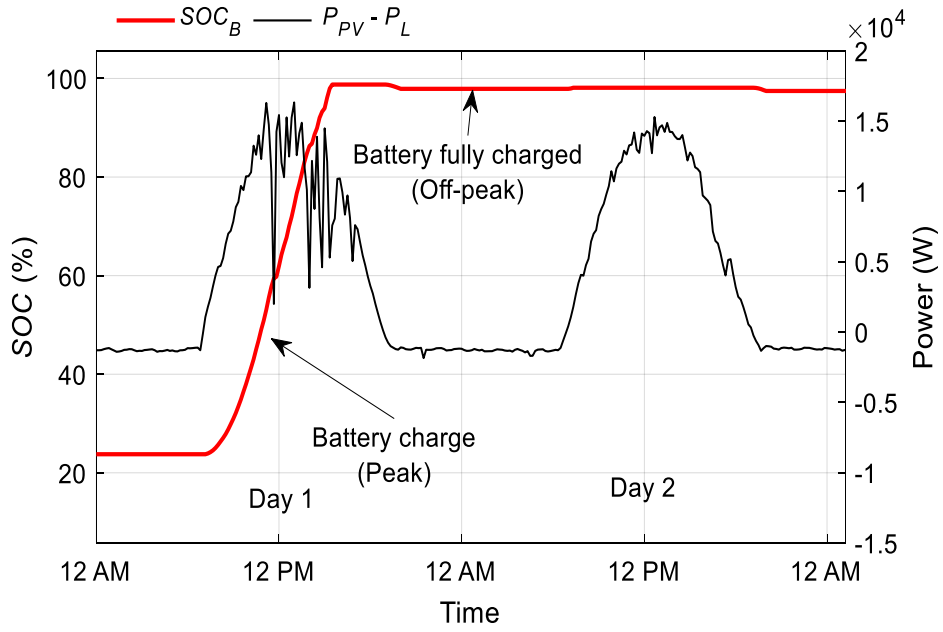

Fig. 3.11. System performance of EMS proposed in [3] for the two test days11th and 12th of May 2019. The red line represents SOC_B, and the black line represents P_{PV} - P_L.

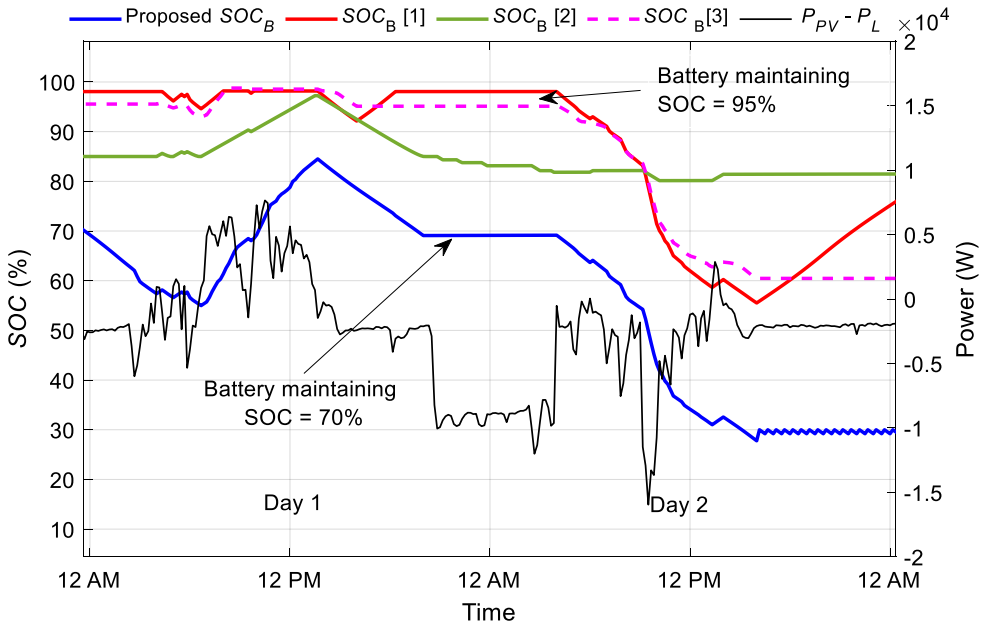

Fig. 3.12. System performance of the EMS proposed in this work and the EMSs proposed in [1], [2], and [3] for 16th and 17th May 2019. The blue, red, green, and purple dashed lines are the SOC_B of the proposed FL-EMS, EMSs in [1], [2], and [3], respectively. The black line represents P_{PV} - P_L.

In comparison, the proposed FL-EMS charges the BSS based on the required energy $E_{Day\text{-}f}$ only to maximise PV self-consumption, while the proposed EMS in [1] fully charges the BSS during the off-peak period. Therefore, any surplus energy from the PV system will be fed to the grid. The proposed EMS in [2], limits BSS capacity to 50 % and feeds any PV surplus energy to the grid. The proposed EMS in [3], despite determining the energy forecast for the following day, does not use surplus energy stored in the BSS to meet off-peak loads. The FL-EMS proposed in this work (the blue line in Fig. 3.12) decreases the amount of energy purchased during peak times by using energy stored in the BSS. In addition, it reduces unnecessary energy exchange with the grid which reduces transmission losses and the requirement for central storages.

3.5.2 Operating Costs and Net Energy Exchanged Comparison

Figs. 3.13, 3.14, and 3.15 show the energy exported during the peak time, the energy imported during the off-peak time and the energy imported during the peak time, respectively, for the six months from May to October 2019. The blue, orange, green, purple and yellow bars denote the results obtained for the proposed FL-EMS, the EMSs used in [1], [2], [3], and the AOB's EMS, respectively.

Fig. 3.13 shows that the proposed FL-EMS enabled maximum usage of PV power by charging the BSS and minimising energy exported to the grid during peak time.

Figs 3.14 and 3.15 show that proposed FL-EMS achieved better management because it purchased less energy during both off-peak and peak periods. Obviously, greater cost reduction is achieved by importing and exporting less energy, i.e., maximising use of the PV power generated. However, the proposed EMS in [1] imported slightly less energy during peak time compared to the proposed FL-EMS, because it adopted the approach that the BSS should be fully charged during off-peak time regardless of the energy forecast for the following peak time.

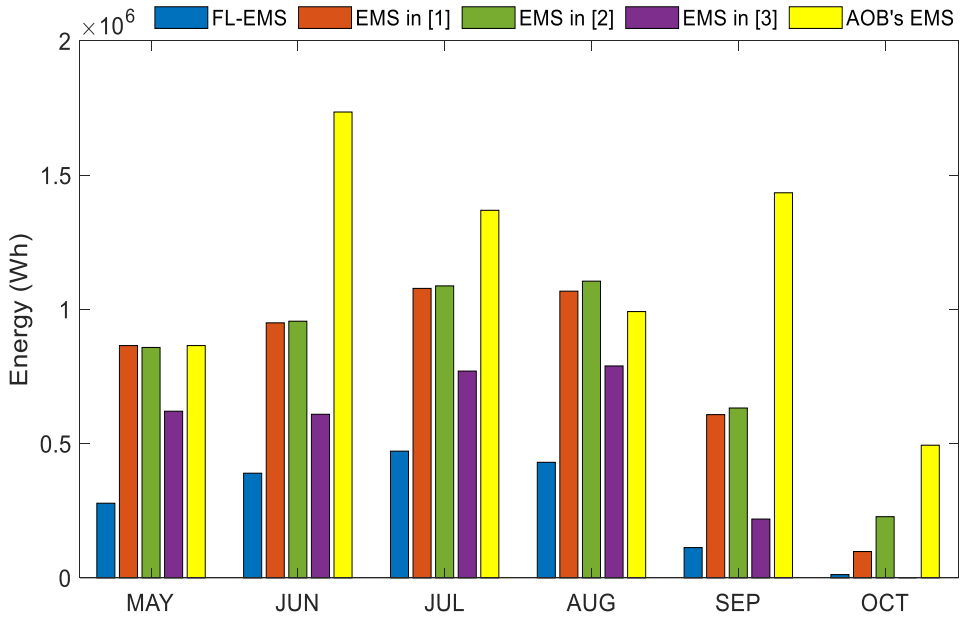

Fig. 3.13. Energy exported during peak time from May to October 2019. The blue, orange, green, purple, and yellow bars denote the results obtained for the proposed FL-EMS, the EMSs used in [1], [2], [3], and the AOB's EMS, respectively.

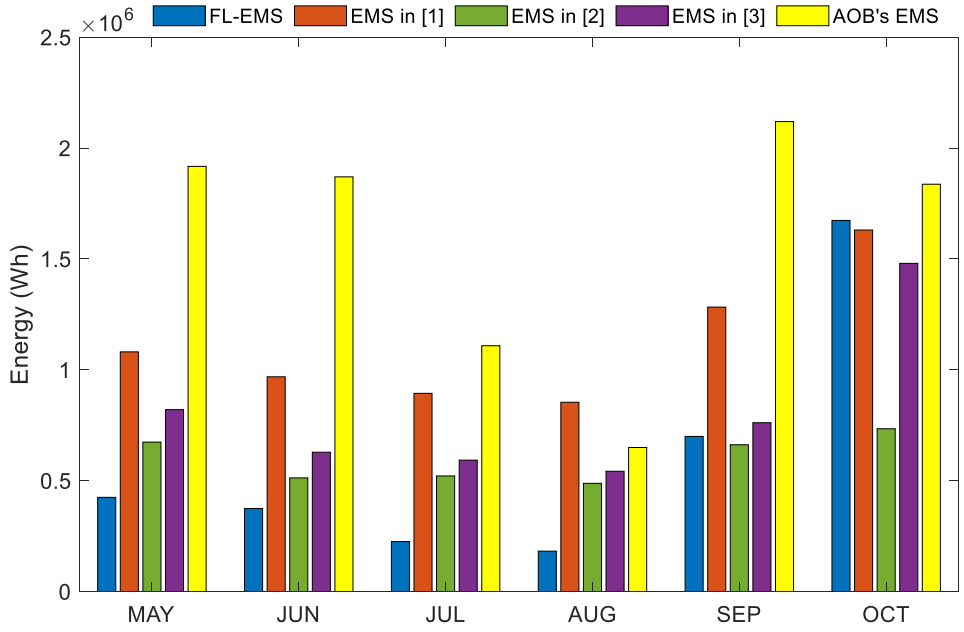

Fig. 3.14. Energy imported during off-peak time from May to October 2019. The blue, orange, green, purple, and yellow bars denote the results obtained for the proposed FL-EMS, the EMSs used in [1], [2], [3], and the AOB's EMS, respectively.

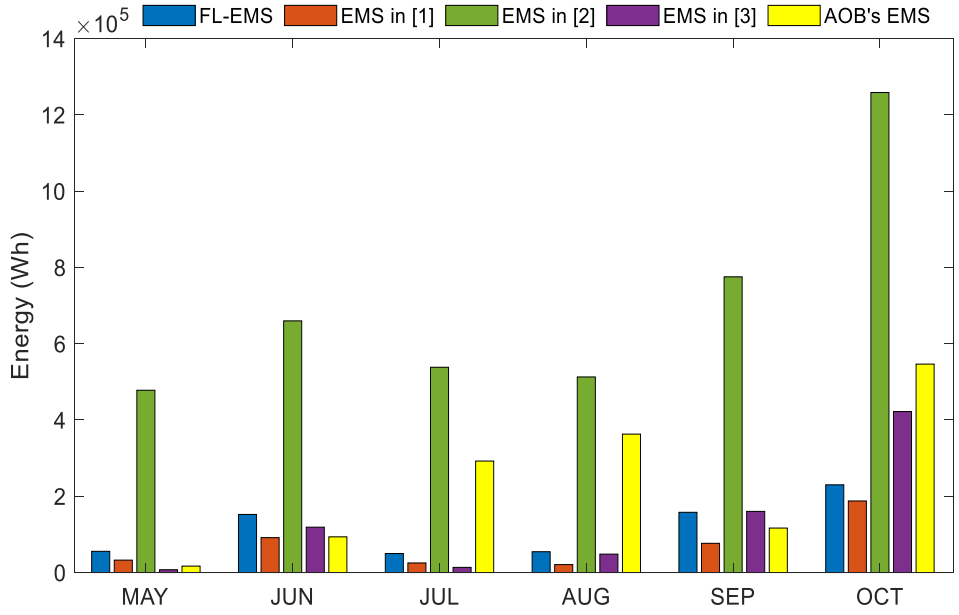

Fig. 3.15. Energy imported during peak time from May to October 2019. The blue, orange, green, purple, and yellow bars denote the results obtained for the proposed FL-EMS, the EMSs used in [1], [2], [3], and the AOB's EMS, respectively.

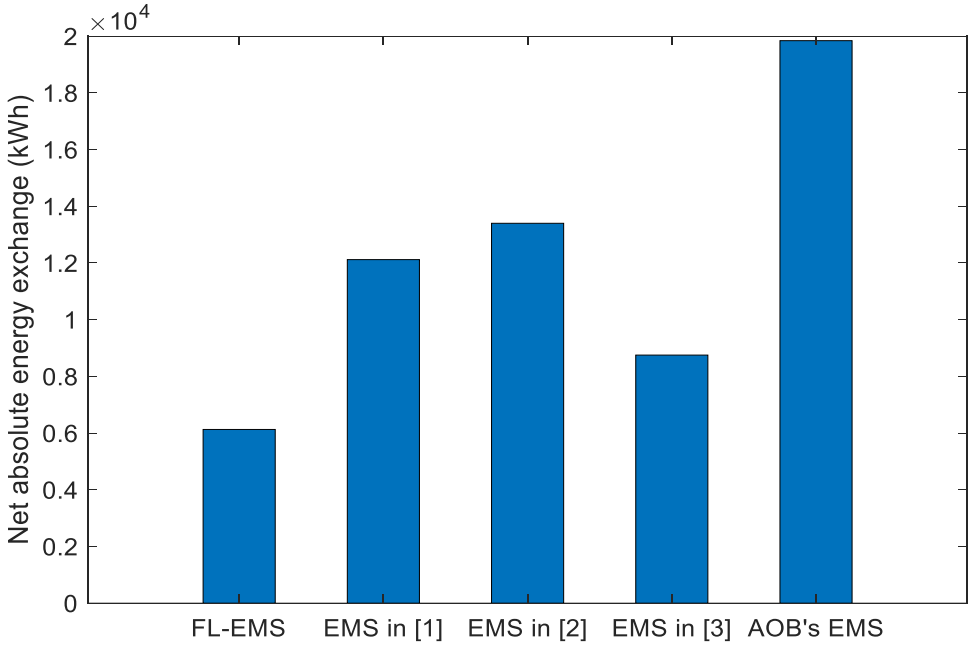

Fig. 3.16. Absolute net energy exchange with the grid for the six months from May to October 2019 for the proposed FL-EMS, the EMSs proposed in [1], [2], [3], and the AOB's EMS, respectively.

Fig. 3.16 shows the absolute net energy exchange with the grid for the six months from May to October 2019 for the proposed FL-EMS, the proposed EMSs in [1], [2], [3], and the AOB's EMS, respectively. The proposed FL-EMS promoted PV self-consumption and reduced the burden on the grid by minimising the total energy exchange with the grid as shown in Fig. 3.16.

Table 3.3 presents the operating costs and net energy exchanged with the grid for the proposed FL-EMS, EMSs proposed in [1], [2], [3], and the AOB's EMS. The proposed FL-EMS in this work achieves savings in energy cost of 33%, 92%, 18%, and 95%, in six months period when compared to [1], [2], [3], and the AOB's EMS, respectively. The proposed FL-EMS uses BSS more frequently, resulting in higher BSS degradation costs compared to [1], [2], and [3]. In addition, it reduced the total operating costs (energy cost + BSS degradation cost) and absolute net energy exchanged with the grid by up to 44% and 69%, respectively, compared to the previous works. Reducing the net energy exchanged with the grid decreases transmission losses and the need for extra energy storage capacity and central generation.

Table 3.3. Operating costs and energy exchanged with the grid for six months.

EMS	Energy cost (£)	Degradation cost (£)	Total operating costs (£)	Absolute net energy exchange (MWh)
FL-EMS	419	298	717	6.127
Ref [1]	556	199	755	12.11
Ref [2]	806	116	922	13.40
Ref [3]	495	185	680	8.751
AOB	816	463	1279	19.84

3.5.3 Battery State-of-Health

Table 3.4 compares the average SOC for the proposed FL-EMS with the EMSs proposed in [1], [2], [3], and AOB's EMS. The FL-EMS monitors the SOH and modifies the BSS utilisation to reduce energy exchanged with the grid. While the SOH remains healthy, the system makes good use of the BSS to reduce the energy exchange with the grid. However, as the SOH degrades, the system considers less BSS utilisation to maintain its heath. It can be seen from Table 3.4, that the average SOC of the new BSS (SOH=100%) for the proposed FL-EMS is 58%; however, it increased to 63% when the SOH dropped to 85%. While the EMSs proposed in [1], [2], [3], and AOB's EMS remain constant. This indicates that the system proposed in [1], [2], [3], and AOB's do not change the BSS performance when the BSS degrades.

Table 3.4. Average SOC for different initial SOH conditions.

Initial SOH	FL-EMS	Ref [1]	Ref [2]	Ref [3]	AOB's EMS
100%	58%	84%	85%	66%	72%
90%	61%	84%	85%	66%	72%
85%	63%	84%	85%	66%	72%

3.5.4 Performance of Algorithm as a Function of System Size

Fig. 3.17, demonstrates how the BSS capacity and size of the PV system affect energy exchange with the grid. The X, Y, and Z axes represent the ratio of PV generation/peak load, the ratio of BSS size/peak load and the net absolute energy exchanged with the grid over six months, respectively. As can be seen from Fig. 3.17, the minimum absolute net energy exchange occurs when the ratio of BSS size/peak load and the ratio of PV size/peak load are 7.3 kWh/kW and 0.6 kW_p/kW, respectively. Either decreasing or increasing the PV size/peak load ratio results in increasing the absolute net energy exchange for a given BSS size/peak load. In addition, it can be observed from Fig. 3.17, that at any ratio of BSS capacity/peak load, the minimum absolute net energy exchanged occurs at a ratio of PV/peak load of 0.6 kW_p/kW. It has been observed that,

as BSS size increases the absolute net energy exchanged with the grid decreases. This is logical as more capacity is accessible for storing energy. If the ratio of BSS size/peak load is increased from 1.0 to 7.3 kWh/kW, the reductions in energy exchanges are 6.4%, 49%, and 39%, corresponding to PV size/peak-load ratios of 0.2, 0.6, and 1.0 kW_p/kW, respectively. This confirms that there is an optimum PV size/peak load (in this case 0.6 kW_p/kW) that uses the BSS most advantageously and produces the greatest reduction in energy exchange with the grid.

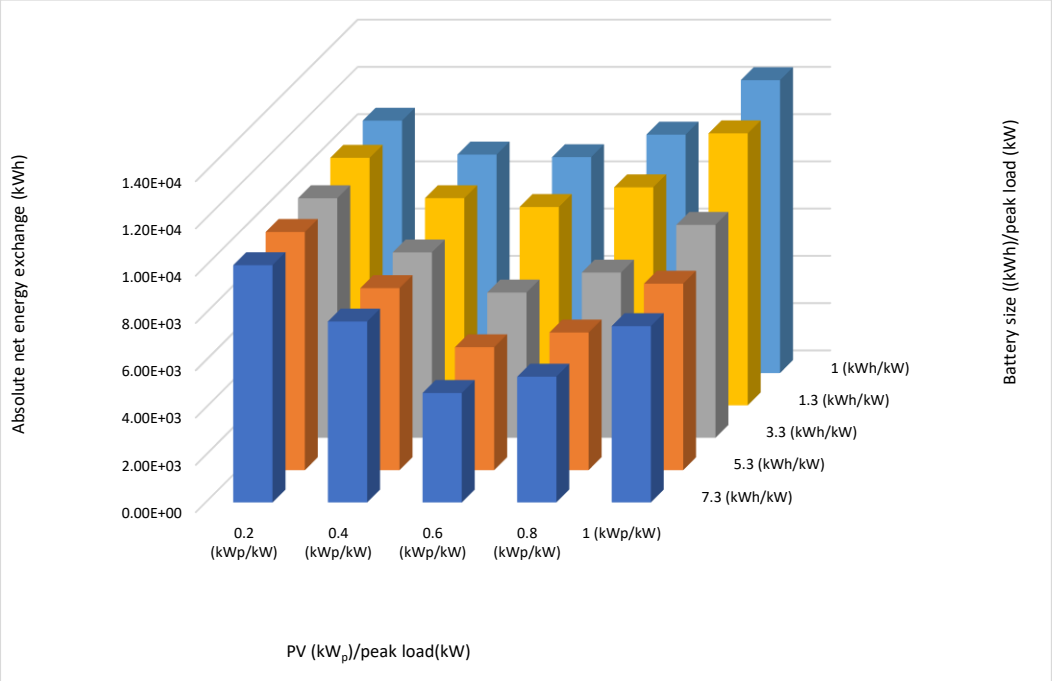

Fig. 3.17. Relationship between the absolute net energy exchanged with different BSS size/rated-load and PV generation/peak-load ratios. The X, Y, and Z axes represent the ratios of PV generation/peak-load, BSS size/peak-load and the absolute net energy exchanged with the grid over six months, respectively.

3.6 Conclusion

This chapter presents a real-time FL-EMS designed to enhance PV self-consumption and reduce net energy exchanged with the grid. The proposed FL-EMS was compared with various EMS approaches. Results demonstrate its effectiveness in reducing both the total energy cost and the net energy exchanged with the grid over a period of six months when

compared with previous EMSs approaches. The proposed FL-EMS optimised BSS performance by avoiding unnecessary charge/discharge cycles and efficiently regulating the difference between the generated PV power and demand. The effect of PV system size and BSS capacity on the net energy exchanged with the grid was also explored.

4 DAY-AHEAD RESIDENTIAL ENERGY MANAGEMENT SYSTEM

4.1 Introduction

Day-ahead planning is required for complex Energy Management Systems (EMSs) to achieve optimal operation of different components. Thus, this chapter proposed a Mixed Integer Linear Programming based Energy Management System (MILP-EMS) which will also be used for developing a Community Energy Management System (CEMS) in the next chapter. The proposed method has been tested using the Active Office Building (AOB) presented in Chapter 3- Section 3.2, as a case study. In addition, it is compared with a recently published state-of-the-art algorithm and with the current EMS utilised in the AOB, to demonstrate the effectiveness of the proposed strategy. The analysis in this chapter has been performed by coding the previous state-of-the-art algorithm and the MILP-EMS in MATLAB software.

Note that the results presented in this chapter have been published in IEEE Access journal:

A. Sorour, M. Fazeli, M. Monfared, A. A. Fahmy, J. R. Searle and R. P. Lewis, “MILP Optimized Management of Domestic PV-Battery Using Two Days-Ahead Forecasts,” *IEEE Access*, vol. 10, pp. 29357-29366, 2022, doi: 10.1109/ACCESS.2022.3158303.

This chapter is structured as follows. Section 4.2 introduces the MILP-EMS. Then, Section 4.3 presents the problem formulation. Section 4.4 discusses the results and compares the proposed MILP-EMS with another cost function that directly promotes reducing the absolute net energy exchange. Finally, Section 4.5 presents the conclusion of Chapter 4.

4.2 MILP-based EMS

The main target of the proposed MILP-EMS is to reduce the net energy exchange with the grid by scheduling the day-ahead Battery Storage System (BSS) setting.

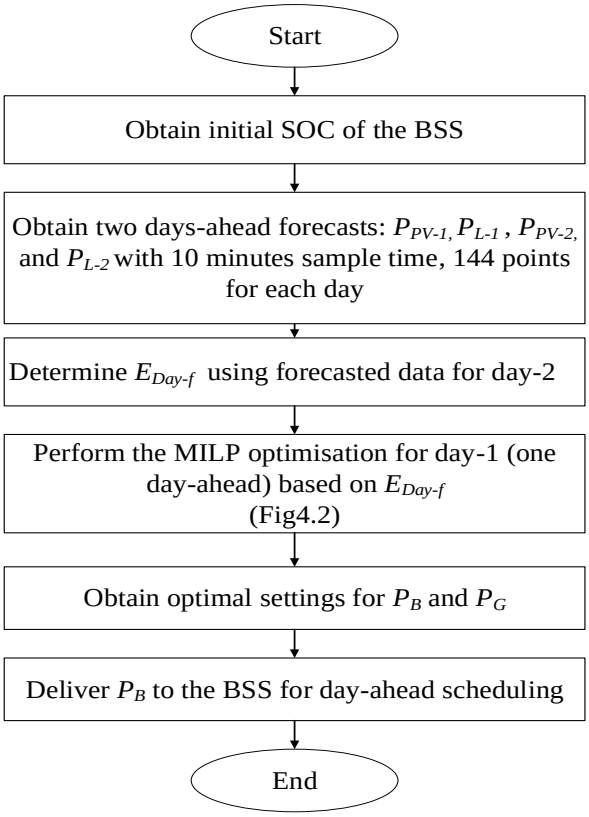

Fig. 4.1. Flowchart of the proposed MILP-EMS.

The proposed MILP-EMS follows the process presented in Fig. 4.1 and the following steps:

1. Input the initial SOC of the BSS.
2. Input the forecasted data for the next two days (day-1 and day-2) assuming that it is provided by a forecasting company, using a 10 minutes sample time, 144 points for each day: day-1 Photovoltaic (PV) generation (P_{PV-1}), day-1 load demand (P_{L-1}), day-2 PV generation (P_{PV-2}), and day-2 load demand (P_{L-2}).
3. Determine the predicted peak-time energy requirement (E_{Day-f}) based on day-2 forecasted data using (4.1):

$$E_{Day\text{-}f} = \int_{t=8\ \mathrm{AM}}^{t=8\ \mathrm{PM}} (P_{PV\text{-}2}(\tau) - P_{L\text{-}2}(\tau))\, d\tau \tag{4.1}$$

4. The MILP optimisation is then carried out for one day-ahead (i.e., day-1) to obtain the optimal BSS scheduling and grid reference.
5. Finally, obtain the decision variables and send the signal to the BSS.

4.3 Problem Formulation

The cost function C_F in (4.2) aims to minimise the absolute net energy exchange with the grid while reducing operating costs. The C_F comprises the costs of the energy purchased from the grid C_{buy}, energy sold to the grid C_{sell} and the degradation cost of the BSS (C_{BSS}).

$$\text{Minimise } C_F = |C_{buy}| + |C_{sell}| + C_{BSS} \tag{4.2}$$

$$C_{buy} = \sum_{t_0}^{T} \Delta T \times f_{buy}(t) \times P_G(t) \quad , P_G(t) > 0 \tag{4.3}$$

$$C_{sell} = \sum_{t_0}^{T} \Delta T \times f_{sell}(t) \times P_G(t) \quad , P_G(t) < 0 \tag{4.4}$$

$$C_{BSS} = \sum_{t_0}^{T} \frac{\mathrm{CC_B} \times \eta_{Conv} \times \eta_c \times \Delta T \times |P_{B\text{-}charg}(t)|}{2 \times N_{Bcycle} \times B_{capacity}(t)} + \frac{\mathrm{CC_B} \times \Delta T \times |P_{B\text{-}disch}(t)|}{\eta_{Conv} \times \eta_d \times 2 \times N_{Bcycle} \times B_{capacity}(t)} \tag{4.5}$$

where T is the duration of the day (24 hours), t_0 is the time of day starting at 12 AM, ΔT (hr) is the sampling time of 10 mins, $f_{buy}(t)$ is the purchasing tariff from the grid (£/kWh), $f_{sell}(t)$ is the selling tariff to the grid (£/kWh), $P_G(t)$ is the grid import/export power (kW), $\mathrm{CC_B}$ represents the cost of a new BSS (£) (without considering the power converters), N_{Bcycle} is the number of BSS life cycles, η_{conv} is the converter efficiency of

the BSS (%), $P_{B\text{-}disch}(t)$ is the BSS discharge power (kW), $P_{B\text{-}charg}(t)$ is the BSS charge power (kW), η_d is the discharging efficiency of the BSS (%), and η_c is the charging efficiency of the BSS (%), $B_{capacity}(t)$ is the current estimated BSS capacity (kWh). The value of $P_G(t)$ is positive when the house imports from the grid and negative when it exports. The values of $P_{B\text{-}disch}(t)$ and $P_{B\text{-}charg}(t)$ are positive and negative, respectively. It worth mentioning that cost function C_F in (4.2) considers the C_{sell} and C_{buy} as absolute values to reduce the total energy transactions.

The system power balance equation is represented as (4.6):

$$P_{L\text{-}1}(t) - P_{PV\text{-}1}(t) = P_G(t) + P_B(t) \tag{4.6}$$

where $P_B(t)$ is the BSS charge/discharge power (kW).

The energy bill C_{bill} is calculated by subtracting C_{sell} and C_{buy} (note that C_{buy} has a positive value and C_{sell} has a negative value):

$$C_{bill} = C_{buy} + C_{sell} \tag{4.7}$$

4.3.1 Battery Storage System Model

The BSS model is presented in this subsection as follows: Equations (4.8), (4.9), and (4.10) are used to estimate the stored energy, SOC and current capacity of the BSS, respectively [4].

$$E_B(t) = E_B(t-1) - \frac{\Delta T \times P_{B\text{-}disch}(t)}{\eta_d} - \Delta T \times \eta_c \times P_{B\text{-}charg}(t) \tag{4.8}$$

$$SOC_B(t) = \frac{E_B(t)}{B_{capacity}(t)} \times 100 \tag{4.9}$$

$$B_{capacity}(t) = \frac{1}{SOC_B(t_\alpha) - SOC_B(t_\beta)} \int_{t_\alpha}^{t_\beta} I_B(\tau)\, d\tau \tag{4.10}$$

where $E_B(t)$ is BSS stored energy at time t (kWh), $E_B(t\text{-}1)$ is BSS energy at time t-1 (kWh), and $I_B(t)$ is the BSS charge/discharge current (A). $SOC_B(t_\alpha)$ and $SOC_B(t_\beta)$ are the SOC of the BSS at times t_α and t_β (%), respectively. The new estimated BSS capacity is fed back into (4.9) to estimate the SOC.

The instantaneous BSS power is given by (4.11) and the BSS maximum and minimum allowable charge/discharge power by (4.12) [4]:

$$P_B(t) = P_{B\text{-}disch}(t) \times \eta_{conv} + \frac{P_{B\text{-}charg}(t)}{\eta_{conv}} \tag{4.11}$$

$$-P_{B\text{-}rating} \leq P_B(t) \leq P_{B\text{-}rating} \tag{4.12}$$

It is worth mentioning that the SOC limit of the BSS depends on when it occurs, at a peak or an off-peak time. During peak time (high tariff), the BSS can be discharged to its minimum limit (i.e., $SOC_{B\text{-}min}$) to supply the load. The allowable limits for the SOC during peak time are represented by (4.13).

$$SOC_{B\text{-}min} \leq SOC_B(t) \leq SOC_{B\text{-}max} \tag{4.13}$$

During the off-peak time, the day-2 forecasted energy requirement for the peak period (i.e., $E_{Day\text{-}f}$) is considered to ensure that any energy needed is stored in the BSS during the off-peak period. The allowable limits for the SOC during off-peak time are given in (4.14).

$$SOC_{B\text{-}min} + \left(100 \times \frac{E_{Day\text{-}f}}{B_{capacity}(t)}\right) \leq SOC_B(t) \leq SOC_{B\text{-}max} \tag{4.14}$$

4.3.2 System Constraints

This subsection introduces four binary variables that act as flags for state transitions of the BSS and the grid. These are Φ_{import}, Φ_{export}, $\Phi_{B\text{-}disch}$, and $\Phi_{B\text{-}charg}$. Where $\Phi_{B\text{-}disch}$ and

$\Phi_{B\text{-}charg}$ are used to guarantee that the BSS is either discharging or charging at any instant by using constraints (4.15)-(4.17) [4].

$$\Phi_{B\text{-}disch}(t) + \Phi_{B\text{-}charg}(t) \leq 1 \tag{4.15}$$

$$\Phi_{B\text{-}disch}(t) = \begin{cases} 1 & , P_B(t) > 0 \\ 0 & , P_B(t) < 0 \end{cases} \tag{4.16}$$

$$\Phi_{B\text{-}charg}(t) = \begin{cases} 1 & , P_B(t) < 0 \\ 0 & , P_B(t) > 0 \end{cases} \tag{4.17}$$

where $\Phi_{B\text{-}disch}(t)$ is equal to 1 when the BSS is discharging, otherwise is equal to 0, $\Phi_{B\text{-}charg}(t)$ is equal to 1 when the BSS is charging, otherwise is equal to 0.

Constraints (4.18) and (4.19) are introduced to link the BSS power limits and the binary variables [4].

$$P_{B\text{-}dish}(t) \leq \Phi_{B\text{-}disch}(t) \times P_{B\text{-}rating} \tag{4.18}$$

$$\left|P_{B\text{-}charg}(t)\right| \leq \Phi_{B\text{-}charg}(t) \times P_{B\text{-}rating} \tag{4.19}$$

where $\Phi_{import}(t)$ and $\Phi_{export}(t)$ are used to guarantee that the building being considered is either importing from, or exporting to, the grid at any time instant using the constraints (4.20) to (4.22) [4].

$$\Phi_{import}(t) + \Phi_{export}(t) \leq 1 \tag{4.20}$$

$$\Phi_{import}(t) = \begin{cases} 1 & , P_G(t) > 0 \\ 0 & , P_G(t) < 0 \end{cases} \tag{4.21}$$

$$\Phi_{export}(t)=\begin{cases}1 & ,P_G(t)<0\\ 0 & ,P_G(t)>0\end{cases} \tag{4.22}$$

where $\Phi_{import}(t)$ is equal to 1 when the building is importing power from the grid, otherwise is equal to 0, $\Phi_{export}(t)$ is equal to 1 when the building is exporting power to the grid, otherwise is equal to 0.

Constraints (4.23) and (4.24) are introduced to link the grid power limits and the binary variables [4].

$$\left|P_{G\text{-}export}(t)\right| \leq \Phi_{export}(t) \times P_{Gmax\text{-}export} \tag{4.23}$$

$$P_{G\text{-}import}(t) \leq \Phi_{import}(t) \times P_{Gmax\text{-}import} \tag{4.24}$$

where $P_{G\text{-}import}(t)$ is the imported power from the grid, $P_{G\text{-}export}(t)$ is the exported power to the grid, while $P_{Gmax\text{-}import}$ and $P_{Gmax\text{-}export}$ are the maximum limits for the power exchanged with the grid, these values are set to infinity unless otherwise specified.

Grid power is represented by (4.25).

$$P_G(t)=P_{G\text{-}import}(t)+P_{G\text{-}export}(t) \tag{4.25}$$

To guarantee that the building is not exporting power from its BSS when exporting excess PV power to the grid, constraint (4.26) is used [4]:

$$\Phi_{B\text{-}disch}(t)+\Phi_{export}(t) \leq 1 \tag{4.26}$$

4.3.3 Mixed Integer Linear Programming

In this work, the MILP optimisation technique and the Gurobi® optimiser tool are used to solve the problem formulation in the MATLAB environment. MILP is a mathematical approach to determining the optimum solution for an objective function

based on constraints and variables [105, 106]. As described in Chapter 2- Subsection 2.4.2, there are three different approaches to solve the MILP problem, namely, Cutting Plane, Feasibility Pump, and Branch and Bound. This study solves the problem using the Branch and Bound algorithm (also known as the Tree search algorithm) [108].

This study achieves the optimal one day-ahead (day-1) BSS scheduling by optimising the cost function in (4.2) using the following steps [109]:

1. The process began with the initial MILP problem, with all constraints removed, the so-called relaxation of the original LP problem.
2. The results obtained are subjected to constraints, and those that are not feasible are rejected.
3. The retained variables generate another generation of variables, then one iteration after another takes place until a solution is found. An optimal solution satisfies the constraints and corresponds to the best objective function value.

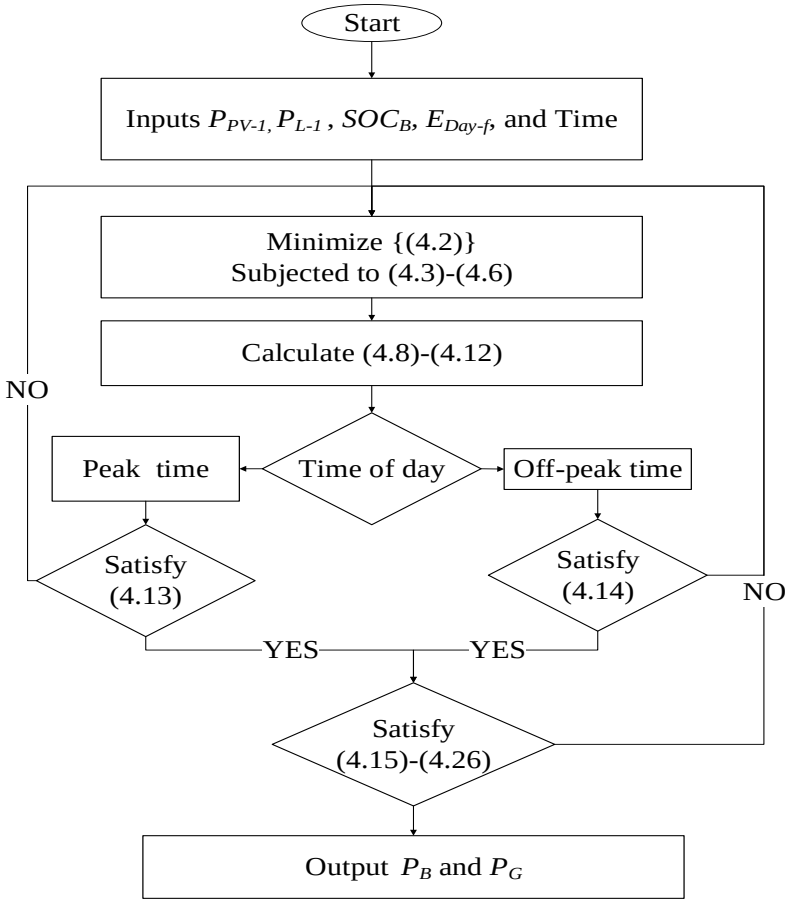

Fig. 4.2. Flowchart of the MILP optimisation process.

Fig. 4.2 shows a detailed flowchart of the optimisation process, demonstrating how the constraints are met:

- First input $P_{PV\text{-}1}$, $P_{L\text{-}1}$, $E_{Day\text{-}f}$, and SOC_B of the BSS to minimise the cost function (4.2), subject to constraints (4.3) and (4.6).
- Then calculate (4.8)-(4.12). Then, if it is a peak time, satisfy (4.13), otherwise satisfy (4.14).
- The constraints (4.15)-(4.26) must be satisfied.
- Finally, send the optimal day-ahead setting to the BSS.

4.4 Case Studies

This study uses the forecast data and tariff prices in Chapter 3- Section 3.3. The proposed algorithm has been tested using the AOB data described in Chapter 3- Section 3.2 This section compares the proposed MILP-EMS performance with the proposed EMS in [4] and the AOB's EMS to emphasise the proposed method's advantages, particularly reducing net energy exchanged with the grid and operating costs. The algorithm in Fig. 4.1 is carried out for each day of the six months from May to October 2019 with a sample time (ΔT) of 10 mins.

4.4.1 Performance Comparison

Figs. 4.3 and 4.4 present the results obtained for BSS performance for the EMS in [4] and the proposed MILP-EMS, respectively, for the two test days (23rd and 24th of May 2019). The red and black lines represent SOC_B and P_{PV} - P_L, respectively. As shown in Figs. 4.3 and 4.4, on the first day (day-1), the PV generation exceeds demand most of the time, but on the second day (day-2), demand exceeds PV generation most of the time.

Fig. 4.3 demonstrates that the algorithm proposed by [4] limits BSS charging and does not maximise the use of the excess PV power. Instead, the excess PV power is exported to the grid to reduce operating costs as the energy is not needed during day-1. This algorithm does not include energy forecasts for day-2 ($E_{Day\text{-}f}$) in its EMS. As a result, on day-2, during off-peak (after 12 AM), the BSS is charged from the grid to meet the peak load requirements. The main objective of the work proposed in [4] is to reduce energy costs

and BSS degradation costs. However, their method results in significant power exchange with the grid and increases energy costs because the system feeds PV power into the grid when it would be more cost-effective to charge the BSS to meet the load for the following day, day-2.

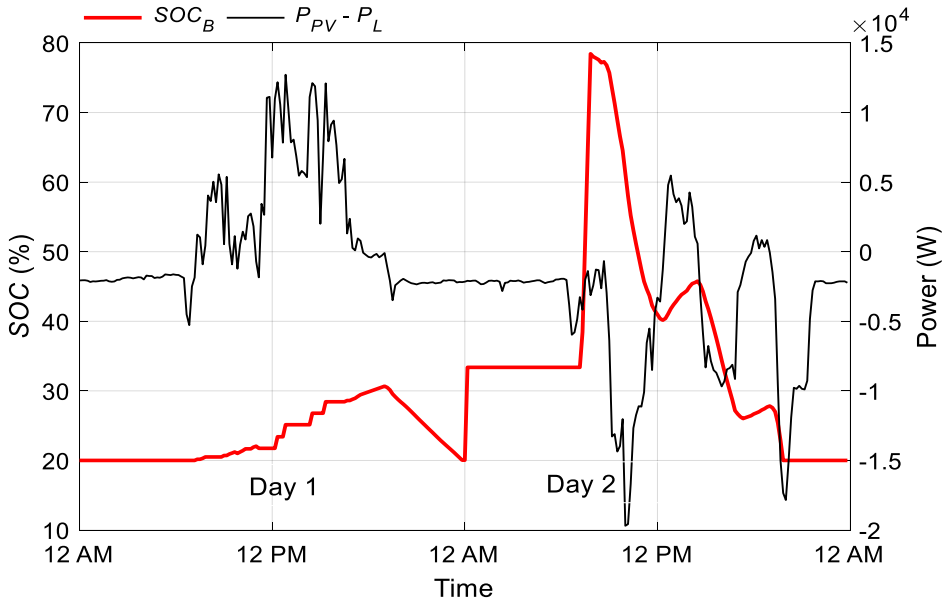

Fig. 4.3. Results for 23rd and 24th of May 2019, for the EMS in [4]. The red and black lines represent SOC_B and P_{PV} - P_L, respectively.

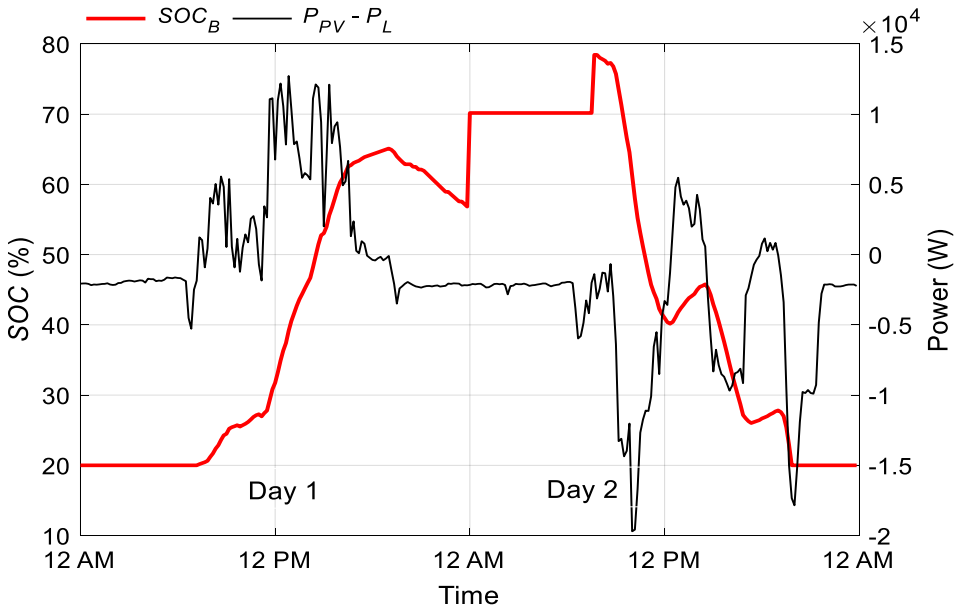

Fig. 4.4. Results for 23rd and 24th May 2019, for the proposed MILP-EMS. The red and black lines represent SOC_B and P_{PV} - P_L, respectively.

As shown in Fig. 4.4, unlike the EMS in [4], the PV excess power is used to charge the BSS rather than be exported to the grid to increase PV self-consumption because it has prior knowledge of day-2's energy forecast ($E_{Day\text{-}f}$). Moreover, the BSS will discharge the stored energy from PV when required to avoid purchasing energy from the grid during peak time. This process maximises the use of PV generated power by reducing absolute net energy exchange with the grid.

4.4.2 Comparison of Operational Costs and Net Energy Exchanged

Fig. 4.5 presents exported energy during peak time, for the six months from May to October 2019. The blue, orange, and yellow bars represent the results obtained for the proposed MILP-EMS, the EMS in [4], and the AOB's EMS, respectively. It is seen from Fig. 4.5 that the proposed MILP-EMS increased utilisation of the PV generated power by reducing the energy exported to the grid during peak time.

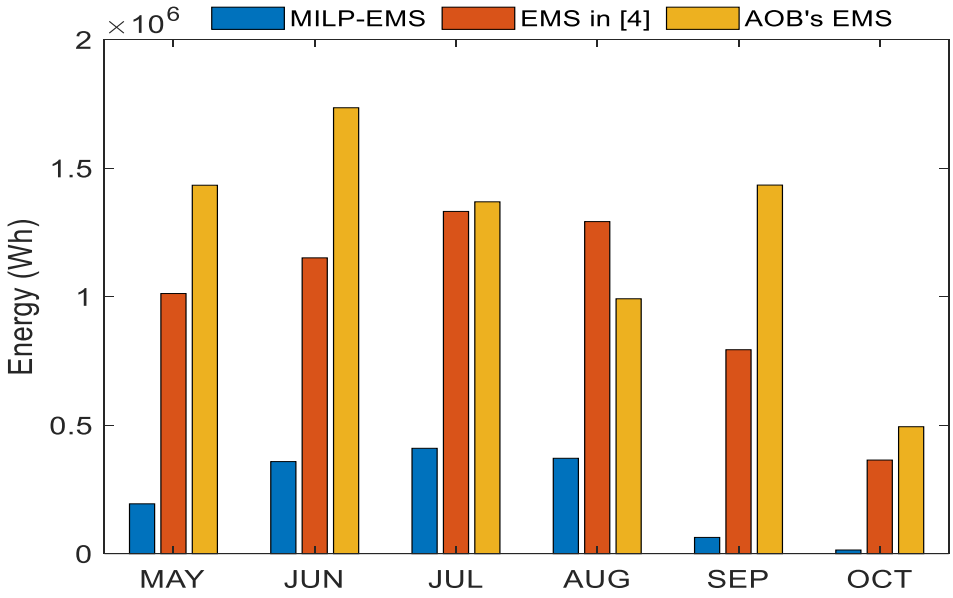

Fig. 4.5. Monthly energy exported during peak time from May to October 2019. The blue, orange, and yellow bars represent the proposed MILP-EMS, the EMS in [4], and the AOB's EMS, respectively.

Figs. 4.6 and 4.7 present the energy imported from the grid during peak and off-peak times, respectively, for the six months from May to October 2019. The blue, orange and yellow bars represent the proposed MILP-EMS, the EMS in [4], and the AOB's EMS,

respectively. As shown in Figs. 4.6 and 4.7, the proposed MILP-EMS imported the least energy of the three systems being considered.

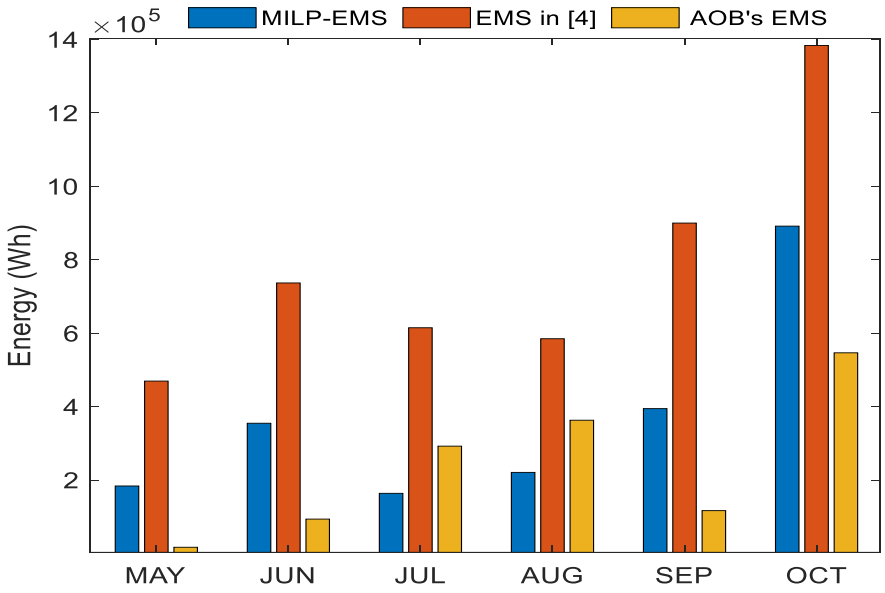

Fig. 4.6. Monthly energy imported during peak time from May to October 2019. The blue, orange, and yellow bars represent the proposed MILP-EMS, the EMS in [4], and the AOB's EMS, respectively.

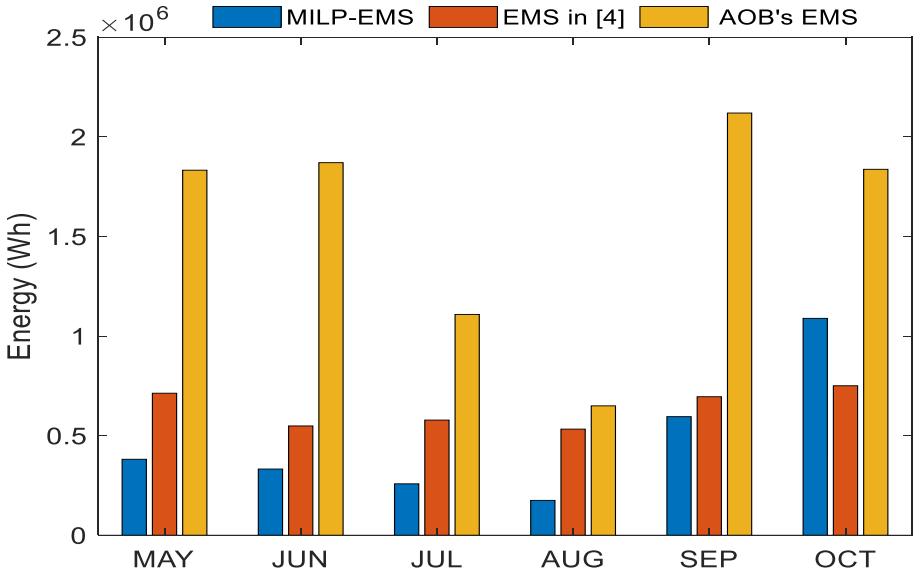

Fig. 4.7. Monthly energy imported during off-peak time from May to October 2019. The blue, orange, and yellow bars represent the proposed MILP-EMS, the EMS in [4], and the AOB's EMS, respectively.

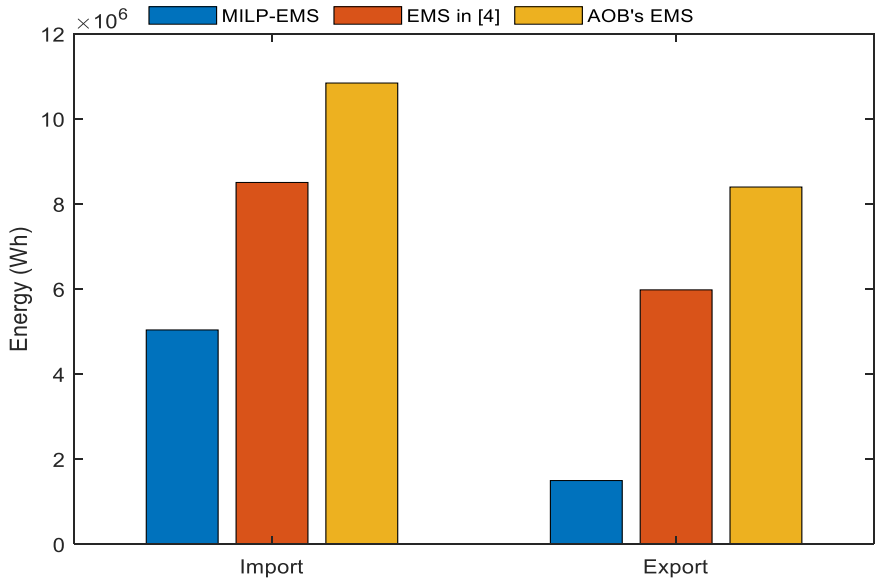

Fig. 4.8. Total imported and exported energy for the six months (May to October 2019). The blue, orange, and yellow bars represent the proposed MILP-EMS, the EMS in [4], and the AOB's EMS, respectively.

Fig. 4.8 shows the total energy imported/exported from/to the grid for the six months from May to October 2019. The blue, orange, and yellow bars represent the proposed MILP-EMS, the EMS in [4], and the AOB's EMS, respectively. Fig. 4.8 shows that the proposed MILP-EMS imported and exported the least energy.

Table 4.1. Operating costs and absolute net energy exchanged with the grid for the six months.

EMS	Energy cost (£)	BSS degradation cost (£)	Total operating costs (£)	Absolute net energy exchange (MWh)
MILP-EMS	598	234	832	6.536
Ref [4]	874	24	898	14.47
AOB	816	463	1279	19.84

Table 4.1 compares the absolute net energy exchange with the grid and the operating costs (energy cost + BSS degradation cost) for the proposed MILP-EMS with the EMS in [4] and the AOB's EMS for the six months from May to October 2019. It can be seen from Table 4.1 that compared to the MILP-EMS, the EMS proposed in [4] increased the absolute net energy exchanged with the grid by 121%. In addition**,** Table 4.1 shows that the proposed MILP-EMS reduced the absolute net energy exchange by using the BSS to a greater extent, reducing energy cost by £276 (a 32% reduction) compared to the EMS in [4], but at the expense of an increase in BSS degradation costs of £210. However, the BSS degradation cost is more than compensated for by the savings on the energy bill, giving a total operating cost reduction of £66 (a 7% reduction). Table 4.1 also shows that compared to the AOB's EMS, the proposed MILP-EMS reduced energy costs by £218 (a 27% reduction) and degradation costs by £229 (a 49% reduction). In addition, the proposed MILP-EMS reduced the total operating cost and absolute net energy exchange by 35% and 67% , respectively, compared to AOB's EMS.

4.4.3 Comparing Different Cost Functions

The main objective when considering cost function (4.2) is to minimise absolute net energy exchanged with the grid and to minimise energy costs, considering tariff prices. From a network operator's viewpoint, minimising net energy exchange might be more favourable since it reduces the transmission losses and the requirement for more central generation/storage systems. Minimised energy exchange with the grid can be used as an indication of the energy independence of a prosumer which, in future networks, with very high integration of distributed generators, might be a definitive factor. With this motivation in mind, this subsection investigates the impact of using the objective function (4.27) on the performance of the proposed MILP-EMS.

$$C_F = |E_{export}| + |E_{import}| \tag{4.27}$$

where the E_{export} and E_{import} are energy exported to and imported from the grid, respectively. Minimising the sum of the absolute values of the exported and imported energies results directly in minimising net energy exchange, maximising self-

consumption of the available Renewable Energy Source (RES). Table 4.2 compares the results for cost functions (4.2) and (4.27).

Table 4.2. Operating costs and absolute net energy exchanged with the grid for six months: May - October 2019.

Cost function	Energy cost (£)	Degradation cost (£)	Total operating costs (£)	Absolute net energy exchanged (MWh)
(4.2)	598	234	832	6.536
(4.27)	642	233	875	6.544

Table 4.2 shows that the cost function (4.27) increases the energy cost by 7% compared to cost function (4.2). However, there is no significant difference in the absolute net energy exchanged between cost functions (4.2) and (4.27). This shows that cost function (4.2) can be considered optimal and best for fulfilling the goals of minimising net energy exchanged with the grid and energy cost.

4.5 Conclusion

The proposed day-ahead MILP-EMS is compared with recent state-of-the-art and the EMS of the AOB to show the effectiveness of the proposed method. The proposed method reduced the total operating cost by up to 35% over six months compared to the other methods. In addition, it reduced net energy exchanged with the grid. The proposed cost function in MILP-EMS shows that it can outperform the performance of alternative cost function that directly reduce the net energy exchange.

5 COMMUNITY ENERGY MANAGEMENT SYSTEM

5.1 Introduction

Several projects reported in the literature have focused on residential house/building Energy Management Systems (EMSs) as standalone systems, but developing smarter electrical networks promises more efficient energy communities [151]. Therefore, a Community Energy Management System (CEMS) that exploits the forecasted two days-ahead demand and Photovoltaic (PV) generation to optimise Battery Storage Systems (BSSs) performance is proposed in this chapter. It should be noted that a "peer" in this chapter refers to a domestic end-user (house) rather than a commercial/industrial end-user. The analysis in this chapter has been performed by coding the previous state-of-the-art algorithm and the CEMS in MATLAB software.

Note that the results presented in this chapter have been published in IEEE Access journal:

A. Al-Sorour, M. Fazeli, M. Monfared, A. Fahmy, J. R. Searle and R. P. Lewis, "Enhancing PV Self-Consumption Within an Energy Community Using MILP-Based P2P Trading," *IEEE Access*, vol. 10, pp. 93760-93772, 2022, doi: 10.1109/ACCESS.2022.3202649.

This chapter is organised as follows. First, Section 5.2 describes the community configuration. Then, Section 5.3 presents the forecast data and tariff prices. The proposed CEMS is presented in Section 5.4. Section 5.5 describes the Central Controller that includes the P2P EMS and Selection level. Section 5.6 compares the results with a recently published state-of-the-art algorithm. Finally, Section 5.7 presents the conclusion of Chapter 5.

5.2 Community Configuration

This study uses measured data obtained from six residential houses located in London, UK [171]. Fig. 5.1 shows that each household comprises a PV system and BSS of 4

kWh connected to the grid. The PV rating, house location and the total load energy for the four months June to September 2014 are shown in Table 5.1. The capital cost of the 4 kWh BSS is assumed to be £3,000 [56]. However, the price of the BSSs is expected to reduce by up to 50% by 2025 [54]. In addition, the rated charge/discharge power ($P_{B\text{-}rating}$), charge/discharge efficiency (η_c^n/η_d^n), and life cycle (N_{Bcycle}^n) of the BSS are 2.7 kW, 95%, and 5,000, respectively [56, 172]. The maximum SOC ($SOC_{B\text{-}max}$) and minimum SOC ($SOC_{B\text{-}min}$) BSS limits are 98% and 20%, respectively [28].

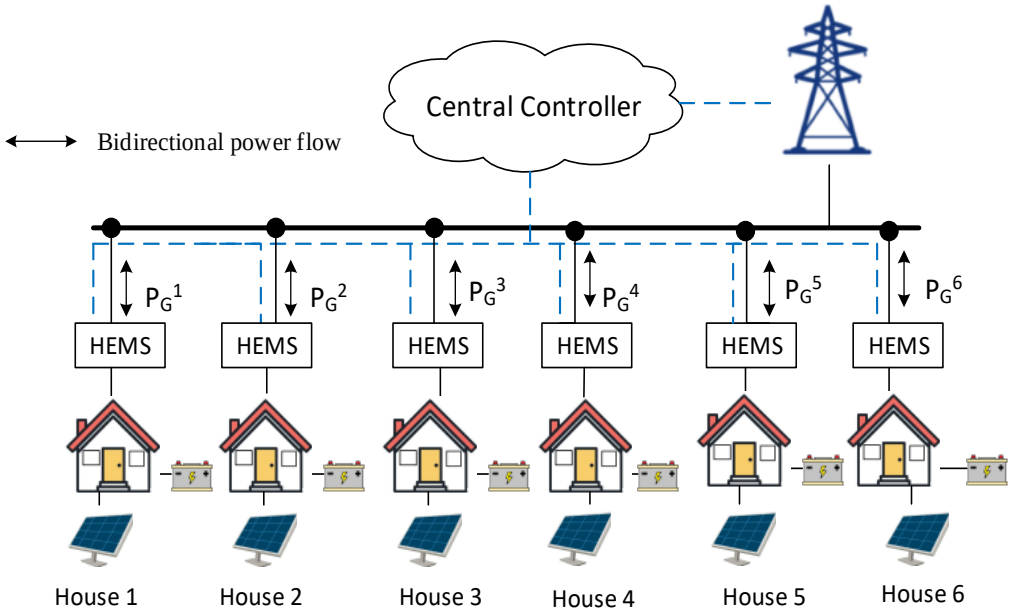

Fig. 5.1. Schematic of the six houses forming the prosumer community.

Table 5.1. Six houses parameters [171]

House number	House location	PV rating (kW_p)	Four month load (kWh)
1	Maple Drive East	0.45	430
2	Suffolk Road	0.50	1072
3	Bancroft Close	3.50	870
4	Alverston Close	3.0	1212
5	YMCA	4.0	1252
6	Forest Road	3.0	732

5.3 Forecast Data and Tariff Prices

A time of use tariff is used in this study, as shown in Table 5.2, whereby a peak rate of 24.99 p/kWh is applied from 4 PM to 7 PM, a mid-peak tariff of 11.99 p/kWh from 6 AM to 4 PM and 7 PM to 11 PM, and an off-peak tariff of 4.99 p/kWh from 11 PM to 6 AM. The tariff for energy exported from the houses to the grid is 3.79 p/kWh [8]. The import/export tariff for energy exchange between pairs of houses is chosen to be 4 p/kWh. The maximum export power from the house to the grid is limited to 3.68 kW [173].

Table 5.2. Tariff rates [5]

Tariff	Time of Day	Price per kWh
Off-peak	11 PM - 6 AM	4.99 p
Mid-peak	6 AM – 4 PM 7 PM – 11 PM	11.99 p
Peak	4 PM – 7 PM	24.99 p

The forecasting methodology is outside the scope of this thesis. Instead, as explained in Chapter 3- Section 3.3, an error with a normal distribution is added to the recorded historical data of PV power (P_{PV}) and load power (P_L) to represent forecasted data. It is assumed that the MAPE for the forecasted energy is 30% over four months.

5.4 Proposed Community Energy Management System

The main objective of the proposed CEMS is to minimise the net absolute energy exchange between the grid and the community, to enhance self-consumption while reducing the community operating costs. As shown in Fig. 5.2, the proposed CEMS consists of three layers:

1. Data collection: The inputs to the House Energy Management System (HEMS) and P2P EMS are (1) initial SOC of the house BSS (SOC_B^n), and (2) two days-ahead forecasts for each house, assuming that it is provided by a forecasting company: day-1 PV generation ($P_{PV\text{-}1}^n$), day-1 load demand ($P_{L\text{-}1}^n$), day-2 PV

generation ($P_{PV\text{-}2}{}^{n}$), and day-2 load demand ($P_{L\text{-}2}{}^{n}$). Where *n* refers to the number of the house within the community.

2. House Energy Management System: Each house has a HEMS installed. This enables the prosumers to manage their energy consumption and production. The optimum house BSS setting is obtained by considering the peak and mid-peak energy forecasts for day-2 ($E_{Day\text{-}f}{}^{n}$) as in (5.1):

$$E_{Day\text{-}f}{}^{n} = \int_{t=6\ \text{AM}}^{t=11\ \text{PM}} (P_{PV\text{-}2}{}^{n}(\tau) - P_{L\text{-}2}{}^{n}(\tau))\, d\tau \tag{5.1}$$

The HEMS enables the energy exchange between each house and grid to be minimised but does not exchange excess energy with other members of the community. The HEMS results are uploaded to the Central Controller. HEMS in this study uses the MILP-EMS system described in Chapter 4.

3. Central Controller consists of two stages:

   a) P2P energy trading for every pair of houses is optimised sequentially via a Central Controller using the data accessible and data uploaded from the HEMS. In this layer, the houses are paired to minimise energy exchanged between the community and the grid while reducing operating costs. The optimum house BSS settings for houses *A* and *B* are obtained by considering the peak and mid-peak energy forecasts for day-2 ($E_{Day\text{-}f}{}^{n}$) using (5.1). The possible number of pairs of houses ($Pair_{no.}$) is:

$$Pair_{no.} = \frac{N_{houses}(N_{houses} - 1)}{2} \tag{5.2}$$

   where N_{houses} is the number of houses in the community, here N_{houses} is 6, resulting in 15 possible pairs. The decision variables are sent to the Selection level to select the best pairs.

   b) The Selection level is where the pairs are chosen based on the percent cost reduction of each house. After obtaining the optimal settings from the

selected pairs of houses, the optimal BSS setting is delivered to each house. A detailed formulation of the P2P EMS problem and Selection level are presented in Section 5.5.

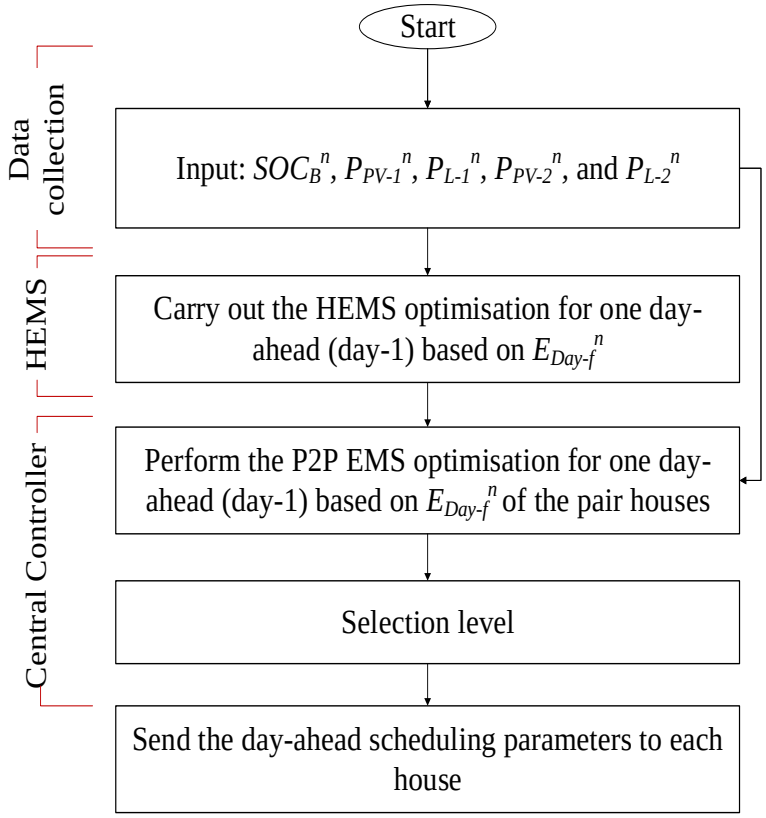

Fig. 5.2. Proposed CEMS.

5.5 Central Controller

The Central Controller is responsible for pairing the houses and choosing the best house pair via P2P EMS and Selection level, respectively. Each pair of houses exports the PV surplus to the grid after satisfying their demands and charging their BSSs sufficiently to meet the energy requirements based on the day-2 forecast (i.e., E_{Day-f}^n). The energy consumption is prioritised from high to low as follows:

1. Consumption of each house.
2. The SOC limit required for each house BSS at the end of the day based on E_{Day-f}^n.
3. Paired house consumption.

4. The SOC limit required for the pair of houses at the end of the day based on $E_{Day\text{-}f}^{n}$.
5. Export energy to the grid.

5.5.1 P2P EMS problem formulation

For the paired houses *A* and *B*, the cost function ($C_{sum\text{-}P2P}$) is formulated as (5.3):

$$\text{Minimise } C_{sum\text{-}P2P} = \sum_{n=A,B} |C_{buy}{}^{n}| + |C_{sell}{}^{n}| + C_{BSS}{}^{n} - |C_{P2P}{}^{n}| \tag{5.3}$$

$$C_{buy}{}^{n} = \sum_{t_0}^{T} \Delta T \times f_{buy}(t) \times P_G{}^{n}(t), \quad P_G{}^{n}(t) > 0 \tag{5.4}$$

$$C_{sell}{}^{n} = \sum_{t_0}^{T} \Delta T \times f_{sell}(t) \times P_G{}^{n}(\mathrm{t}), \quad P_G{}^{n}(t) < 0 \tag{5.5}$$

$$C_{P2P}{}^{n} = \begin{cases} \Delta T \times \sum_{t_0}^{T} f_{P2P\text{-}exp}(t) \times P_{P2P}{}^{A \leftrightarrow B}(t), P_{P2P}{}^{A \leftrightarrow B}(t) > 0 \\ \Delta T \times \sum_{t_0}^{T} f_{P2P\text{-}imp}(t) \times P_{P2P}{}^{A \leftrightarrow B}(t), P_{P2P}{}^{A \leftrightarrow B}(t) < 0 \end{cases} \tag{5.6}$$

$$C_{BSS}{}^{n} = \sum_{t_0}^{T} \frac{\mathrm{CC_B}{}^{n} \times \eta_{Conv}{}^{n} \times \eta_{c}{}^{n} \times \Delta T \times \left| P_{B\text{-}charg}{}^{n}(t) \right|}{2 \times N_{Bcycle}{}^{n} \times B_{capacity}{}^{n}(t)} + \frac{\mathrm{CC_B}{}^{n} \times \Delta T \times |P_{B\text{-}disch}{}^{n}(t)|}{\eta_{Conv}{}^{n} \times \eta_{d}{}^{n} \times 2 \times N_{Bcycle}{}^{n} \times B_{capacity}{}^{n}(t)} \tag{5.7}$$

where *n* refers to the house number of *A* and *B*, $C_{buy}{}^{n}$ is cost of energy purchased from the grid (£), $C_{sell}{}^{n}$ is the price of the energy sold to the grid (£), $C_{BSS}{}^{n}$ is the BSS degradation cost (£), $C_{P2P}{}^{n}$ is the cost of energy exchanged per day between paired

houses A and B (£), T is the duration of the day (24 hours), t_0 is the time of day starting at 12 AM, ΔT is the sampling time (hr), $f_{buy}(t)$ is the purchasing tariff from the grid (£/kWh), $f_{sell}(t)$ is the selling tariff to the grid (£/kWh), $P_G^n(t)$ is power exchanged between house and the grid (kW), $f_{P2P\text{-}exp}(t)$ is the tariff for energy exported from one house in the pair to the other (£/kWh), $f_{P2P\text{-}imp}(t)$ is the tariff for energy imported by one house in the pair from the other (£/kWh), $P_{P2P}^{A\leftrightarrow B}(t)$ is the power exchanged between the paired houses (kW), CC_B^n is the cost of a new BSS for a house (£) (without considering the power converters), N_{Bcycle}^n is the number of house BSS life cycles, η_{conv}^n is converter efficiency of the house BSS (%), $P_{B\text{-}disch}^n(t)$ is the house BSS discharge power (kW), $P_{B\text{-}charg}^n(t)$ is the BSS charge power (kW), η_d^n is the discharging efficiency of the house BSS (%), η_c^n is the charging efficiency of the house BSS (%), and $B_{capacity}^n(t)$ is the current estimated house BSS capacity (kWh). The value of $P_G^n(t)$ is positive when the house n imports from the grid and negative when it exports. The values of $P_{B\text{-}disch}^n(t)$ and $P_{B\text{-}charg}^n(t)$ are positive and negative, respectively. The value of $P_{P2P}^{A\leftrightarrow B}(t)$ is positive when the house is exporting energy and is negative when it is importing energy from its neighbour.

Note, in (5.3) the C_{buy}^n and C_{sell}^n are absolute values to reduce the total grid energy transactions. In addition, C_{P2P}^n is an absolute value subtracted from the overall cost function, so when minimising $C_{sum\text{-}P2P}$ the total energy exchanged between neighbours is maximised. Note also that $C_{sum\text{-}P2P}$ includes the term C_{BSS}^n to take into consideration the lifetimes of the BSSs.

The system power balance equation for houses A and B and when they are paired are:

For house A:

$$P_{L\text{-}1}^{A}(t)-P_{PV\text{-}1}^{A}(t) = P_G^A(t)+P_B^A(t)-P_{P2P}^{A\leftrightarrow B}(t) \tag{5.8}$$

For house B:

$$P_{L\text{-}1}^{B}(t)-P_{PV\text{-}1}^{B}(t)=P_G^B(t)+P_B^B(t)-P_{P2P}^{B\leftrightarrow A}(t) \tag{5.9}$$

For houses *A* and *B*:

$$\sum_{n=A,B} P_G{}^n(t)+P_B{}^n(t) = \sum_{n=A,B} P_{L\text{-}1}{}^n(t)-P_{PV\text{-}1}{}^n(t) \tag{5.10}$$

where $P_B{}^n(t)$ is the house BSS charge/discharge power (kW).

5.5.1.1 House BSS model

The house BSS model presented in Chapter 4- Subsection 4.3.1 is used for houses *A* and *B.*

5.5.1.2 System Constraints for P2P EMS

Each house is associated with six binary variables: $\Phi_{B\text{-}disch}{}^n$, $\Phi_{B\text{-}charg}{}^n$, $\Phi_{import}{}^n$, $\Phi_{export}{}^n$, $\delta_{import}{}^n$, and $\delta_{export}{}^n$. Where $\Phi_{B\text{-}charg}{}^n$ and $\Phi_{B\text{-}disch}{}^n$ are used for house BSS charge and discharge modes, respectively. $\Phi_{import}{}^n$ and $\Phi_{export}{}^n$ are used for energy import from and export to the grid, respectively. $\delta_{import}{}^n$ and $\delta_{export}{}^n$ are used for energy import from and export to the neighbour.

To ensure that the power flowing between houses *A* and *B* is always in only one direction, constraint (5.11) is used [5].

$$\delta_{import}{}^n(t)+\delta_{export}{}^n(t)\leq 1 \tag{5.11}$$

$$\delta_{export}(t)=\begin{cases} 1 & , \; P_{P2P}{}^{A\leftrightarrow B}(t)>0 \\ 0 & , \; P_{P2P}{}^{A\leftrightarrow B}(t)<0 \end{cases} \tag{5.12}$$

$$\delta_{import}(t)=\begin{cases} 1 & , \; P_{P2P}{}^{A\leftrightarrow B}(t)<0 \\ 0 & , \; P_{P2P}{}^{A\leftrightarrow B}(t)>0 \end{cases} \tag{5.13}$$

where $\sigma_{export}^{n}(t)$ is equal to 1 when house n is exporting power to its neighbour, otherwise is equal to 0. $\sigma_{import}^{n}(t)$ is equal to 1 when house n is importing power from its neighbour, otherwise is equal to 0.

Constraints (5.14) and (5.15) link binary variables and exchanged power between paired houses [5].

$$\left| P_{P2P}^{A \leftrightarrow B}(t) \right| \leq \sigma_{import}^{n}(t) \times P_{P2P\text{-}max}^{n}(t) \tag{5.14}$$

$$P_{P2P}^{A \leftrightarrow B}(t) \leq \sigma_{export}^{n}(t) \times P_{P2P\text{-}max}^{n}(t) \tag{5.15}$$

where $P_{P2P\text{-}max}^{n}(t)$ is the maximum permitted value of power exchanged between houses A and B, which is set to infinity unless otherwise specified.

To prevent the condition where one house in a pair exports power to the grid whilst simultaneously importing power from the other house, constraint (5.16) is applied [5].

$$\sigma_{import}^{n}(t) + \Phi_{export}^{n}(t) \leq 1 \tag{5.16}$$

To prevent one house in a pair importing power from the grid whilst simultaneously exporting power to the other house, constraint (5.17) is applied [5].

$$\sigma_{export}^{n}(t) + \Phi_{import}^{n}(t) \leq 1 \tag{5.17}$$

where $\Phi_{import}^{n}(t)$ is equal to 1 when house n is importing power from the grid, otherwise is equal to 0.

Constraint (5.18) prevents the house BSS from charging and discharging at the same time [5].

$$\Phi_{B\text{-}disch}^{n}(t) + \Phi_{B\text{-}charg}^{n}(t) \leq 1 \tag{5.18}$$

The house BSS discharges when $\Phi_{B\text{-}disch}^{n}(t)$ is equal to 1, and charges when $\Phi_{B\text{-}charg}^{n}(t)$ is equal to 1. When the $\Phi_{B\text{-}disch}^{n}(t)$ and $\Phi_{B\text{-}charg}^{n}(t)$ are equal to 0, the BSS is neither charging nor discharging and hence $P_{B}^{n}(t)$ is equal to 0.

Constraints (5.19) and (5.20) link binary variables and house BSS power [5].

$$P_{B\text{-}disch}^{\ n}(t) \leq \Phi_{B\text{-}disch}^{\ n}(t) \times P_{B\text{-}rating}^{\ n} \tag{5.19}$$

$$\left|P_{B\text{-}charg}^{\ n}(t)\right| \leq \Phi_{B\text{-}charg}^{\ n}(t) \times P_{B\text{-}rating}^{\ n} \tag{5.20}$$

Constraint (5.21) ensures that the house only imports or exports power at any one instant [5].

$$\Phi_{import}^{\ n}(t) + \Phi_{export}^{\ n}(t) \leq 1 \tag{5.21}$$

When a house imports power from the grid, $\Phi_{import}^{\ n}(t)$ is equal to 1, otherwise is equal to 0. Similarly, if a house exports power to the grid, $\Phi_{export}^{\ n}(t)$ is equal to 1, otherwise is equal to 0.

Constraints (5.22)-(5.24) link the binary variables with the grid power [5].

$$P_{G\text{-}import}^{\ n}(t) \leq \Phi_{import}^{\ n}(t) \times P_{G\text{-}max\text{-}import}^{\ n} \tag{5.22}$$

$$\left|P_{G\text{-}export}^{\ n}\right|(t) \leq \Phi_{export}^{\ n}(t) \times P_{G\text{-}max\text{-}export}^{\ n} \tag{5.23}$$

$$P_{G}^{\ n}(t) = P_{G\text{-}import}^{\ n}(t) + P_{G\text{-}export}^{\ n}(t) \tag{5.24}$$

where $P_{G\text{-}import}^{\ n}(t)$ and $P_{G\text{-}export}^{\ n}(t)$ are power transferred from and to the grid, respectively. $P_{G\text{-}max\text{-}import}^{\ n}$ and $P_{G\text{-}max\text{-}export}^{\ n}$ are the limits of power transferred from and to the grid, respectively.

To prevent the house BSS discharging when the PV system is transferring surplus power to the grid, constraint (5.25) is used [5].

$$\Phi_{B\text{-}disch}^{\ n}(t) + \Phi_{export}^{\ n}(t) \leq 1 \tag{5.25}$$

where $\Phi_{B\text{-}disch}^{n}(t)$ is equal to 1, when the BSS is discharging and otherwise equal to 0. $\Phi_{export}^{n}(t)$ is equal to 1 when the house transfers power to the grid and otherwise equal to 0.

Constraint (5.26) ensures that any solution obtained from P2P optimisation for houses *A* and *B* is more cost-effective than the houses operating individually (i.e., solution from HEMS) [5].

$$C_{house\text{-}cost}^{P2P(n)} \leq C_{house\text{-}cost}^{individual(n)} \tag{5.26}$$

$$C_{house\text{-}cost}^{individual(n)} = C_{buy}^{n} + C_{sell}^{n} + C_{BSS}^{n} \tag{5.27}$$

$$C_{house\text{-}cost}^{P2P(n)} = C_{buy}^{n} + C_{sell}^{n} + C_{BSS}^{n} - C_{P2P}^{n} \tag{5.28}$$

where $C_{house\text{-}cost}^{individual(n)}$ is the daily operational cost when a house operates individually, $C_{house\text{-}cost}^{P2P(n)}$ is the daily operational cost for house *n* when paired with another house.

Fig. 5.3 represents the process described above for P2P EMS and follows the steps:

- First input $P_{PV\text{-}1}^{n}$, $P_{L\text{-}1}^{n}$, SOC_B^{n} and $E_{Day\text{-}f}^{n}$ along with operating costs of the house being operating individually ($C_{house\text{-}cost}^{individual\ (n)}$) from HEMS; for the pair of houses *A* and *B*, in order to minimise the cost function (5.3), subject to constraints (5.4)-(5.10).
- Then calculate (4.8)-(4.12).
- During off-peak hours, the system determines whether the house BSS has enough energy for the next mid-peak and peak periods by satisfying constraint (4.14), else constraint (4.13) must be satisfied.
- Finally, system constraints (5.11)-(5.28) must be satisfied and the output parameters are uploaded into the Selection level.

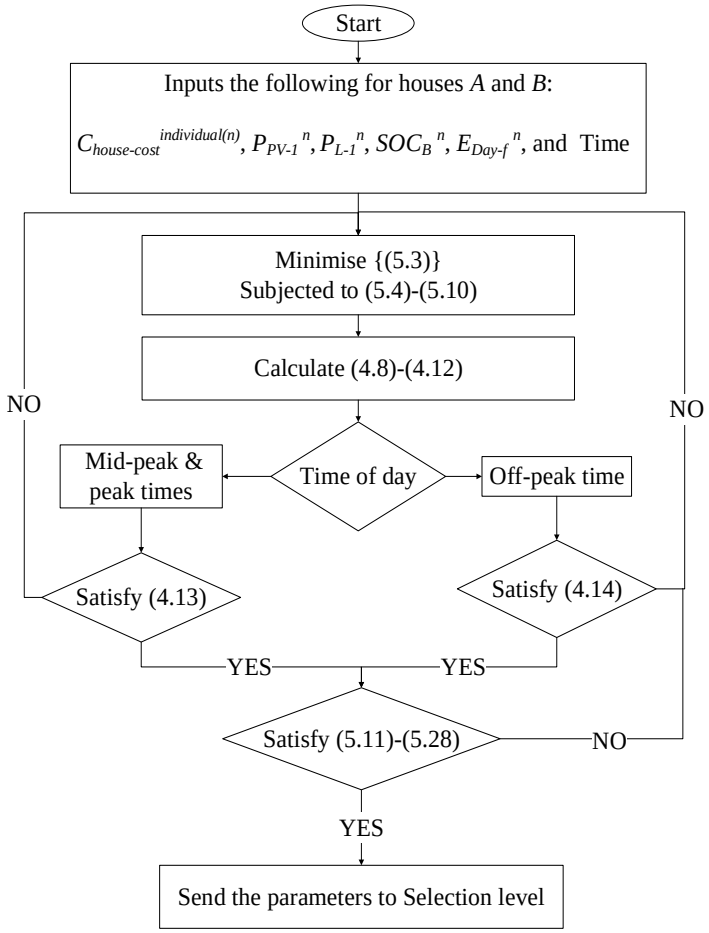

Fig. 5.3. Flowchart for P2P EMS.

5.5.2 Selection Level

Fig. 5.4 presents the process used to identify and select the pairs of houses from the P2P EMS results:

1. Determine operating costs for every possible pair of houses from the P2P EMS and operating costs of each house when operating individually from HEMS.
2. Determine the percentage reduction for every pair of houses using (5.29).

$$\frac{\sum_{n=A,B} C_{house\text{-}cost}^{individual(n)} - \sum_{n=A,B} C_{house\text{-}cost}^{P2P(n)}}{\sum_{n=A,B} C_{house\text{-}cost}^{individual(n)}} \times 100\% \qquad (5.29)$$

3. Arrange all the percentage reductions in descending order to choose the pair of houses with the greatest reduction.

4. Remove from the list every other score which includes either of these houses to prevent these houses being a member of multiple pairs. Then repeat steps 3 until all P2P scores are determined.
5. Send optimal settings for all houses.

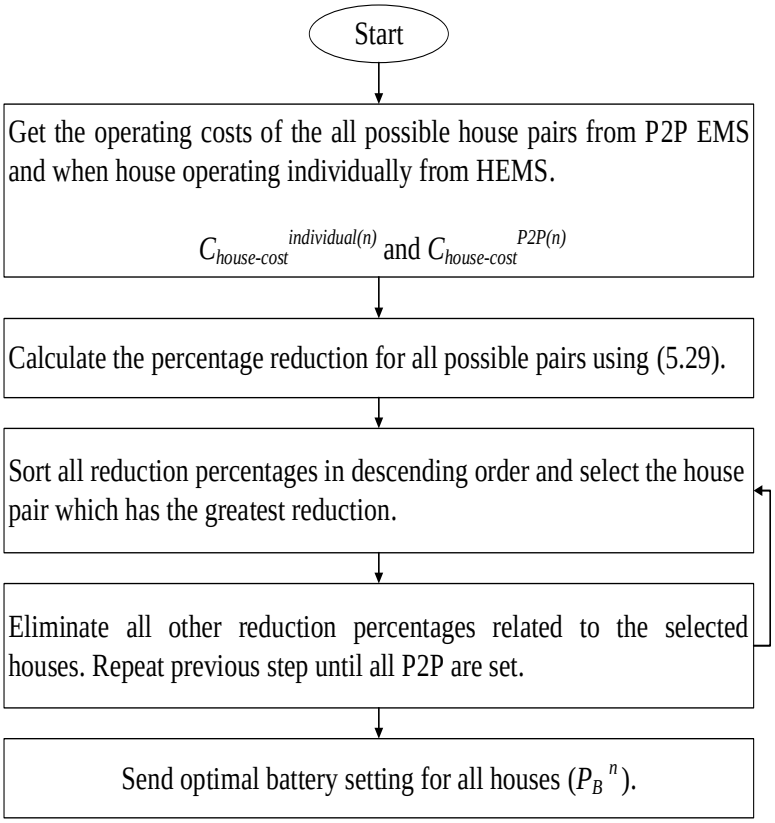

Fig. 5.4. Flowchart of the Selection level.

5.6 Case Studies

The proposed system is implemented in MATLAB software and compared with the system proposed in [5]. The proposed system in [5] is chosen for comparison as it has a similar system configuration (i.e., P2P EMS at the domestic community level) and aims to minimise operating costs while maximising self-consumption. The proposed algorithm has been tested using the community data described in Section 5.2. The algorithm in Fig. 5.2 is carried out for each day of the four months from June to September 2014 with a sample time (ΔT) of 10 mins.

5.6.1 Performance Comparison

This subsection presents the performance of the proposed CEMS on four houses chosen from the community (houses nos. 1, 2, 3, and 4), because they are sufficient to demonstrate the method and concepts involved.

Figs. 5.5 (a-1), (a-2), and (a-3) show generation and load for houses nos. 1, 2, and 3, respectively, for the two days 17th and 18th of June 2014. The red and black solid lines represent P_{PV}^{n} and P_{L}^{n}, respectively. Figs 5.5 (b-1), (b-2), and (b-3) present the optimal house BSS settings for each house and the power exchanged with neighbours for houses nos. 1, 2, and 3, respectively. The red solid and blue dashed lines represent SOC_{B}^{n} and P_{p2p}^{n}, respectively. Where *n* refers to the house number.

Figs 5.5 (a-1) and (a-2) show the energy consumed by houses nos. 1 and 2 is greater than the power generated from the PV for most of the time during day-1 and day-2. However, house no. 3 generates more in PV power than it consumes, as shown in Fig. 5.5 (a-3).

Figs 5.5 (b-1), (b-2), and (b-3), illustrate that house no. 1 exchanges power with house no. 2 during day-1, and with house no. 3 during day-2. Fig. 5.5 (b-2) illustrates that during day-2 house no. 2 does not exchange energy with its neighbours ($P_{P2P}^{n} = 0$). Instead, during the off-peak period the BSS is charged to just above 40% and holds the charge from 5 AM to 8 AM, then it is again charged from the surplus PV power (according to the $E_{Day\text{-}f}{}^{n}$). Similarly, as shown in Fig. 5.5 (b-3), house no. 3 does not exchange energy with its neighbours on day-1. This reduces the household's energy cost by maximising PV self-consumption.

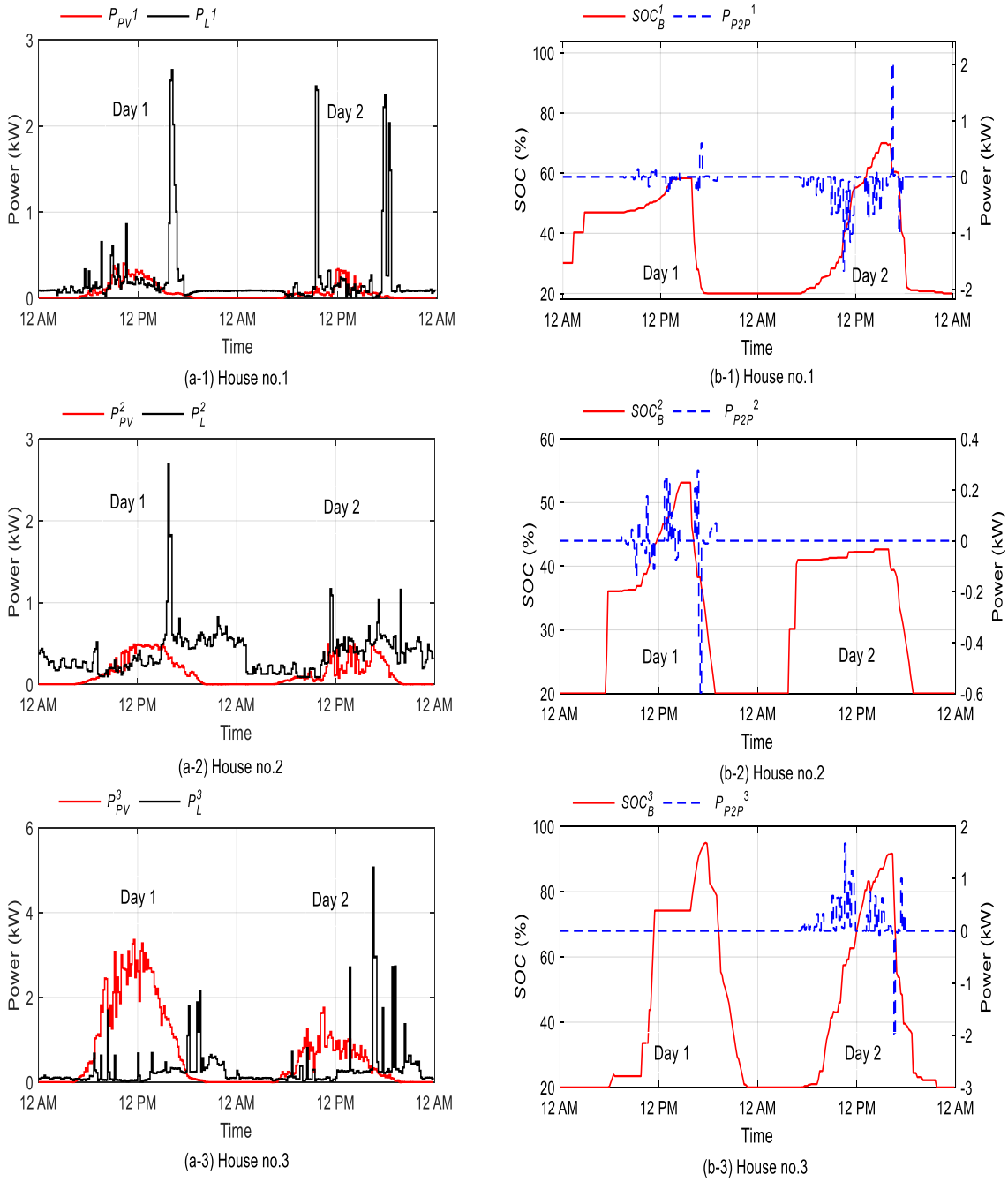

Fig. 5.5. Power and SOC of the house BSS for the proposed CEMS system applied to houses nos. 1, 2, and 3 for the 17th and 18th of June 2014. Figs. (a-1), (a-2), and (a-3) represent the P_{PV} and P_L for houses nos. 1, 2, and 3, respectively. The red and black solid lines represent $P_{PV}{}^n$ and $P_L{}^n$, respectively. Figs. (b-1), (b-2), and (b-3) represent the $SOC_B{}^n$ and $P_{P2P}{}^n$ for houses nos. 1, 2 and 3, respectively. The red solid and blue dashed lines represent $SOC_B{}^n$ and $P_{p2p}{}^n$, respectively.

Fig. 5.6 shows the performance of house no. 4 for the two days 17th and 18th June 2014. The red solid, blue dashed, and black solid lines represent SOC_B^4, P_{P2P}^4, and P_{PV}^4-P_L^4, respectively. During day-1, the PV power generated is greater than the demand ($P_{PV}^4 > P_L^4$), the surplus energy is used to charge the BSS. As can be seen the SOC is maintained at 45% during the off-peak period as it knows the day-2 energy forecast (i.e., $E_{Day\text{-}f}$). Thus, during day-1 and day-2, house no. 4 did not share excess energy with its neighbours. This process maximises PV self-consumption and reduces the net energy exchanged with the grid. In addition, storing the energy required for day-2 prevents purchasing unnecessary energy from the grid or neighbours.

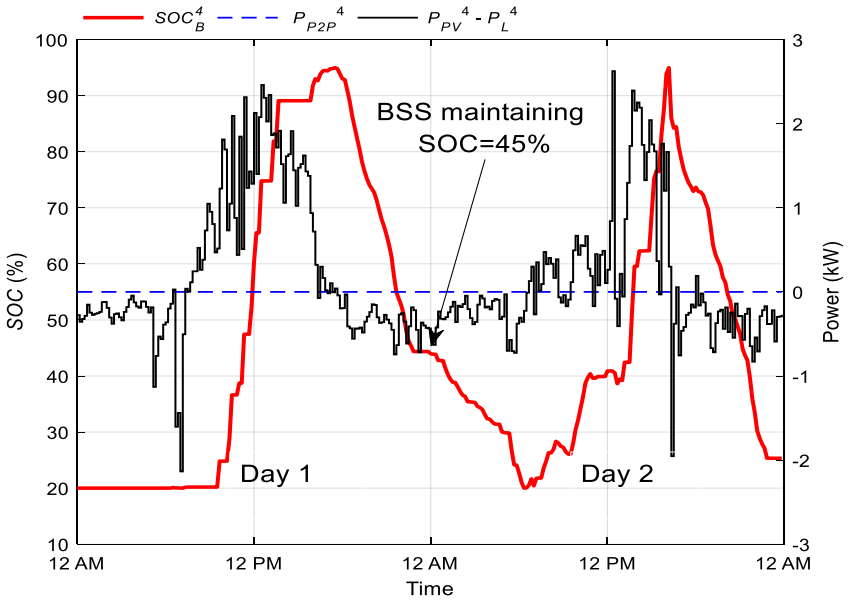

Fig. 5.6. The proposed CEMS system applied to house no. 4 for the 17th and 18th of June 2014. The red solid, blue dashed, and black solid lines represent SOC_B^4, P_{P2P}^4, and P_{PV}^4-P_L^4, respectively.

5.6.2 Operating Costs and Energy Exchange Comparison

Table 5.3 compares the total operating costs of the proposed CEMS for the four months from June to September 2014 for each household operating as part of the community, compared to operating individually. The proposed CEMS reduced the total operating

cost of the community by 7.6% when compared to the six houses being operated individually.

Table 5.4 compares the total operating costs of the proposed method in [5] for the four months June to September 2014 for each household when they are operating as part of the community, compared to operating individually. The method proposed in [5] reduces the operating costs of all houses (except house no. 5) by up to 45%. In addition, the total operating cost of the community is reduced by 11% when compared to the six houses being operated individually.

Comparing Tables 5.3 and 5.4, it is seen that the proposed CEMS in this work operates at higher cost than the method proposed in [5]. This is because the proposed CEMS aims to reduce the net energy exchange with the grid rather than reducing the operating costs, which promotes a self-consumption approach. As a result, the BSSs will be used more frequently compared with the method described in [5], which increases the operating costs of each house. Nevertheless, since the method in [5] exchanges more energy with the grid (see Table 5.5), it requires more distribution/transmission and storage capacity on the network side; consequently, the overall network operating cost increases. Therefore, if the network operators are interested in promoting self-consumption, the energy tariff and/or storage price must be changed accordingly.

Table 5.5 compares the total absolute net energy exchange of the proposed CEMS with the method proposed in [5] from June to September 2014. The proposed CEMS reduces the total absolute net energy exchange for the six houses by 25.3% compared to the method in [5].

Fig. 5.7 illustrates the total imported energy during peak and mid-peak periods for the four months from June to September 2014. The blue and green bars represent the proposed CEMS and the method proposed in [5], respectively. The proposed CEMS reduces the total energy imported from the grid during peak and mid-peak periods, which is most beneficial as it is at these times that the tariffs are highest.

Table 5.3. Operating costs for individual and community operations for the proposed method in this work from June to September 2014.

House number	Operating costs for individual operation (HEMS) (£)	Operating costs for community operation (CEMS) (£)	Percentage (%)
1	32	26	18.8
2	112	96	14.2
3	32	31	3.1
4	47	49	4.3
5	47	48	2.1
6	61	56	8.2
Total	331	306	7.6

Table 5.4. Operating costs for individual and community operations for the method proposed in [5] from June to September 2014.

House number	Operating costs for individual operation (HEMS) (£)	Operating costs for community operation (CEMS) (£)	Percentage (%)
1	19	18	5.3
2	116	105	9.5
3	40	22	45
4	32	31	3.1
5	27	27	0
6	63	62	1.6
Total	297	265	11

Table 5.5. Absolute net energy exchange with the grid from June to September 2014.

House number	Absolute net energy exchanged (kWh) (Ref [5])	Absolute net energy exchanged (kWh) (CEMS)	Percentage (%)
1	1166	818	29.9
2	681	624	8.4
3	1427	1052	26.3
4	1378	964	30
5	1660	1188	28.4
6	351	328	6.6
Total	6663	4974	25.3

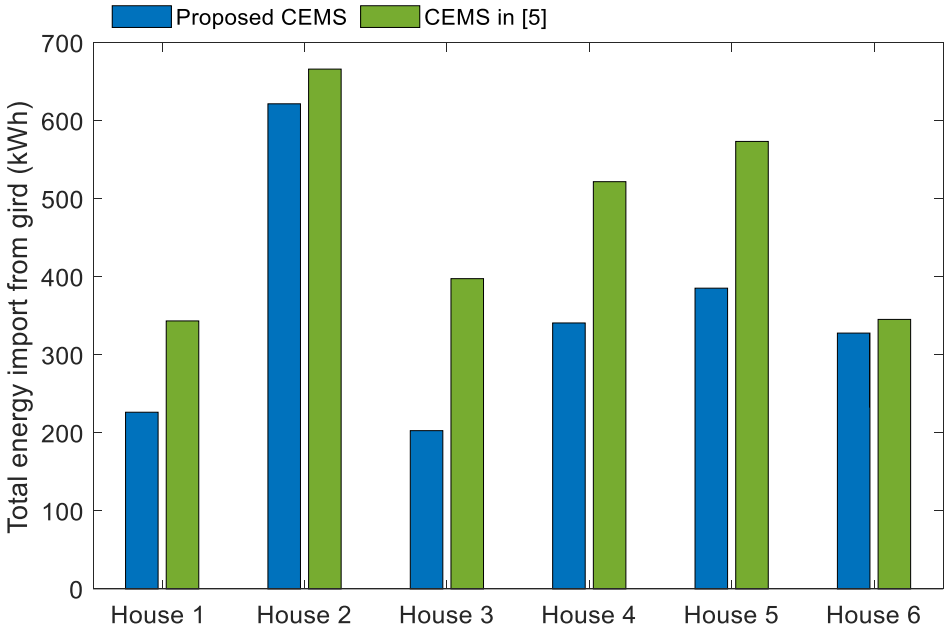

Fig. 5.7. Total imported energy for all six houses during peak and mid-peak periods for June to September 2014. The blue and green bars represent the proposed CEMS and the method reported in [5], respectively.

5.7 Conclusion

This chapter used the proposed MILP-EMS in Chapter 4 as the foundation for a CEMS based on the energy trading between prosumers. The main target of the CEMS was enhancing self-consumption within the community and reducing: (1) energy exchange between the community and the grid, (2) operating costs of the community, (3) transmission losses and (4) the required central generation, transmission, and storage facilities. In addition, the proposed CEMS optimised BSS performance by avoiding unnecessary charge/discharge cycles by including the next day-ahead forecast (i.e., day-2) and BSS degradation cost in the optimisation process. Results compared with a similar state-of-the-art approach showed a significant reduction in energy exchange between the grid and community by 25.3% over four months. The proposed CEMS also reduced community operating costs by 7.6%. However, based on the outcomes, it should be pointed out that with today's energy tariffs and storage costs, enhancing a self-consumption approach may not be economical for individual houses. Consequently, if network operators intend to enhance self-consumption, energy tariffs and/or storage prices must be changed.

6 INVESTIGATION OF THE CONTRIBUTION OF EVs TO A COMMUNITY ENERGY SYSTEM

6.1 Introduction

The widespread use of Electric Vehicles (EVs) has created many new challenges for network operators and the need for new infrastructure [73]. In addition, the EV charging/discharging activities can increase peak demand, overload transmission lines, and damage local distribution transformers [57, 74]. In this regard, several countries, including the UK, promote a self-consumption approach to reduce infrastructure development costs and the burden on the grid [6, 7]. This chapter focuses on investigating the impact of EVs and shiftable appliances on the proposed Community Energy Management System (CEMS) presented on Chapter 5. The analysis in this chapter has been performed by coding the system in MATLAB software.

Note that the results presented in this chapter have been published in IEEE Access journal:

A. Al-Sorour, M. Fazeli, M. Monfared, and A. A. Fahmy, "Investigation of Electric Vehicles Contributions in an Optimized Peer-to-Peer Energy Trading System," *IEEE Access*, vol. 11, pp. 12489-12503, 2023, doi: 10.1109/ACCESS.2023.3242052.

This chapter is organised as follows. First, Sections 6.2 and 6.3 describe the community configuration and structure of the proposed CEMS, respectively. Next, Sections 6.4 and 6.5 describe the House Energy Management System (HEMS) and Central Controller, respectively. The results are presented in Section 6.6. Finally, Section 6.7 presents the conclusion of Chapter 6.

6.2 Community Configuration

This study uses the community described in Chapter 5- Section 5.2, which consists of six houses, each occupied with a Battery Storage System (BSS) and Photovoltaic (PV) system. However, it is assumed that all six households use an EV and are equipped with a bidirectional charger to facilitate the V2H mode, as shown in Fig. 6.1. Two types of

EVs are used, which are Nissan and Tesla. The EV battery costs of Nissan and Tesla are equivalent to 110£/kWh and 100£/kWh, respectively [174]. It is assumed that the charge/discharge efficiency ($\eta_{EVc}^{n}/\eta_{EVd}^{n}$) and the life cycle ($N_{EVcycle}^{n}$) of both types of EV battery are 90% and 5,000, respectively [57]. The maximum SOC ($SOC_{EV\text{-}max}^{n}$) and the minimum SOC ($SOC_{EV\text{-}min}^{n}$) limits of the EV batteries are set to 90% and 10%, respectively [175]. In addition, this study considers two shiftable appliances, which are a washing machine and a dishwasher. Tables 6.1 and 6.2 show each house's shiftable appliances ratings ($P_{rate\text{-}L}^{n}$) and EV parameters, respectively.

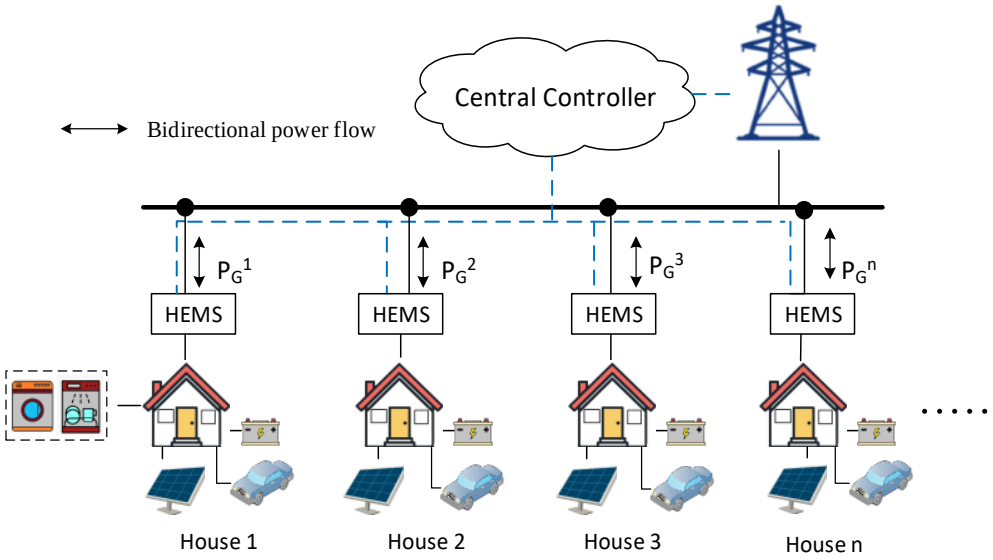

Fig. 6.1. System configuration.

Table 6.1. Shiftable appliances

House number	Washing machine (kWh) [176]	Dishwasher (kWh) [177]
1	0.8	1.6
2	1.1	1.5
3	1.2	1.7
4	0.9	1.1
5	No	1.3
6	No	1.2

Table 6.2. EV parameters [178]

House number	EV type	EV capacity (kWh)	Average EV consumption (kWh/km)	Maximum charge/discharge power of EV (kW)
1	Nissan Leaf	40	0.18	6.6
2	Tesla Model 3 Long Range Dual Motor	79	0.17	11
3	Nissan Leaf e+	62	0.18	6.6
4	Tesla Model 3	60	0.16	11
5	Tesla Long Range Dual Motor	82	0.16	11
6	Nissan Leaf	40	0.18	6.6

6.3 Proposed CEMS

The CEMS proposed in Chapter 5 is developed further to include shiftable appliances and EVs. The new system is divided into three stages, as shown in Fig. 6.2:

1. Data collection: The inputs to the HEMS and P2P EMS are:

    a) Household data: Initial SOC of the house BSS (SOC_B^n) and EV battery (SOC_{EV}^n), travel distance (T_D^n), EV arrival time (EV_A^n), EV departure time (EV_D^n), desired SOC of the EV battery for the second journey ($SOC_{EV\text{-}desired}^n$), appliance start time (T_{start}^n (i)), appliance maximum waiting time (T_{wait}^n (i)), where n refers to the number of the house within the community, i refers to the appliance (i = 1 for the washing machine and i = 2 for the dishwasher).

    b) Two days-ahead generation and demand forecasts for each house assumed that is provided by forecasting company: day-1 PV generation ($P_{PV\text{-}1}^n$), day

1 load demand ($P_{L\text{-}1}^{n}$), day-2 PV generation ($P_{PV\text{-}2}^{n}$), and day-2 load demand ($P_{L\text{-}2}^{n}$).

2. House Energy Management System: A HEMS is used in each house to minimise the energy exchanged with the grid and reducing energy costs by scheduling shiftable appliances, EVs and house BSSs. The optimum house BSS setting is obtained by considering the peak and mid-peak energy forecasts for day-2 ($E_{Day\text{-}f}^{n}$). After determining optimal system settings, energy costs and the relevant parameters for each house are uploaded into the Central Controller to perform P2P EMS optimisation.
3. The Central Controller consists of two stages:

   a) P2P EMS where every possible pair of the given houses are generated. Here the number of houses is 6 resulting in 15 pairs. The optimum house BSS of houses *A* and *B* is obtained by considering the peak and mid-peak energy forecasts for day-2 ($E_{Day\text{-}f}^{n}$).

   b) The Selection level where each pair of houses is selected to establish: (1) minimum cost of the energy consumed by the pair, and (2) a profile of the daily energy exchange between the two houses and between the pair and the grid with sample time (ΔT) of 10 min. The best pairs are chosen based on percentage cost reductions. After the optimal settings are obtained from the selected house pairs, the BSS, EV battery and shiftable appliances settings are sent to each house.

6.4 House Energy Management System

The HEMS in this study is an updated version of the MILP-EMS system described in Chapter 4. The main goal of the updated cost function (C_{house}^{n}) in (6.1) is to minimise the net energy exchanged with the grid by considering the absolute costs of the energy imported from, and energy exported to, the grid. The cost function of C_{house}^{n} comprises the costs of the energy purchased from the grid (C_{buy}^{n}), energy sold to the grid (C_{sell}^{n}), the degradation cost of the house BSS (C_{BSS}^{n}) and the degradation cost of the EV battery (C_{EV}^{n}). It should be noted that the EV battery degradation cost is only taken into account when EV battery is in V2H mode, i.e., when it is being discharged to supply a house.

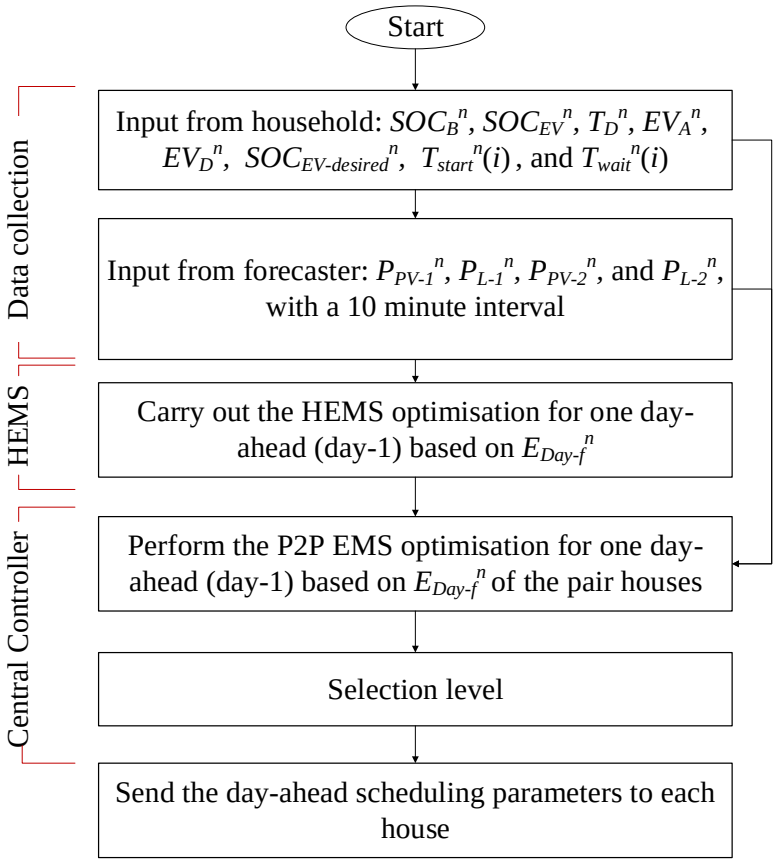

Fig. 6.2. Proposed CEMS.

$$\text{Minimise } C_{house}^{\,n} = |C_{buy}^{\,n}| + |C_{sell}^{\,n}| + C_{BSS}^{\,n} + C_{EV}^{\,n} \tag{6.1}$$

$$C_{buy}^{\,n} = \sum_{t_0}^{T} \Delta T \times f_{buy}(t) \times P_G^{\,n}(t),\ P_G^{\,n}(t) > 0 \tag{6.2}$$

$$C_{sell}^{\,n} = \sum_{t_0}^{T} \Delta T \times f_{sell}(t) \times P_G^{\,n}(t),\ P_G^{\,n}(t) < 0 \tag{6.3}$$

$$C_{BSS}^{\,n} = \sum_{t_0}^{T} \frac{\mathrm{CC_B}^{n} \times \eta_{Conv}^{\,n} \times \eta_c^{\,n} \times \Delta T \times \left| P_{B\text{-}charg}^{\,n}(t) \right|}{2 \times N_{Bcycle}^{\,n} \times B_{capacity}^{\,n}(t)} + \tag{6.4}$$

$$\frac{\mathrm{CC_B}^{n}\times\Delta T\times\left|P_{B\text{-}disch}{}^{n}(t)\right|}{\eta_{Conv}{}^{n}\times\eta_{d}{}^{n}\times 2\times N_{Bcycle}{}^{n}\times B_{capacity}{}^{n}(t)}$$

$$C_{EV}{}^{n}=\sum_{t_0}^{T}\frac{\mathrm{CC_{EV}}^{n}\times\Delta T\times\left|P_{EV\text{-}disch}{}^{n}(t)\right|}{\eta_{EV}{}^{n}\times\eta_{EVd}{}^{n}\times 2\times N_{EVcycle}{}^{n}\times EV_{capacity}{}^{n}(t)} \tag{6.5}$$

where n is the house number, T is the day duration of 24 hours, t_0 is the time of day starting at 12 AM, ΔT is the sampling time (hr), $f_{buy}(t)$ is the purchasing tariff from the grid (£/kWh), $f_{sell}(t)$ is the selling tariff to the grid (£/kWh), $P_G{}^{n}(t)$ is the grid import/export power (kW), $\mathrm{CC_B}^{n}$ represents the cost the cost of a new BSS for a house (£) (without considering the power converters), $N_{Bcycle}{}^{n}$ is the number of house BSS life cycles, $\eta_{conv}{}^{n}$ is the converter efficiency of the house BSS (%), $P_{B\text{-}disch}{}^{n}(t)$ is the house BSS discharge power (kW), $P_{B\text{-}charg}{}^{n}(t)$ is the house BSS charge power (kW), $\eta_d{}^{n}$ is the discharging efficiency of the house BSS (%), $\eta_c{}^{n}$ is the charging efficiency of the house BSS (%), $B_{capacity}{}^{n}(t)$ is the current estimated house BSS capacity (kWh), $\mathrm{CC_{EV}}^{n}$ is the cost of a new EV battery (£), $N_{EVcycle}{}^{n}$ is the number of EV battery life cycles, $\eta_{EV}{}^{n}$ is the EV converter efficiency (%), $\eta_{EVd}{}^{n}$ is the discharging efficiency of the EV battery (%), $P_{EV\text{-}disch}{}^{n}$ is the EV discharge power (kW), and $EV_{capacity}{}^{n}(t)$ is the current estimated EV battery capacity (kWh). Note that the value of $P_G{}^{n}(t)$ is positive when the house n imports from the grid and negative when it exports. In addition, the values of $P_{B\text{-}disch}(t)$ and $P_{B\text{-}charg}(t)$ are positive and negative, respectively. the values of $P_{EV\text{-}disch}(t)$ and $P_{EV\text{-}charg}(t)$ are positive and negative, respectively.

The system power balance equation is presented as (6.6):

$$P_{L\text{-}1}{}^{n}(t)+P_{L\text{-}sh}{}^{n}(i,t)-P_{PV\text{-}1}{}^{n}(t)=P_G{}^{n}(t)+P_B{}^{n}(t)+P_{EV}{}^{n}(t) \tag{6.6}$$

where $P_{EV}{}^{n}(t)$ is charge/discharge of EV battery power (kW), $P_B{}^{n}(t)$ is charge/discharge of house BSS power (kW), $P_{L\text{-}sh}{}^{n}(i,t)$ is the power required for shiftable appliance i at time t (kW). Note that the $P_{EV}{}^{n}(t)$ is equal to 0 when the EV is not available.

6.4.1 Demand-Side Management

Scheduling the domestic load motivates consumers and prosumers to change their daily consumption patterns by considering relevant factors, such as the electricity price and the available local generation and storage. This study considers two categories of domestic loads:

1. Fixed appliances, such as TV and refrigerators, which cannot be scheduled.
2. Shiftable appliances, such as dishwashers, which can be time-shifted to the low-price tariff (i.e., off-peak and mid-peak times) or when there is surplus energy to reduce energy costs.

This study considers two shiftable appliances: a washing machine and a dishwasher. The shiftable appliances are scheduled using the following steps:

- Appliance *i* transmits the ON signal state to the HEMS.
- The HEMS then schedules a start time for appliance *i.*
- The appliance *i* will wait for the ON signal from HEMS.
- Once started, the appliance *i* stops when it completes its cycle.

In this study, the time that the appliance *i* can wait is between 1 and 8 hours, depending on the household's preferences. When $T_{wait}^{n}(i)$ is equal to 0, it specifies that appliance *i* will begin operation immediately once it is switched ON. To ensure that an appliance *i* begins operation within the specified wait time, the constraint (6.7) is imposed [5].

$$\Delta T \times \sum_{T_{start}^{n}(i)}^{24} \text{logic NOT}(\sigma_L^{n}(i,t)) \leq T_{wait}^{n}(i) \tag{6.7}$$

where $T_{wait}^{n}(i)$ is the permitted maximum wait time of appliance *i* (hr) and $T_{start}^{n}(i)$ is the moment at which the HEMS gets an ON command from appliance *i* (hr). when $i = 1$ refers to the washing machine and $i = 2$ refers to the dishwasher. $\sigma_L^{n}(i, t)$ is a binary variable that indicates the operational status of appliance *i*. $\sigma_L^{n}(i, t)$ is equal to 1 if appliance *i* is ON, else is equal to 0.

For starting up the appliance *i* constraint (6.8) is introduced [5].

$$\sigma_L^{\,n}(i,t+1)-\sigma_L^{\,n}(i,t)-\sigma_{startup}^{\,n}(i,t)\leq 0 \tag{6.8}$$

where $\sigma_{startup}^{n}(i,\ t)$ is a binary variable that indicates that appliance i is in operating mode. $\sigma_{startup}^{n}(i,\ t)$ is equal to 1 when the appliance i status shifts from OFF to ON, otherwise is equal to 0.

To ensure appliance i is continuously operating without any sudden interruptions (i.e., switched OFF), constraint (6.9) is applied [5].

$$\Delta T\times\sum_{T_{start}^{\,n}(i)}^{T_{end}^{\,n}(i)}\sigma_L^{\,n}(i,t)=T_{cycle}^{\,n}(i) \tag{6.9}$$

where $T_{cycle}^{n}(i)$ is the required operation time for appliance i (hr) and $T_{end}^{n}(i)$ is the time at which the operation of appliance i ends (hr).

To make sure the appliance i starts only on request and switches OFF after completing its operational cycle, $\sigma_L^{n}(i,\ t)$ is set to 0 before the HEMS receives a start signal and after completion of the operation [5]. The washing machine and the dishwasher take 1 hour to complete their cycles.

$$\sigma_L^{\,n}(i,t)=0 \quad \text{at } t<T_{start}^{\,n}(i), \quad t>T_{end}^{\,n}(i) \tag{6.10}$$

Equation (6.11) represents the power consumed by appliance i [5].

$$P_{L\text{-}sh}^{\,n}(i,t)=P_{rate\text{-}L}^{\,n}(i)\times\sigma_L^{\,n}(i,t) \tag{6.11}$$

where $P_{rate\text{-}L}^{\,n}(i)$ is the appliance's power rating (Wh).

6.4.2 EV Battery Model

At the start of every day, the EV begins its first journey of the day with fully charged battery according to (6.12):

$$SOC_{EV}{}^{n}\,(t=EV_{D}{}^{n}) = SOC_{EV\text{-}max}{}^{n} \tag{6.12}$$

where EV_D^n is the EV departure time (hr).

It is assumed that an EV does not receive any charge during its journey so when an EV returns to its house and is plugged in, a new SOC_{EV}^n ($t=EV_A^n$) is determined corresponding to the energy consumed during the journey using (6.13) [57]. Otherwise, precise information on the SOC is obtained once the EV is connected to the house's charging/discharging control unit. The estimated energy consumed during the journey (E_{reduce}^n) is presented in (6.14).

$$SOC_{EV}{}^{n}\,(t=EV_{A}{}^{n}) = SOC_{EV}{}^{n}\,(t=EV_{D}{}^{n}) - E_{reduce}{}^{n}\,(t) \tag{6.13}$$

$$E_{reduce}{}^{n}\,(t) = \frac{T_{D}{}^{n} \times E_{cons}{}^{n}}{EV_{capacity}{}^{n}} \times 100 \tag{6.14}$$

The current capacity of the EV battery is estimated using (6.15).

$$EV_{capacity}{}^{n}\,(t) = \frac{1}{SOC_{EV}{}^{n}\,(t_{\alpha}) - SOC_{EV}{}^{n}\,(t_{\beta})} \int_{t_{\alpha}}^{t_{\beta}} I_{EV}{}^{n}\,(\tau)\, d\tau \tag{6.15}$$

where EV_A^n is the time of arrival of the EV (hr), E_{cons}^n is the energy consumption per km (kWh/km), T_D^n is the travel distance (km), I_{EV}^n (t) is the EV battery charge/discharge current (A), SOC_{EV}^n (t_α) is the SOC of the EV battery at time t_α (%), and SOC_{EV}^n (t_β) is the SOC of the EV battery at time t_β (%).

For a second journey on the same day, the user would estimate the required minimum charge before commencing the journey ($SOC_{EV\text{-}desired}^n$). The constraint represented by (6.16) makes sure that the EV battery has the necessary energy before departure.

$$SOC_{EV}{}^{n}\,(t=EV_{D}{}^{n}) \geq SOC_{EV\text{-}min}{}^{n} + \frac{T_{D}{}^{n} \times E_{cons}{}^{n}}{EV_{capacity}{}^{n}\,(t)} \times 100 \tag{6.16}$$

Equations (6.17) and (6.18) are used to estimate the energy stored and SOC of the EV battery, respectively.

$$E_{EV}^{n}(t) = E_{EV}^{n}(t\text{-}1) - \frac{\Delta T \times P_{EV\text{-}disch}^{n}(t)}{\eta_{EVd}^{n}} - \Delta T \times \eta_{EVc}^{n} \times P_{EV\text{-}charg}^{n}(t) \quad (6.17)$$

$$SOC_{EV}^{n}(t) = \frac{E_{EV}^{n}(t)}{EV_{capacity}^{n}(t)} \times 100 \quad (6.18)$$

where $E_{EV}^{n}(t)$ is EV battery stored energy at time t, $E_{EV}^{n}(t\text{-}1)$ is EV battery energy at time t-1, η_{EVc}^{n} represents the EV charging efficiency (%), $P_{EV\text{-}disch}^{n}$ is the EV discharging power (kW), and $P_{EV\text{-}charg}^{n}$ is the EV charging power (kW).

The constraint presented in (6.19) ensures that the SOC of the EV battery does not exceed permitted limits.

$$SOC_{EV\text{-}min}^{n} \leq SOC_{EV}^{n}(t) \leq SOC_{EV\text{-}max}^{n} \quad (6.19)$$

The instantaneous EV battery power (P_{EV}^{n}) is given by (6.20) and the EV battery maximum and minimum allowable charge/discharge power limits by (6.21):

$$P_{EV}^{n}(t) = P_{EV\text{-}disch}^{n}(t) \times \eta_{EV}^{n} + \frac{P_{EV\text{-}charg}^{n}(t)}{\eta_{EV}^{n}} \quad (6.20)$$

$$-P_{EV\text{-}rating}^{n} \leq P_{EV}^{n}(t) \leq P_{EV\text{-}rating}^{n} \quad (6.21)$$

where $P_{EV\text{-}rating}^{n}$ represents the rated charging/discharging power of the EV battery (kW).

6.4.3 House BSS Model

The BSS model presented in Chapter 4- Subsection 4.3.1 is used here for the house n BSS.

6.4.4 System Constraints for HEMS

In addition to the system constraints presented in Chapter 4- Subsection 4.3.2, the following constraints are defined by introducing two additional binary variables for the

EV battery, $\Phi_{EV\text{-}disch}^{n}$ and $\Phi_{EV\text{-}charg}^{n}$, which are used to prevent the EV battery from being both charged and discharged simultaneously. See constraint (6.22).

$$\Phi_{EV\text{-}disch}^{n}(t)+\Phi_{EV\text{-}charg}^{n}(t)\leq 1 \tag{6.22}$$

$$\Phi_{EV\text{-}charg}^{n}(t)=\begin{cases}1 & , P_{EV}^{n}(t)<0\\ 0 & , P_{EV}^{n}(t)>0\end{cases} \tag{6.23}$$

$$\Phi_{EV\text{-}disch}^{n}(t)=\begin{cases}1 & , P_{EV}^{n}(t)>0\\ 0 & , P_{EV}^{n}(t)<0\end{cases} \tag{6.24}$$

where $\Phi_{EV\text{-}disch}^{n}(t)$ is equal to 1 when the EV battery is discharging, otherwise, is equal to 0. The $\Phi_{EV\text{-}charg}^{n}(t)$ is equal to 1 when the EV battery is charging, otherwise, is equal to 0.

Constraints (6.25) and (6.26) are introduced to prevent the house BSS and EV battery from charging each other.

$$\Phi_{EV\text{-}disch}^{n}(t)+\Phi_{B\text{-}charg}^{n}(t)\leq 1 \tag{6.25}$$

$$\Phi_{EV\text{-}charg}^{n}(t)+\Phi_{B\text{-}disch}^{n}(t)\leq 1 \tag{6.26}$$

Constraints (6.27) and (6.28) are introduced to ensure the EV battery is charged and discharged within allowable limits.

$$P_{EV\text{-}disch}^{n}(t)\leq \Phi_{EV\text{-}disch}^{n}(t)\times P_{EV\text{-}rating}^{n} \tag{6.27}$$

$$\left|P_{EV\text{-}charg}^{n}(t)\right|\leq \Phi_{EV\text{-}charg}^{n}(t)\times P_{EV\text{-}rating}^{n} \tag{6.28}$$

Constraint (6.29) is introduced to guarantee that the EV battery is not exporting power to the grid when the house is exporting excess PV power.

$$\Phi_{EV\text{-}disch}{}^{n}(t) + \Phi_{export}{}^{n}(t) \leq 1 \tag{6.29}$$

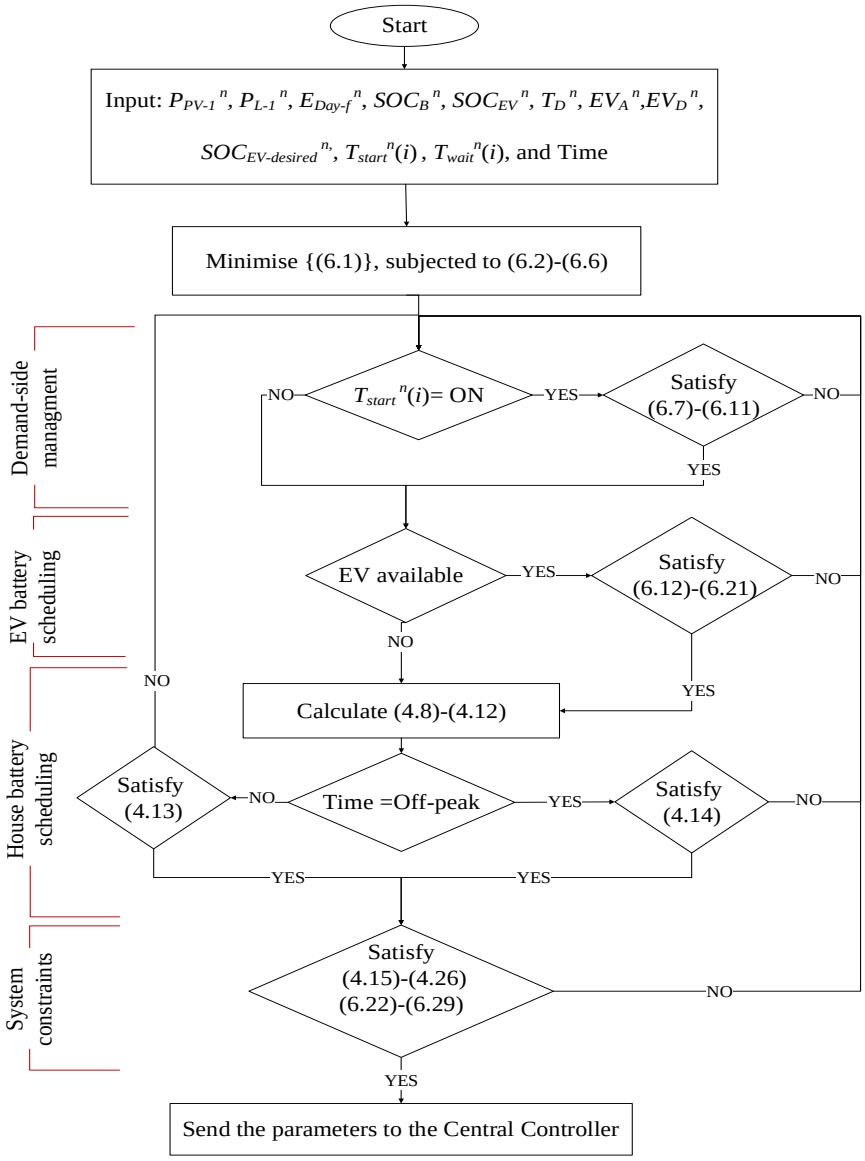

Fig. 6.3. Flowchart of the HEMS.

Fig. 6.3 illustrates the flowchart of the HEMS and follows the procedures below:

- Input the parameters to the HEMS to minimise the cost function of (6.1), which is subjected to constraints in (6.2)-(6.6).

- Next, if appliances are ON, constraints in (6.7)-(6.11) must be met.
- The system checks if the EV is connected, and if so, constraints (6.12)-(6.21) must be met.
- Then the system calculates (4.8)-(4.12).
- During the off-peak hours, the system will verify if the house BSS has sufficient energy for the next peak hour by satisfying constraint (4.14), otherwise, constraint (4.13) must be satisfied.
- Finally, after satisfying system constraints (4.15)-(4.26) and (6.22)-(6.29) the output parameters are uploaded into the Central Controller.

6.5 Central Controller

The Central Controller consists of two stages which are P2P EMS and Selection level. The Central Controller in this study is an updated version of the Central Controller described in Chapter 5- Section 5.5.

6.5.1 P2P Problem Formulation

The updated cost function ($C_{sum\text{-}P2P}$) for paired houses *A* and *B* is presented in (6.30):

$$\text{Minimise } C_{sum\text{-}P2P} = \sum_{n=A,\,B} |{C_{buy}}^{n}|+|{C_{sell}}^{n}|+{C_{BSS}}^{n} + {C_{EV}}^{n} - \left|{C_{P2P}}^{n}\right| \tag{6.30}$$

$${C_{buy}}^{n}=\sum_{t_0}^{T} \Delta T\times f_{buy}\,(t)\times {P_G}^{n}\,(t),\;\; {P_G}^{n}\,(t)>0 \tag{6.31}$$

$${C_{sell}}^{n}=\sum_{t_0}^{T} \Delta T\times f_{sell}\,(t)\times {P_G}^{n}\,(t),\;\;\; {P_G}^{n}\,(t)<0 \tag{6.32}$$

$${C_{BSS}}^{n}=\sum_{t_0}^{T} \frac{{CC_B}^{n}\times {\eta_{Conv}}^{n}\times {\eta_c}^{n}\times \Delta T\times \left|{P_{B\text{-}charg}}^{n}\,(t)\right|}{2\times {N_{Bcycle}}^{n}\times {B_{capacity}}^{n}\,(t)} + \frac{{CC_B}^{n}\times \Delta T\times \left|{P_{B\text{-}disch}}^{n}\,(t)\right|}{{\eta_{Conv}}^{n}\times {\eta_d}^{n}\times 2\times {N_{Bcycle}}^{n}\times {B_{capacity}}^{n}\,(t)} \tag{6.33}$$

$$C_{EV}{}^{n}=\sum_{t_0}^{T}\frac{\mathrm{CC_{EV}}^{\mathrm{n}}\times\Delta T\times|P_{EV\text{-}disch}{}^{n}(t)|}{\eta_{EV}{}^{n}\times\eta_{EVd}{}^{n}\times 2\times N_{EVcycle}{}^{n}\times EV_{capacity}{}^{n}(t)} \tag{6.34}$$

$$C_{P2P}{}^{n}=\begin{cases}\Delta T\times\sum_{t_0}^{T} f_{P2P\text{-}exp}(t)\times P_{P2P}{}^{A\leftrightarrow B}(t)\,,\ P_{P2P}{}^{A\leftrightarrow B}(t)>0\\ \Delta T\times\sum_{t_0}^{T} f_{P2P\text{-}imp}(t)\times P_{P2P}{}^{A\leftrightarrow B}(t)\,,\ P_{P2P}{}^{A\leftrightarrow B}(t)<0\end{cases} \tag{6.35}$$

where n refers to the house number of A and B, $C_{buy}{}^{n}$ is the cost of energy purchased from the grid (£), $C_{sell}{}^{n}$ is the price of the energy sold to the grid (£), $C_{BSS}{}^{n}$ is the house BSS degradation cost (£), $C_{EV}{}^{n}$ is the degradation cost of the EV battery (£), $C_{P2P}{}^{n}$ is the cost of energy exchanged per day between paired houses A and B (£), t_0 is the time of day starting at 12 AM, ΔT is the sampling time (hr), $f_{buy}(t)$ is the tariff for purchasing from the grid (£/kWh), $f_{sell}(t)$ is the tariff for selling to the grid (£/kWh), $P_G{}^{n}(t)$ is power exchanged between the house and the grid (kW), $f_{P2P\text{-}exp}(t)$ is the tariff for energy exported from one house in the pair to the other (£/kWh), $f_{P2P\text{-}imp}(t)$ is the tariff for energy imported by one house in the pair from the other (£/kWh), $P_{P2P}{}^{A\leftrightarrow B}(t)$ is the power exchanged between the paired houses (kW), $\mathrm{CC_B}^{\mathrm{n}}$ is the cost of a new house BSS (£), $N_{Bcycle}{}^{n}$ is the number of life cycles of a house BSS, $\eta_{conv}{}^{n}$ is converter efficiency of the house BSS (%), $P_{B\text{-}disch}{}^{n}(t)$ is the house BSS discharge power (kW), $P_{B\text{-}charg}{}^{n}(t)$ is the house BSS charge power (kW), $\eta_d{}^{n}$ is the discharging efficiency of the house BSS (%), $\eta_c{}^{n}$ is the charging efficiency of the house BSS (%), $\mathrm{CC_{EV}}^{\mathrm{n}}$ is the cost of a new EV battery (£), $N_{EVcycle}{}^{n}$ is the number of life cycles of the EV battery, $\eta_{EV}{}^{n}$ is the EV converter efficiency (%), $\eta_{EVd}{}^{n}$ is the discharging efficiency of the EV battery (%), $B_{capacity}{}^{n}(t)$ is the current estimated house BSS capacity (kWh), $EV_{capacity}{}^{n}(t)$ is the current estimated EV battery capacity (kWh), and $P_{EV\text{-}disch}{}^{n}(t)$ is the EV discharge power (kW). The value of $P_G{}^{n}(t)$ is positive when the house n imports from the grid and negative when it exports. The values of $P_{B\text{-}disch}{}^{n}(t)$ and $P_{EV\text{-}disch}{}^{n}(t)$ are positive. In addition, the values of $P_{B\text{-}charg}{}^{n}(t)$ and $P_{EV\text{-}charg}{}^{n}(t)$ are negative. The value of $P_{P2P}{}^{A\leftrightarrow B}(t)$ is positive when the house is exporting energy and is negative when it is importing energy from its neighbour.

The system power balance equations for houses *A* and *B* separately and when they are paired are:

For house *A*:

$$P_{L\text{-}1}{}^{A}(t) + P_{L\text{-}sh}{}^{A}(i,t) - P_{PV\text{-}1}{}^{A}(t) = P_{G}{}^{A}(t) + P_{B}{}^{A}(t) + P_{EV}{}^{A}(t) - P_{P2P}{}^{A\leftrightarrow B}(t) \quad (6.36)$$

For house *B*:

$$P_{L\text{-}1}{}^{B}(t) + P_{L\text{-}sh}{}^{B}(i,t) - P_{PV\text{-}1}{}^{B}(t) = P_{G}{}^{B}(t) + P_{B}{}^{B}(t) + P_{EV}{}^{B}(t) - P_{P2P}{}^{B\leftrightarrow A}(t) \quad (6.37)$$

For houses *A* and *B* when paired:

$$\sum_{n=A,\,B} P_{G}{}^{n}(t) + P_{B}{}^{n}(t) + P_{EV}{}^{n}(t) = \sum_{n=A,\,B} P_{L\text{-}1}{}^{n}(t) + P_{L\text{-}sh}{}^{n}(i,t) - P_{PV\text{-}1}{}^{n}(t) \quad (6.38)$$

where $P_{EV}{}^{n}(t)$ is charge/discharge of EV battery power, $P_{B}{}^{n}(t)$ is charge/discharge of house BSS power, $P_{L\text{-}sh}{}^{n}(i, t)$ is the power required for shiftable appliance *i*, at time *t* (kW). Note that the $P_{EV}{}^{n}(t)$ is equal to 0 when the EV is not available.

6.5.1.1 Demand-side Management

The equations presented in Chapter 6- Subsection 6.4.1 are used for the appliances in houses *A* and *B.*

6.5.1.2 EV Battery Model

EV model presented in Chapter 6- Subsection 6.4.2 is used for EV batteries for houses *A* and *B.*

6.5.1.3 House BSS Model

The BSS model presented in Chapter 4- Section 4.3.1 is used here for BSSs in houses *A* and *B.*

6.5.1.4 System Constraints for P2P-EMS

In addition to the system constraints presented in Chapter 5- Subsection 5.5.1.2, the following constraints are introduced:

Constraint in (6.39) is used to prevent the EV battery from both charging and discharging at the same time.

$$\Phi_{EV\text{-}disch}^{\ n}(t)+\Phi_{EV\text{-}charg}^{\ n}(t)\leq 1 \tag{6.39}$$

where $\Phi_{EV\text{-}disch}^{\ n}(t)$ is equal to 1 when the EV battery is discharging, otherwise is equal to 0. $\Phi_{EV\text{-}charg}^{\ n}(t)$ is equal to 1 when the EV battery is charging, otherwise is equal to 0.

By using constraints in (6.40) and (6.41) the house BSS and EV battery are prevented from charging from each other.

$$\Phi_{EV\text{-}disch}^{\ n}(t)+\Phi_{B\text{-}charg}^{\ n}(t)\leq 1 \tag{6.40}$$

$$\Phi_{EV\text{-}charg}^{\ n}(t)+\Phi_{B\text{-}disch}^{\ n}(t)\leq 1 \tag{6.41}$$

Constraints in (6.42) and (6.43) are used to ensure the EV battery is charged and discharged within allowable limits.

$$P_{EV\text{-}disch}^{\ n}(t)\leq \Phi_{EV\text{-}disch}^{\ n}(t)\times P_{EV\text{-}rating}^{\ n} \tag{6.42}$$

$$\left|P_{EV\text{-}charg}^{\ n}(t)\right|\leq \Phi_{EV\text{-}charg}^{\ n}(t)\times P_{EV\text{-}rating}^{\ n} \tag{6.43}$$

To ensure that the EV battery does not export energy to the grid, constraint (6.44) is used.

$$\Phi_{EV\text{-}disch}{}^{n}(t) + \Phi_{export}{}^{n}(t) \leq 1 \tag{6.44}$$

The operational costs $C_{house\text{-}cost}{}^{individual(n)}$ and $C_{house\text{-}cost}{}^{P2P(n)}$ for houses *A* and *B* when they are operating individually and when they are operating as a pair are updated for the presence of EVs and shiftable appliances as shown in (6.45) and (6.46), respectively:

$$C_{house\text{-}cost}{}^{individual(n)} = C_{buy}{}^{n} + C_{sell}{}^{n} + C_{BSS}{}^{n} + C_{EV}{}^{n} \tag{6.45}$$

$$C_{house\text{-}cost}{}^{P2P(n)} = C_{buy}{}^{n} + C_{sell}{}^{n} + C_{BSS}{}^{n} + C_{EV}{}^{n} - C_{P2P}{}^{n} \tag{6.46}$$

Fig. 6.4 illustrates the flowchart of the P2P EMS, which follows the procedure below:

- Input the parameters to the P2P EMS to minimise the cost function (6.30), which is subjected to constraints (6.31)-(6.38).
- Next, if appliances are on, constraints (6.7)-(6.11) must be met.
- The system checks if the EV is connected, and if so, constraints (6.12)-(6.21) must be met.
- Then calculate (4.8)-(4.12).
- During the off-peak hours, the system will verify if the house BSS has sufficient energy for the next peak hour by satisfying constraint (4.14), otherwise, constraint (4.13) must be satisfied.
- Finally, system constraints in (5.11)-(5.26) and (6.39)-(6.46) must be met and the output parameters are uploaded into the Central Controller.

6.5.2 Selection Level

The Selection level, described in Chapter 5- Subsection 5.5.2, is used here to choose the best pairs of houses.

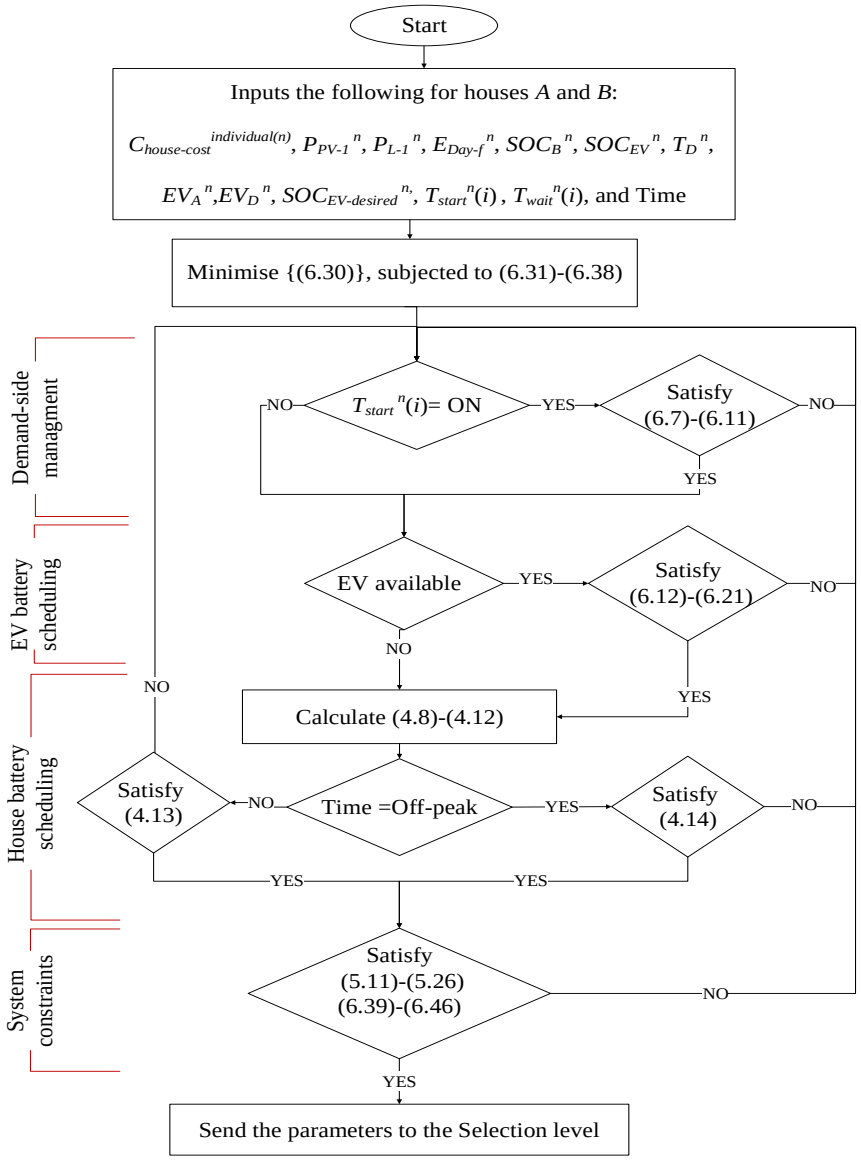

Fig. 6.4. Flowchart of the proposed P2P-EMS.

6.6 Case Studies

This study uses the forecast data and tariff prices in Chapter 5- Section 5.3. The proposed algorithm has been tested using the community data described in Section 6.2. The probability distribution functions of EV arrival and departure times are obtained from the National Household Travel Survey [179]. The algorithm in Fig. 6.2 is carried out in MATLAB software for each day of the four months from June to September 2014 with a sample time (ΔT) of 10 mins.

6.6.1 System Behaviour

This subsection discusses how the V2H mode and shiftable appliances affected houses nos. 1, 2 and 3 for 17th and 18th June 2014. Three houses are chosen from the six houses because they are sufficient to demonstrate the method and concepts involved.

Figs. 6.5 (a-1), (a-2), and (a-3) show generation and load demand for houses nos. 1, 2, and 3, respectively, for the two days 17th and 18th June 2014. The red solid and black solid lines represent P_{PV}^{n} and P_{L}^{n}, respectively, where n is the house number. Figs. 6.5 (b-1), (b-2), and (b-3) show the SOC of the house BSS, the SOC of the EV battery, EV departure time and EV arrival time for houses nos. 1, 2, and 3, respectively. The red solid and blue solid lines are SOC_{EV}^{n} and SOC_{B}^{n}, respectively. The first and second vertical black dashed lines show EV_{D}^{n} and EV_{A}^{n}, respectively. Figs. 6.5 (c-1), (c-2), and (c-3) present the power exchanged with the grid and neighbours. The red solid and blue dashed lines represent P_{P2P}^{n} and P_{G}^{n}, respectively. Figs. 6.5 (d-1), (d-2), and (d-3) present the schedules of the shiftable appliance in houses nos. 1, 2, and 3, respectively. The red solid and blue solid lines represent the users' requested operation for the dishwasher $P_{D\text{-}Sh}^{n}$ and the washing machine $P_{W\text{-}Sh}^{n}$, respectively. The red dashed and blue dashed represent the scheduled operation of the dishwasher P_{D}^{n} and the washing machine P_{W}^{n}, respectively, as operated by the CEMS.

From Figs. 6.5 (a-1) and (a-2), it can be seen that the energy consumed by houses nos. 1 and 2 is greater than the power generated from the PV for most of the time during day-1 and day-2. However, Fig. 6.5 (a-3) shows that for house no. 3 the PV power generated is greater than the demand for most of the time during both days.

Figs. 6.5 (b-1) and (b-3) show that for houses nos. 1 and 3 the EVs made only one journey per day for the two days considered, while for house no. 2 the EV made two journeys on day-1 and one journey on day-2 as shown in Fig. 6.5 (b-2). In addition, the EV batteries for all houses are fully charged during off-peak time to reduce energy purchases from the grid at high tariffs. It is noticeable from Figs. 6.5 (b-1) and (b-3) that the BSS of houses nos. 1 and 3 are not fully charged on either day, but the BSS of house no. 2 is fully charged from its neighbour during the second day, as shown in highlighted

box in Fig. 6.5 (c-2). This is because the forecasted energy for day-3 ($E_{Day\text{-}f}$) indicates that the generation is lower than demand. More detailed data for day-3 is presented in Figs. 6.8 and 6.9.

Figs. 6.5 (c-1), (c-2), and (c-3) show that during days 1 and 2, house no.1 exchanged power with houses nos. 2 and 3, respectively, and house no. 3 exchanged no power with its neighbour on day-1.

Figs. 6.5 (d-1), (d-2), and (d-3), show that the ON times of the shiftable appliances are moved to times where there is a surplus of PV power or times where the house can import power from a neighbour to reduce energy costs and peak load.

Figs. 6.6 and 6.7 present power exchange between houses nos. 1 and 3 during peak time on day-2. The red dashed, black solid, and blue solid lines represent P_{P2P}^{n}, P_{L}^{n}-P_{PV}^{n}, and P_{EV}^{n}, respectively. Where *n* refers to houses 1 and 3. As it can be seen, around 3:50 PM, the EV belonging to house no.1 discharged power to supply house no. 3 (see the black arrows in Figs. 6.6 and 6.7). In addition, around 4:45 PM, the EV belonging to house no.1 supplied power to houses nos. 1 (its own house) and 3. At 5:30 PM, the EV belonging to house no. 3 was plugged in and began to provide energy to house no. 1.

Fig. 6.8 presents the PV and load power for house no. 2 on day-3 (19th June 2014). The red solid and black solid lines represent P_{PV}^{2} and P_{L}^{2}, respectively. As seen in Fig. 6.8 the demand greatly exceeded generation. Thus, during day-2 the house BSS will be charged by a neighbour to meet the demands for day-3, see Figs. 6.5 (b-2), (c-2) and Fig. 6.9.

Fig. 6.9 presents the SOCs for EV battery and house BSS for house no. 2 on day-3. The blue solid and red solid lines are SOC_{B}^{2} and SOC_{EV}^{2}, respectively. The first and second vertical black dashed lines represent EV_{D}^{2} and EV_{A}^{2}, respectively. Fig. 6.9 shows that the house BSS is used to supply demands during day-3 to reduce the amount of energy purchased from the grid at high tariffs.

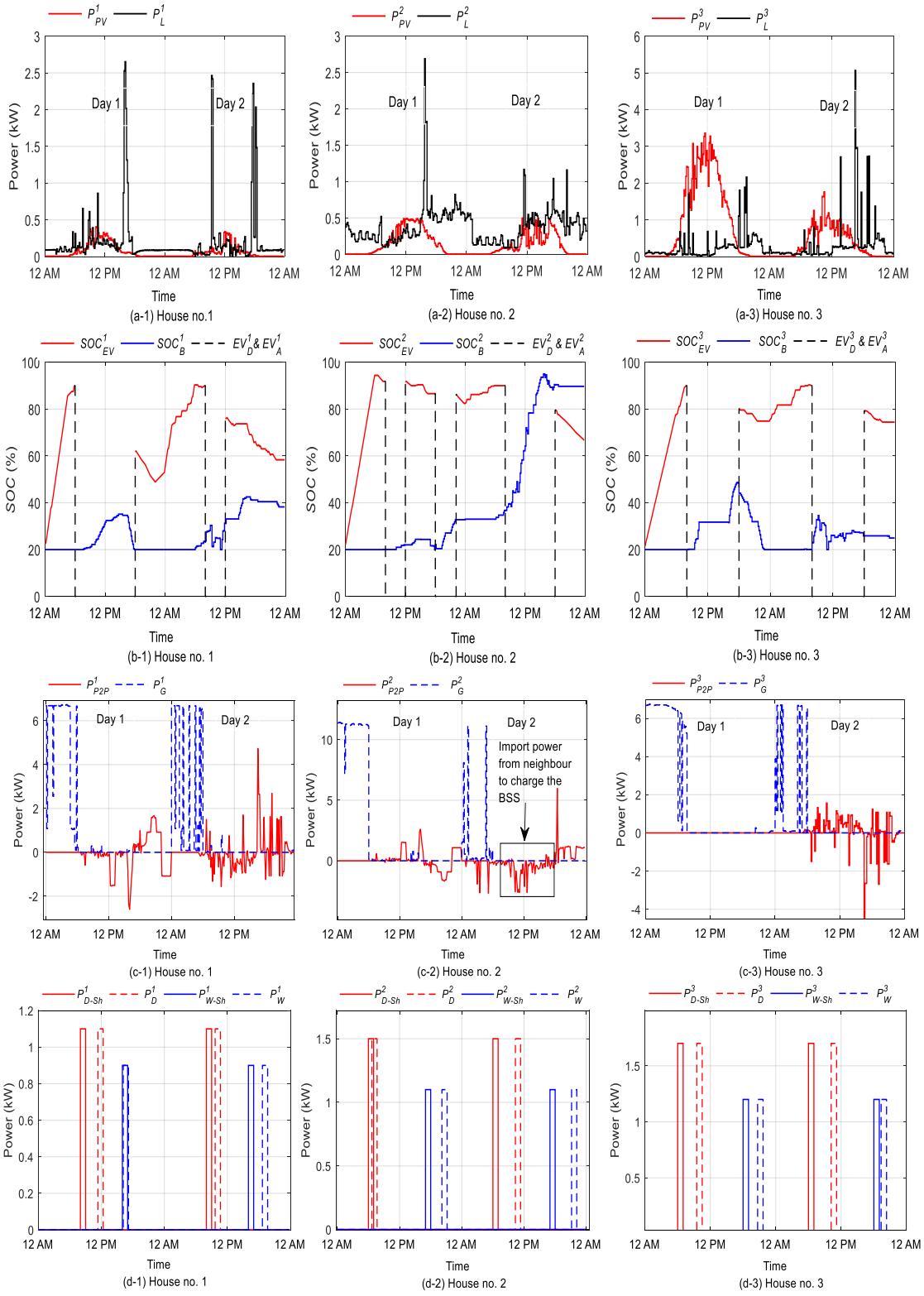

Fig. 6.5. System performance for houses nos. 1, 2 and 3 for 17th and 18th June 2014. Figs. (a-1), (a-2), and (a-3) present PV and load of houses nos. 1, 2 and 3, respectively. The red solid and black solid lines represent P_{PV}^{n} and P_{L}^{n}, respectively, where n is the

house number. Figs. (b-1), (b-2), and (b-3) present the SOC of the EV battery and house BSS, EV departure time, and EV arrival time of houses nos. 1, 2, and 3, respectively. The red solid and blue solid lines are SOC_{EV}^{n} and SOC_{B}^{n}, respectively. The first and second vertical black dashed lines show EV_{D}^{n} and EV_{A}^{n}, respectively. Figs. (c-1), (c-2), and (c-3) present the power exchanged by each house with the grid and neighbours. The red solid and blue dashed lines represent P_{P2P}^{n} and P_{G}^{n}, respectively. Figs (d-1), (d-2), and (d-3) present the schedules of the shiftable appliance in houses nos. 1, 2, and 3, respectively. The red solid and blue solid lines represent the users' requested operation for the dishwasher $P_{D\text{-}Sh}^{n}$ and the washing machine $P_{W\text{-}Sh}^{n}$, respectively. The red dashed and blue dashed represent the scheduled operation of the dishwasher P_{D}^{n} and the washing machine P_{W}^{n}, respectively, as operated by the CEMS.

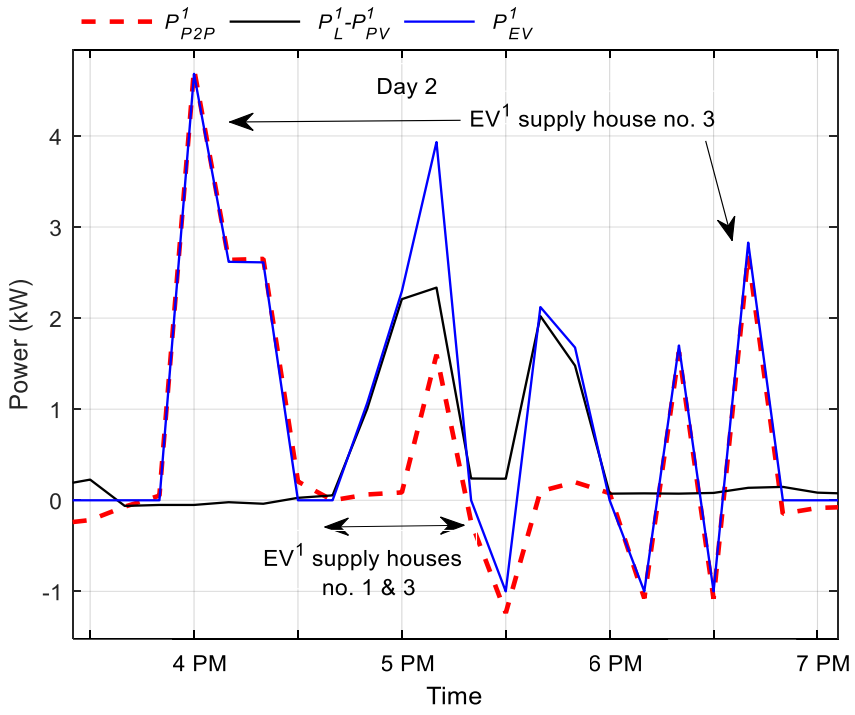

Fig. 6.6. Power exchanged by house no. 1 during peak time on day-2. The red dashed, black solid, and blue solid lines represent P_{P2P}^{1}, P_{L}^{1}-P_{PV}^{1}, and P_{EV}^{1}, respectively.

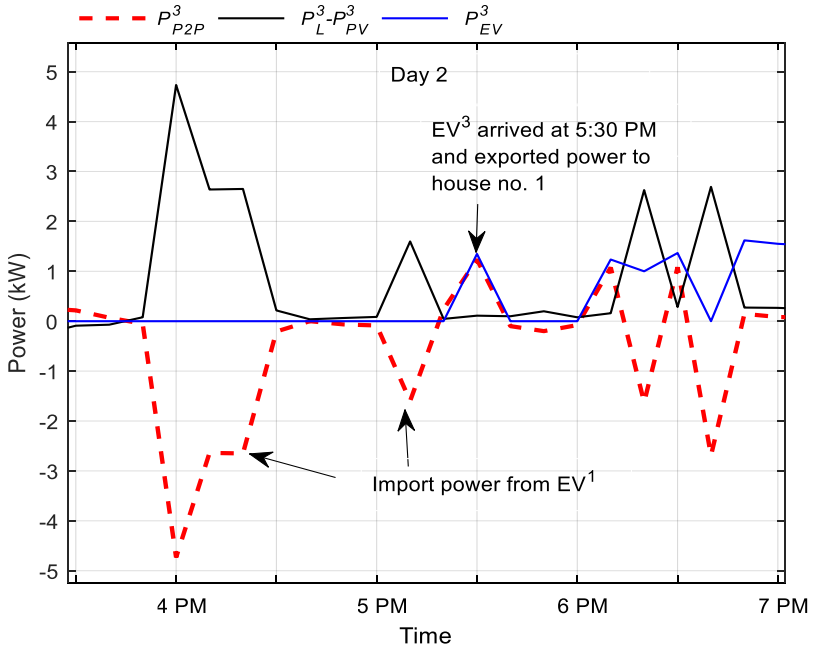

Fig. 6.7. Power exchanged by house no. 3 during peak times on day-2. The red dashed, black solid, and blue solid lines represent P_{P2P}^3, P_L^3-P_{PV}^3, and P_{EV}^3, respectively.

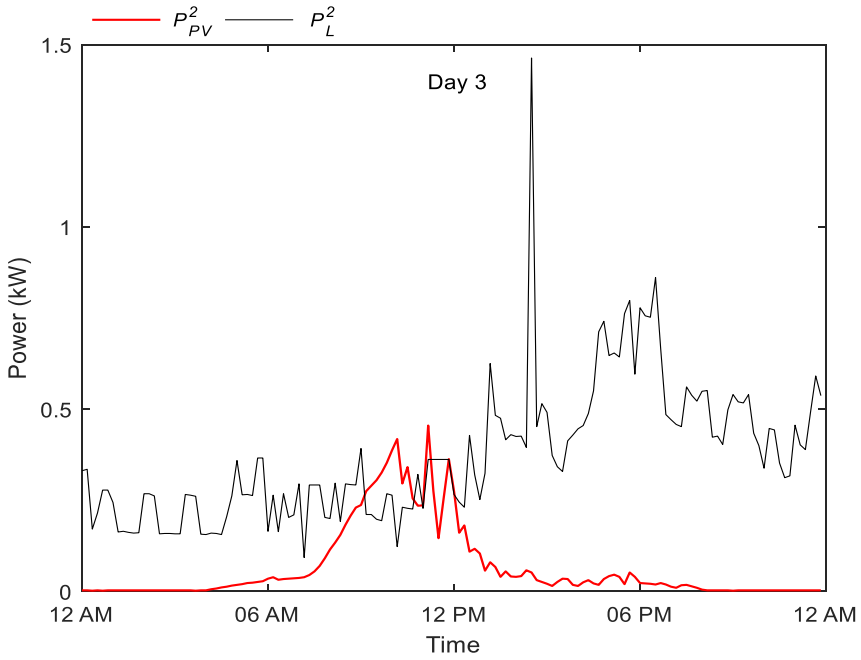

Fig. 6.8. PV and load for house no. 2 for day-3 (19th June 2014). The red solid and black solid lines represent P_{PV}^2 and P_L^2, respectively.

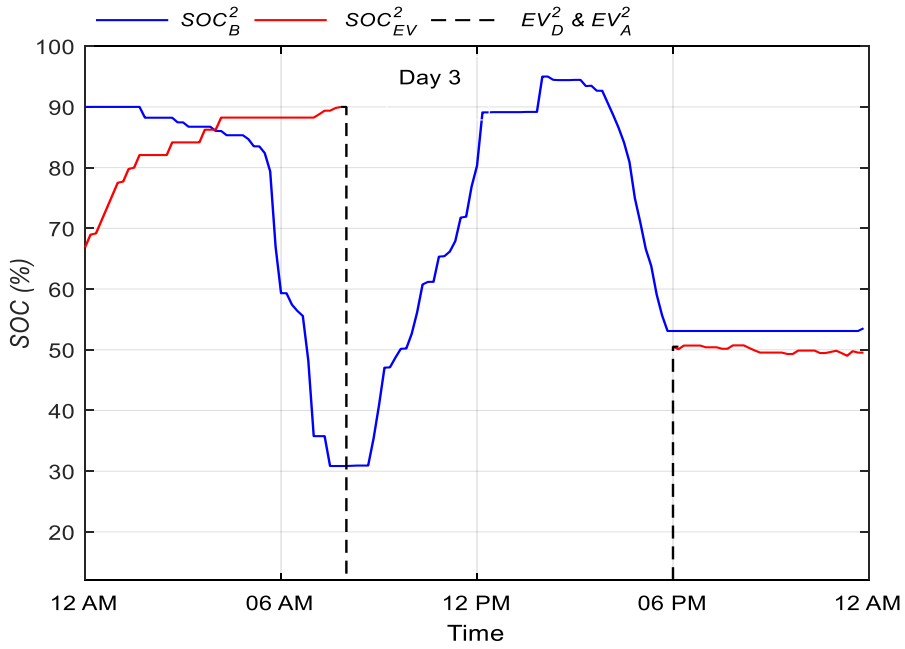

Fig. 6.9. The SOC of the EV battery and house BSS for house no. 2 during day-3 (19th June 2014). The blue solid and red solid lines are SOC_B^2 and SOC_{EV}^2, respectively. The first and second vertical dashed lines show EV_D^2 and EV_A^2, respectively.

6.6.2 Comparing Energy Exchange and Energy Costs

Table 6.3 presents operating costs for each of the six houses with and without V2H mode operational for the four months from June to September 2014. By introducing the V2H mode the overall operating costs for individual houses in the community are reduced by up to 23%, while the total operating cost (energy cost + BSS degradation cost) for the community (all six houses) is reduced by 15%.

Table 6.4 presents the absolute net energy exchange with the grid, with and without V2H mode operational for the four months from June to September 2014. Table 6.4 shows that introducing the V2H mode reduced the overall absolute net energy exchange between the community (i.e., 6 houses) and the grid by 3%. However, while not all houses experienced a reduction, the aim of this system is to reduce the overall energy exchange.

Table 6.3. Energy costs for the community with and without V2H mode for four months from June to September 2014

House number	Operating cost without V2H mode (£)	Operating cost with V2H mode (£)	Percentage (%)
1	139	123	12
2	210	175	17
3	112	86	23
4	119	110	8
5	132	114	14
6	107	87	19
Total	819	695	15

Table 6.4. Absolute net energy exchange between the houses and grid with and without V2H mode for the four months from June to September 2014

House number	Absolute net energy exchanged for P2P EMS without V2H (kWh)	Absolute net energy exchanged for P2P EMS with V2H (kWh)
1	1661	1674
2	2329	2517
3	1474	1273
4	1849	2222
5	1933	1829
6	1946	1384
Total	11192	10898

6.7 Conclusion

The proposed system in this chapter was an extended version of the CEMS presented in Chapter 5. This study verified the importance of the contribution of the EVs to reducing the burden on the grid. Introducing the V2H mode in the CEMS reduced the total

operating cost of the community by 15% in comparison to being without the V2H mode. The absolute net energy exchange between the community and the grid was reduced by 3%. The proposed system also considered shifting usage times of appliances, such as washing machines and dishwasher to off-peak and/ or when PV energy is surplus which reduced the grid's burden and energy costs.

7 CONCLUSIONS AND FUTURE WORK

The penetration of Distributed Energy Resources (DERs) at consumption and distribution levels is increasing dramatically, necessitating robust electrical network systems. Unlike traditional fuel sources, DERs are intermittent, which challenges network operators to balance generation and demand [180]. To address these challenges, several countries are promoting the utilisation of the self-consumption approach for Renewable Energy Sources (RESs) within Energy Management Systems (EMS) to reduce the burden on the national grid [6, 7].

In this work, real-time Fuzzy Logic-based EMS (FL-EMS) and day-ahead Mixed Integer Linear Programming-based EMS (MILP-EMS) are proposed to maximise PV self-consumption by reducing the net energy exchange between Active Office Building (AOB) and the grid. The results demonstrate that both methods effectively reduce the net energy exchange with the grid compared to other approaches.

Then, the problem is expanded to incorporate a community energy management controller capable of collectively controlling the Battery Storage Systems (BSSs), Electric Vehicles (EVs), and shiftable appliances within a community of houses. The Community Energy Management System (CEMS) aims to reduce the net energy exchange with the grid by optimising the community's overall energy consumption and generation rather than each house operating individually. The proposed CEMS demonstrates further reductions in the net energy exchange with the grid compared to individual house operations. In addition, utilising EVs and shiftable appliances within the CEMS can offer significant benefits. This includes enhanced efficiency, cost-effectiveness, and overall performance. Moreover, incorporating EV batteries as additional energy storage can reduce the need for new infrastructure, additional charging stations, and centralised storage facilities [3].

Some research gaps remain to be addressed, including:

1. An economic analysis that includes the cost of system components and profitability need to be carried out, analysing the effect of different sizes of the

Battery Storage System (BSS) and the Photovoltaic (PV) generation in a CEMS. In addition, different tariffs and policies in both residential EMS and CEMS need to be explored.

2. Investigating the application of a CEMS in a more complex management strategy comprising peer to system to peer trading architecture, such as method proposed in [181].
3. Considering different loads such as semi-controlled appliances (e.g., heaters) at household and community levels to achieve further benefits.
4. Study different P2P energy trading methods, such as auction or game theory trading, to reduce energy exchange with the grid instead of reducing energy costs.
5. Explore more advanced EMS using Artificial Intelligence (AI) schemes.
6. Implement MILP-EMS and CEMS in real-time to validate the profitability of such systems.

REFERENCES

[1] K. Mansiri, S. Sukchai, and C. Sirisamphanwong, ‘‘Fuzzy Control Algorithm for Battery Storage and Demand Side Power Management for Economic Operation of the Smart Grid System at Naresuan University, Thailand,’’ *IEEE Access*, vol. 6, pp. 32440-32449, 2018, doi: 10.1109/ACCESS.2018.2838581.

[2] J. C. Peña-Aguirre, A. Barranco-Gutiérrez, J. A. Padilla-Medina, A. Espinosa-Calderon, and F. J. Pérez-Pinal, ‘‘Fuzzy Logic Power Management Strategy for a Residential DC-Microgrid,’’ *IEEE Access*, vol. 8, pp. 116733-116743, 2020, doi: 10.1109/ACCESS.2020.3004611.

[3] M. Elkazaz, M. Summer, S. Pholboon, R. Davies, and D. Thomas, ‘‘Performance Assessment of an Energy Management System for a Home Microgrid with PV Generation,’’ *Energies*, vol. 13, pp. 3436, 2020, doi: https://doi.org/10.3390/en13133436.

[4] M. Elkazaz, M. Sumner, E. Naghiyev, S. Pholboon, R. Davies, and D. Thomas, ‘‘A hierarchical two-stage energy management for a home microgrid using model predictive and real-time controllers,’’ *Applied Energy*, vol. 269, pp. 115118, 2020, doi: https://doi.org/10.1016/j.apenergy.2020.115118.

[5] M. Elkazaz, M. Sumner, and D. Thomas, ‘‘A hierarchical and decentralized energy management system for peer-to-peer energy trading,’’ *Applied Energy*, vol. 291, pp. 116766, 2021, doi: https://doi.org/10.1016/j.apenergy.2021.116766.

[6] V. Jately, B. Azzopardi, B. Bartolo, R. Mikalauskiene and S. Bhattacharya, ‘‘Techno-Economic Assessment of PV System for self-consumption Case Study of Malta”, *47th IEEE Photovoltaic Specialists Conference* (PVSC), Calgary, Canada, 2020, pp. 2151-2153, doi: 10.1109/PVSC45281.2020.9300680.

[7] M. Monfared, M. Fazeli, R. Lewis, and J. Searle,‘‘Fuzzy Predictor With Additive Learning for Very Short-Term PV Power Generation,’’ *IEEE Access*, vol. 7, pp. 91183-91192, 2019, doi: 10.1109/ACCESS.2019.2927804.

[8] GreenMatch (2021). *Smart Export Guarantee*. Accessed: 1/1/2021. [Online]. Available: https://www.greenmatch.co.uk/green-energy/grants/smart-export-guarantee.

[9] N. Liu, X. Yu, C. Wang, C. Li, L. Ma and J. Lei, ‘‘Energy-Sharing Model With Price-Based Demand Response for Microgrids of Peer-to-Peer Prosumers,’’ *IEEE Transactions on Power Systems*, vol. 32, no. 5, pp. 3569-3583, Sept. 2017, doi: 10.1109/TPWRS.2017.2649558.

[10] E. Mckenna, J. Pless, and S. J. Darby, ‘‘Solar photovoltaic self-consumption in the UK residential sector: New estimates from a smart grid demonstration project,’’ *Energy Policy*, 2018, vol. 118, pp. 482-491, doi: https://doi.org/10.1016/j.enpol.2018.04.006.

[11] GOV. UK (2021). *UK ENERGY IN BRIEF 2021*. Accessed: 4/1/2022. [Online]. Available: https://www.gov.uk/government/statistics/uk-energy-in-brief-2021.

[12] GOV.UK (2022). *Transport and environment statistics 2022.* Accessed: 22/1/2023. [Online]. Available at: https://www.gov.uk/government/statistics/transport-and-environment-statistics-2022/transport-and-environment-statistics-2022.

[13] S. Gao, K. T. Chau, C. Liu, D. Wu, and C. C. Chan, ‘‘Integrated Energy Management of Plug-in Electric Vehicles in Power Grid With Renewables,’’ *IEEE Transactions on Vehicular Technology*, vol. 63, no. 7, pp. 3019-3027, 2014, doi: 10.1109/TVT.2014.2316153.

[14] SOLAR POWER PORTAL (2020). *Solar PV costs fall 82% over the last decade, says IRENA.* Accessed: 6/1/2021. [Online]. Available: https://www.solarpowerportal.co.uk/news/solar_pv_costs_fall_82_over_the_last_decade_says_irena.

[15] IMAGES (2023). *Photovoltaic Cells – Generating electricity.* Accessed: 25/6/2023. [Online]. Available: https://www.imagesco.com/articles/photovoltaic/photovoltaic-pg4.html.

[16] R. Hledik, J. Lazarim, and L. Schwartz. ‘‘Distribution System Pricing with Distributed Energy Resources, ’’ *Future Electric Utility Regulation,* United States, 2017, doi:10.2172/1375194.

[17] M. Fazeli, P. M. Holland, and M. Baruwa, ‘‘‘‘Grid”-Less Power Systems: A Vision for Future Structure of Power Networks,’’ *IEEE Access,* vol. 8, pp. 159120-159131, 2020, doi: 10.1109/ACCESS.2020.3020455.

[18] Professional Electrician & Installer (2022). *What is a prosumer?.* Accessed: 19/3/2022. [Online]. Available: https://professional-electrician.com/technical/as-concerns-grow-about-the-increase-in-energy-crisis-and-security-of-supply-niceic-explains-what-is-a-prosumer/#:~:text=However%2C%20in%20our%20world%20(electrotechnical,1%20million%20back%20in%202015.

[19] C. Zhang, J. Wu, Y. Zhou, M. Cheng, and C. Long, ‘‘Peer-to-Peer energy trading in a Microgrid,’’ *Applied Energy*, vol. 220, pp. 1–12, 2018, doi: https://doi.org/10.1016/j.apenergy.2018.03.010.

[20] Microgrid Knowledge (2023). *What is a microgrid ?*. Accessed: 12/2/2023. [Online]. Available: https://www.microgridknowledge.com/about-microgrids/article/11429017/what-is-a-microgrid.

[21] C. García-Santacruz, P. J. Gómez, J. M. Carrasco and E. Galván, ‘‘Multi P2P Energy Trading Market, Integrating Energy Storage Systems and Used for Optimal Scheduling,’’ *IEEE Access*, vol. 10, pp. 64302-64315, 2022, doi: 10.1109/ACCESS.2022.3182698.

[22] T. D. Hutty, A. Pena-Bello, S. Dong, D. Parra, R. Rothman, and S. Brown, ‘‘Peer-to-peer electricity trading as an enabler of increased PV and EV ownership,’’ *Energy Conversion and Management*, vol. 245, pp. 114634, 2021, doi: https://doi.org/10.1016/j.enconman.2021.114634.

[23] greentechedia (2020). *Germany's Maxed-Out Grid Is Causing Trouble Across Europe*. Accessed: 7/2/2022. [Online]. Available: https://www.greentechmedia.com/articles/read/germanys-stressed-grid-is-causing-trouble-across-europe.

[24] Eenergy saving trust (2020). *Time of use tariffs: all you need to know*. Accessed: 3/4/2022. [Online]. Available: https://energysavingtrust.org.uk/time-use-tariffs-all-you-need-know/.

[25] International district energy association (2020). *Wind Power Monthly*. Accessed: 6/3/2022. [Online]. Available: https://www.districtenergy.org/blogs/district-energy/2020/05/01/germanys-negative-price-rules-bring-negative-conse.

[26] Los Angeles Times (2017). *California invested heavily in solar power. Now there's so much that other states are sometimes paid to take it*. Accessed: 4/2/2022. [Online]. Available: https://www.latimes.com/projects/la-fi-electricity-solar/.

[27] Ofgem (2020). *Feed-in Tariff (FIT) Rates.* Accessed: 4/5/2020. [Online]. Available: https://www.ofgem.gov.uk/environmental-programmes/fit/fit-tariff-rates.

[28] A. Sorour, M. Fazeli, M. Monfared, A. A. Fahmy, J. R. Searle, and R. P. Lewis, ‘‘Forecast-Based Energy Management for Domestic PV-Battery Systems: A U.K. Case Study,’’ *IEEE Access*, vol. 9, pp. 58953-58965, 2021, doi: 10.1109/ACCESS.2021.3072961.

[29] H. Shareef, M. S. Ahmed, A. Mohamed, and E. Al Hassan, ‘‘Review on Home Energy Management System Considering Demand Responses, Smart Technologies, and Intelligent Controllers,’’ *IEEE Access*, vol. 6, pp. 24498-24509, 2018, doi: 10.1109/ACCESS.2018.2831917.

[30] Department for business, energy and industrial strategy (2022). *Review of solar PV capacity publications.* Accessed: 6/10/2022. [Online]. Available: https://assets.publishing.service.gov.uk/government/uploads/system/uploads/attachment_data/file/1064817/Review_of_solar_PV_capacity_publications.pdf.

[31] Which? (2021). *What was the feed-in tariff?*. Accessed: 5/1/2022. [Online]. Available: https://www.which.co.uk/reviews/feed-in-tariffs/article/feed-in-tariffs/what-was-the-feed-in-tariff-aAsa36S95iJy.

[32] The greenage (2013). *What is Economy 7*. Accessed: 6/10/2021. [Online]. Available: https://www.thegreenage.co.uk/what-is-economy-7-tariff/#:~:text=Economy%207%20is%20simply%20a,energy%20at%20off%20peak%20times.&text=As%20a%20result%20Economy%207,find%20a%20use%20for%20it.

[33] Simple switch (2020). *Innovative ‘Time of Day’ Tariff Launched by Green Energy UK.* Accessed: 9/2/2022. [Online]. Available: https://www.simplyswitch.com/innovative-time-of-day-tariff-launched-by-green-energy-uk/.

[34] Y. Lin, H. Tang, T. Shen and C. Hsia, ‘‘A Smart Home Energy Management System Utilizing Neurocomputing-Based Time-Series Load Modeling and Forecasting Facilitated by Energy Decomposition for Smart Home Automation,’’ *IEEE Access,* vol. 10, pp. 116747-116765, 2022, doi: 10.1109/ACCESS.2022.3219068.

[35] J. Zhao, S. Kucuksari, E. Mazhari, and Y. J. Son, ‘‘Integrated analysis of high-penetration PV and PHEV with energy storage and demand response,’’ *Applied Energy,* vol. 112, pp. 35–51, 2013, doi: http://dx.doi.org/10.1016/j.apenergy.2013.05.070.

[36] M. Monfared, M. Fazeli, R. Lewis, and J. Searle, ‘‘Day-Ahead Prediction of PV Generation Using Weather Forecast Data: a Case Study in the UK,’’ *International Conference on Electrical, Communication, and Computer Engineering* (*ICECCE*), Istanbul, Turkey, 2020, pp. 1-5, doi: 10.1109/ICECCE49384.2020.9179454.

[37] M. Seyedmahmoudian, E. Jamei et al., ‘‘Short-Term Forecasting of the Output Power of a Building-Integrated Photovoltaic System Using a Metaheuristic Approach,’’ *Energies,* vol. 11, pp. 1260, 2018, doi: 10.3390/en11051260.

[38] M. Ali, M. Adnan, M. Tariq and H. V. Poor, ‘‘Load Forecasting Through Estimated Parametrized Based Fuzzy Inference System in Smart Grids,’’ *IEEE Transactions on Fuzzy Systems,* vol. 29, no. 1, pp. 156-165, Jan. 2021, doi: 10.1109/TFUZZ.2020.2986982.

[39] M. S. Hossain and H. Mahmood, ‘‘Short-Term Photovoltaic Power Forecasting Using an LSTM Neural Network and Synthetic Weather Forecast,’’ *IEEE Access,* vol. 8, pp. 172524-172533, 2020, doi: 10.1109/ACCESS.2020.3024901.

[40] DNV (2023). *Forecaster.* Accessed: 3/1/2023. [Online]. Available: https://www.dnv.com/power-renewables/services/forecaster/index.html.

[41] VAISALA (2023). *Forecaster For Renewable Energy.* Accessed: 4/1/2023. [Online]. Available: https://www.vaisala.com/en/products/renewable-energy/forecaster.

[42] AleaSoft Energy Forecasting (2023). *AleaSoft Energy Forecasting.* Accessed: 4/1/2023. [Online]. Available: https://aleasoft.com/products-and-services/.

[43] A. Yoza, A. M. Howlader, K. Uchida, A. Yona, and T. Senjyu,‘‘Optimal scheduling method of controllable loads in smart house considering forecast error,’’ *IEEE 10th International Conference on Power Electronics and Drive Systems (PEDS),* 2013, pp. 84-89, doi: 10.1109/PEDS.2013.6526993.

[44] A. Guwaeder and R. Ramakumar, ‘‘Statistical analysis of PV insolation data,’’ *IEEE 44th Photovoltaic Specialist Conference (PVSC),* 2017, pp. 1122-1126, doi: 10.1109/PVSC.2017.8366723.

[45] X. Yan, D. Abbes, and B. Francois, ‘‘Uncertainty analysis for day ahead power reserve quantification in an urban microgrid including PV generators,’’

Renewable Energy, vol. 106, pp. 288-297, 2017, doi: https://doi.org/10.1016/j.renene.2017.01.022.

[46] H. Bri-Mathias, F. Anthony , O. Kirsten , L. Debra , and M.Michael, ‘‘A Comparison of Wind Power and Load Forecasting Error Distributions,’’ *World Renewable Energy Forum,* CO, USA, 2012.

[47] British Gas (2023). *Help with Hive Active Heating*. Accessed: 2/3/2023. [Online]. Available: https://www.britishgas.co.uk/help-and-support/smart-home/help-with-hive-active-heating.

[48] S. B. Raha and D. Biswas, ‘‘Fuzzy Controlled Demand Response Energy Management for Economic Microgrid Planning,’’ *IEEE International Conference on Power Electronics, Smart Grid and Renewable Energy* (*PESGRE2020*), Cochin, India, 2020, pp. 1-6, doi: 10.1109/PESGRE45664.2020.9070451.

[49] M. K. Mishra and S. K. Parida, ‘‘A Game Theoretic Approach for Demand-Side Management Using Real-Time Variable Peak Pricing Considering Distributed Energy Resources,’’ *IEEE Systems Journal*, vol. 16, no. 1, pp. 144-154, 2022, doi: 10.1109/JSYST.2020.3033128.

[50] S. Malik, K. Lee and D. Kim, ‘‘Optimal Control Based on Scheduling for Comfortable Smart Home Environment,’’ *IEEE Access*, vol. 8, pp. 218245-218256, 2020, doi: 10.1109/ACCESS.2020.3042534.

[51] R. Manojkumar, C. Kumar, and S. Ganguly, ‘‘Optimal Demand Response in a Residential PV Storage System Using Energy Pricing Limits,’’*IEEE Transactions on Industrial Informatics,* vol. 18, pp. 2497-2507, 2022, doi: 10.1109/TII.2021.3103014.

[52] W. Schram, I. Lampropoulos, and W. Sark, ‘‘Photovoltaic systems coupled with batteries that are optimally sized for household self-consumption: Assessment of peak shaving potential,’’*Applied Energy,* vol. 223, pp. 69-81, 2018, doi: https://doi.org/10.1016/j.apenergy.2018.04.023.

[53] M. A. Hannan, M. M. Hoque, A. Hussain, Y. Yusof, and P. J. Ker, ‘‘State-of-the-Art and Energy Management System of Lithium-Ion Batteries in Electric Vehicle Applications: Issues and Recommendations,’’ *IEEE Access*, vol. 6, pp. 19362-19378, 2018, doi: 10.1109/ACCESS.2018.2817655.

[54] DNV. *TESLA’S BATTERY DAY AND THE ENERGY TRANSITION.* Accessed: 2/2/2022. [Online]. Available: https://www.dnv.com/feature/tesla-battery-day-energy-transition.html.

[55] BloombergNEF (2023). *A Behind the Scenes Take on Lithium-ion Battery Prices.* Accessed: 2/1/2023. [Online]. Available at: https://about.bnef.com/blog/behind-scenes-take-lithium-ion-battery-prices/.

[56] Which?(2022). *Solar panel battery storage.* Accessed: 12/5/2022. [Online]. Available: https://www.which.co.uk/reviews/solar-panels/article/solar-panels/solar-panel-battery-storage-a2AfJ0s5tCyT.

[57] G. Abdelaal, M. I. Gilany, M. Elshahed, M. Elshahed, H. M. Sharaf, and A. EL'Gharably, ‘‘Integration of Electric Vehicles in Home Energy Management Considering Urgent Charging and Battery Degradation,’’ *IEEE Access,* vol. 9, P. 47713-47730, 2021, doi: 10.1109/ACCESS.2021.3068421.

[58] B. Xu, J. Zhao, T. Zheng, E. Litvinov, and D. S. Kirschen, ‘‘Factoring the Cycle Aging Cost of Batteries Participating in Electricity Markets,’’ *IEEE Transactions on Power Systems,* vol. 33, no. 2, pp. 2248-2259, March 2018, doi: 10.1109/TPWRS.2017.2733339.

[59] V. Diaz, D. Cantane, A. Santos, and O. Junior, ‘‘Comparative Analysis of Degradation Assessment of Battery Energy Storage Systems in PV Smoothing Application,’’ *Energies* 2021, 14 (12), 3600, dio: https://doi.org/10.3390/en14123600.

[60] N. Narayan, T. Papakosta, V. Vega-Garita, Z. Qin, J. Popovic-Gerber, P. Bauer, and M. Zeman, ‘‘Estimating battery lifetimes in Solar Home System design using a practical modelling methodology,’’ *Applied Energy,* vol. 288, pp. 1629-1639, 2018. doi: ttps://doi.org/10.1016/j.apenergy.2018.06.152.

[61] F. Y. Melhem, O. Grunder, Z. Hammoudan, and N. Moubayed, ‘‘Optimization and Energy Management in Smart Home Considering Photovoltaic, Wind, and Battery Storage System With Integration of Electric Vehicles,’’ *Canadian Journal of Electrical and Computer Engineering,* vol. 40, pp. 128-138, 2017, doi: 10.1109/CJECE.2017.2716780.

[62] A. Sorour, M. Fazeli, M. Monfared, A. A. Fahmy, J. R. Searle, and R. P. Lewis, ‘‘MILP Optimized Management of Domestic PV-Battery Using Two Days-Ahead Forecasts,’’ *IEEE Access*, vol. 10, pp. 29357-29366, 2022, doi: 10.1109/ACCESS.2022.3158303.

[63] A. Al-Ogaili, T. Hashim, et al., ‘‘Review on Scheduling, Clustering, and Forecasting Strategies for Controlling Electric Vehicle Charging: Challenges and Recommendations,’’ *IEEE Access*, vol. 7, pp. 128353-128371, 2019, doi: 10.1109/ACCESS.2019.2939595.

[64] T. Chen, X. Zhang, J. Wang, J. Li, C. Wu, et al., ‘‘A Review on Electric Vehicle Charging Infrastructure Development in the UK,’’ *Journal of Modern Power Systems and Clean Energy*, vol. 8, no. 2, pp. 193-205, March 2020, doi: 10.35833/MPCE.2018.000374.

[65] Iea (2023). *Electric Vehicles.* Accessed: 2/3/2023. [Online]. Available: https://www.iea.org/reports/electric-vehicles.

[66] GOV.UK (2022). *Plug-in grant for cars to end as focus moves to improving electric vehicle charging.* Accessed: 1/2/2023. [Online]. Available at: https://www.gov.uk/government/news/plug-in-grant-for-cars-to-end-as-focus-moves-to-improving-electric-vehicle-charging.

[67] SMS (2019). *UK peer-to-peer energy trading trials get underway.* Accessed: 6/1/2023. [Online]. Available at: https://www.sms-plc.com/insights/blogs-news/uk-peer-to-peer-energy-trading-trials-get-underway/.

[68] S. Shahriar, A. R. Al-Ali, A. H. Osman, S. Dhou, and M. Nijim, ‘‘Machine Learning Approaches for EV Charging Behavior: A Review,’’ *IEEE Access*, vol. 8, pp. 168980-168993, 2020, doi: 10.1109/ACCESS.2020.3023388.

[69] Mr. Sustainability (2023). *EV Battery Prices Plunge 89% in Ten Years.* Accessed: 4/2/2023. [Online]. Available:https://www.mr-sustainability.com/stories/2021/ev-battery-prices-plunge-89-in-ten-years.

[70] EDF energy (2023). *Road tax & company car tax on electric cars.* Accessed: 12/1/2023. [Online]. Available at: https://www.edfenergy.com/electric-cars/tax-road-company.

[71] GOV.UK (2022). *Grant schemes for electric vehicle charging infrastructure.* Accessed: 12/1/2023. [Online]. Available at: https://www.gov.uk/government/collections/government-grants-for-low-emission-vehicles.

[72] City of Westminster (2023). *Electric vehicles.* Accessed: 20/1/2023. [Online]. Available at: https://www.westminster.gov.uk/parking/electric-vehicles.

[73] R. Carmichael, R. Gross, R. Hanna, A. Rhodes, and T. Green, ‘‘The Demand Response Technology Cluster: Accelerating UK residential consumer engagement with time-of-use tariffs, electric vehicles and smart meters via digital comparison tools,’’ *Renewable and Sustainable Energy Reviews*, vol. 139, pp. 110701, 2021, dio: https://doi.org/10.1016/j.rser.2020.110701.

[74] N. G. Paterakis, O. Erdinc, I. N. Pappi, A. G. Bakirtzis, and J. P. S. Catalao, ‘‘Coordinated operation of a neighborhood of smart households comprising electric vehicles, energy storage and distributed generation,’’ *IEEE Trans. Smart Grid*, vol. 7, no. 6, , pp. 2736-2747, 2016, doi: 10.1109/TSG.2015.2512501.

[75] M. Amir, Zaheeruddin, and A. Haque, ‘‘Optimal Scheduling of Charging/Discharging Power and EVs Pattern Using Stochastic Techniques in V2G System,’’ *IEEE Transportation Electrification Conference* (ITEC-India), pp. 1-6, 2021, doi: 10.1109/ITEC-India53713.2021.9932455.

[76] K. Ginigeme and Z. Wang, ‘‘Distributed Optimal Vehicle-To-Grid Approaches With Consideration of Battery Degradation Cost Under Real-Time Pricing,’’ *IEEE Access*, vol. 8, pp. 5225-5235, 2020, doi: 10.1109/ACCESS.2019.2963692.

[77] K. Kaur, N. Kumar, and M. Singh, ‘‘Coordinated Power Control of Electric Vehicles for Grid Frequency Support: MILP-Based Hierarchical Control Design,’’ *IEEE Transactions on Smart Grid*, vol. 10, no. 3, pp. 3364-3373, 2019, doi: 10.1109/TSG.2018.2825322.

[78] X. Chen and K. -C. Leung, ‘‘Non-Cooperative and Cooperative Optimization of Scheduling With Vehicle-to-Grid Regulation Services,’’ *IEEE Transactions on Vehicular Technology*, vol. 69, no. 1, pp. 114-130, 2020, doi: 10.1109/TVT.2019.2952712.

[79] Y. Huang, ‘‘Day-Ahead Optimal Control of PEV Battery Storage Devices Taking Into Account the Voltage Regulation of the Residential Power Grid,’’ *IEEE*

Transactions on Power Systems, vol. 34, no. 6, pp. 4154-4167, Nov. 2019, doi: 10.1109/TPWRS.2019.2917009.

[80] Project Sciurus (2022). *Sciurus: Domestic V2G Demonstration*. Accessed: 11/12/2022. [Online]. Available: https://www.cenex.co.uk/projects-case-studies/sciurus/.

[81] R. Hemmati, H. Mehrjerdi, N. A. Al-Emadi, and E. Rakhshani, ‘‘Mutual Vehicle-to-Home and Vehicle-to-Grid Operation Considering Solar-Load Uncertainty,’’ *2nd International Conference on Smart Grid and Renewable Energy (SGRE)*, 2019, pp. 1-4, doi: 10.1109/SGRE46976.2019.9020685.

[82] B. Zafar and S. Slama,‘‘PV-EV integrated home energy management using vehicle-to-home (V2H) technology and household occupant behaviors’’, *Energy Strategy Reviews*, vol. 44, pp. 101001, 2022, doi: https://doi.org/10.1016/j.esr.2022.101001.

[83] R. Roche, F. Berthold, F. Gao, F. Wang, A. Ravey, and S. Williamson, ‘‘A model and strategy to improve smart home energy resilience during outages using vehicle-to-home,’’ *IEEE International Electric Vehicle Conference*, 2014, pp. 1-6, doi: 10.1109/IEVC.2014.7056106.

[84] T. Moreno, G. Fernandez, P. Garcia, and F. Rodriguez, ‘‘Energy Management Strategy for Micro-Grids with PV-Battery Systems and Electric Vehicles,’’ *Energies*, vol. 11, pp. 522, 2018, dio: https://doi.org/10.3390/en11030522.

[85] B. Sharma and J. Maherchandani, ‘‘A Review on Integration of Electric Vehicle in Smart Grid: Operational modes, Issues and Challenges,’’ *International Conference on Computer Communication and Informatics*, pp. 1-5, 2022, doi: 10.1109/ICCCI54379.2022.9740940.

[86] Y. Wang and D. Infield, ‘‘Markov Chain Monte Carlo simulation of electric vehicle use for network integration studies,’’ *International Journal of Electrical Power & Energy Systems*, vol. 99, pp. 85-94, 2018, dio: https://doi.org/10.1016/j.ijepes.2018.01.008.

[87] M. Di Somma, G. Graditi, E. Heydarian-Forushani, M. Shafie-khah, and P. Siano. ‘‘Stochastic optimal scheduling of distributed energy resources with renewables considering economic and environmental aspects,’’ *Renewable Energy, vol.116, pp.* 272–287, 2018, doi: https://doi.org/10.1016/j.renene.2017.09.074.

[88] R. Zhang, S. E, and R. Samuel, ‘‘Fuzzy Efficient Energy Smart Home Management System for Renewable Energy Resources,’’ Sustainability, vol. 12, no. 8, 2020, doi: 10.3390/su12083115.

[89] S. A. Pourmousavi, M. H. Nehrir, C. M. Colson, and C.Wang, ‘‘Real-Time Energy Management of a Stand-Alone Hybrid Wind-Microturbine Energy System Using Particle Swarm Optimization,’’ *IEEE Transactions on Sustainable Energy*, vol. 1, no. 3, pp. 193-201, 2010, doi:10.1109/TSTE.2010.2061881.

[90] C. M. Colson, M. H. Nehrir, and S. A. Pourmousavi, ‘‘Towards real-time microgrid power management using computational intelligence methods,’’ *IEEE PES General Meeting*, 2010, pp. 1-8, doi:10.1109/PES.2010.5588053.

[91] J. Y. Lee and S. G. Choi, ‘‘Linear programming based hourly peak load shaving method at home area,’’ *Proc. 16th Int. Conf. Adv. Commun. Technol*., Feb. 2014, pp. 310–313.

[92] H. T. Dinh, J. Yun, D. M. Kim, K. Lee, and D. Kim, ‘‘A Home Energy Management System With Renewable Energy and Energy Storage Utilizing Main Grid and Electricity Selling,’’ *IEEE Access*, vol. 8, pp. 49436-49450, 2020, doi: 10.1109/ACCESS.2020.2979189.

[93] M. Jafari, Z. Malekjamshidi, J. Zhu, and M. -H. Khooban,‘‘A Novel Predictive Fuzzy Logic-Based Energy Management System for Grid-Connected and Off-Grid Operation of Residential Smart Microgrids,’’ *IEEE Journal of Emerging and Selected Topics in Power Electronics*, vol. 8, no. 2, pp. 1391-1404, 2020, doi: 10.1109/JESTPE.2018.2882509

[94] Y. Jin, J. Choi, and D. Won, ‘‘Pricing and Operation Strategy for Peer-to-Peer Energy Trading Using Distribution System Usage Charge and Game Theoretic Model,’’ *IEEE Access*, vol. 8, pp. 137720-137730, 2020, doi: 10.1109/ACCESS.2020.3011400.

[95] W. Tushar, T. K. Saha, C. Yuen, P. Liddell, R. Bean, and H. V. Poor, ‘‘Peer-to-Peer Energy Trading With Sustainable User Participation: A Game Theoretic Approach,’’ *IEEE Access*, vol. 6, pp. 62932-62943, 2018, doi: 10.1109/ACCESS.2018.2875405.

[96] H. T. Doan, J. Cho, and D. Kim, ‘‘Peer-to-Peer Energy Trading in Smart Grid Through Blockchain: A Double Auction-Based Game Theoretic Approach,’’ *IEEE Access*, vol. 9, pp. 49206-49218, 2021, doi: 10.1109/ACCESS.2021.3068730.

[97] P. Shamsi, H. Xie, A. Longe, and J. Y. Joo, ‘‘Economic Dispatch for an Agent-Based Community Microgrid,’’ *IEEE Transactions on Smart Grid*, vol. 7, no. 5, pp. 2317-2324, 2016, doi: 10.1109/TSG.2015.2487422.

[98] W. Liu, D. Qi, and F. Wen, ‘‘Intraday Residential Demand Response Scheme Based on Peer-to-Peer Energy Trading,’’ *IEEE Transactions on Industrial Informatics*, vol. 16, no. 3, pp. 1823-1835, 2020, doi: 10.1109/TII.2019.2929498.

[99] Y. Liu, L. Wu, J. Li, ‘‘Peer-to-peer (P2P) electricity trading in distribution systems of the future,’’ *The Electricity Journal*, 2019, pp. 2-6, vol. 32, doi: https://doi.org/10.1016/j.tej.2019.03.002.

[100] T. AlSkaif, J. L. Crespo-Vazquez, M. Sekuloski, G. v. Leeuwen, and J. P. S. Catalão, ‘‘Blockchain-Based Fully Peer-to-Peer Energy Trading Strategies for Residential Energy Systems,’’ *IEEE Transactions on Industrial Informatics*, vol. 18, no. 1, pp. 231-241, 2022, doi: 10.1109/TII.2021.3077008.

[101] N. Z. Aitzhan and D. Svetinovic, ‘‘Security and Privacy in Decentralized Energy Trading Through Multi-Signatures, Blockchain and Anonymous Messaging Streams,’’ *IEEE Transactions on Dependable and Secure Computing*, vol. 15, no. 5, pp. 840-852, 2018, doi: 10.1109/TDSC.2016.2616861.

[102] L. Suganthi, S. Iniyan, and A. Samuel, ‘‘Applications of fuzzy logic in renewable energy systems – A review,’’ *Renewable and Sustainable Energy Reviews*, vol. 48, pp. 585-607, March 2015, doi: https://doi.org/10.1016/j.rser.2015.04.037.

[103] W. Abdellatif, M. Mohamed, S. Barakat, and A. Brisha, ‘‘A Fuzzy Logic Controller Based MPPT Technique for Photovoltaic Generation System,’’ *International Journal on Electrical Engineering and Informatic*s, vol. 13, 2021.

[104] W. Dong, Q. Yang, X. Fang, and W. Ruan, ‘‘Adaptive optimal fuzzy logic based energy management in multi-energy microgrid considering operational uncertainties,’’ *Applied Soft Computing*, vol. 98, pp.106882, 2021, doi: https://doi.org/10.1016/j.asoc.2020.106882.

[105] M. Jünger, T. M. Liebling, D. Naddef, G. L. Nemhauser, W. R. Pulleyblank, G. Reinelt, G. Rinaldi, and L. A. Wolsey, Eds., *50 Years of Integer Programming 1958–2008: From the Early Years to the State-of-the-Art*. Springer, 2009. [Online]. Available: https://books.google.co.uk/books?hl=en&lr=&id=bUJc_weiYfkC&oi=fnd&pg=PR5&dq=50+Years+of+Integer+Programming+597+1958%3F2008:&ots=0zEUMmsmLT&sig=WF6McR9OYG1UoXa26pe0-kyWAS8#v=onepage&q=50%20Years%20of%20Integer%20Programming%20597%201958%3F2008%3A&f=false.

[106] J. P. Vielma, ‘‘Mixed integer linear programming formulation techniques,’’ SIAM Rev., vol. 57, no. 1, pp. 3–57, 2015.

[107] M. Elkazaz, M. Sumner, S. Pholboon, and D. Thomas, ‘‘Microgrid Energy Management Using a Two Stage Rolling Horizon Technique for Controlling an Energy Storage System”, *7th International Conference on Renewable Energy Research and Applications (ICRERA),* vol. 3, pp. 324-329, 2018, doi: 10.1109/ICRERA.2018.8566761.

[108] Gurobi Optimization. *Mixed-Integer Programming (MIP) – A Primer on the Basics.* Accessed: 22/2/2022. [Online]. Available: https://www.gurobi.com/resource/mip-basics/.

[109] J. C. Smith and Z. C. Taskin, ‘‘A tutorial guide to mixed-integer programming models and solution techniques,’’ Optim. Med. Biol., pp. 521–548, 2008, doi: 10.1201/9780849305696.axa.

[110] D. A. Aviles, J. Pascual, F. Guinjoan, L. Marroyo, P. Sanchis, and M. P. Marietta, ‘‘Low complexity energy management strategy for grid profile smoothing of a residential grid-connected microgrid using generation and demand forecasting,’’ *Applied Energy*, vol. 205, pp. 69-84, Nov. 2017, doi: https://doi.org/10.1016/j.apenergy.2017.07.123.

[111] S. Marzal, R. Salas-Puente, R. González-Medina, E. Figueres, and G. Garcerá, ‘‘Peer-to-peer decentralized control structure for real time monitoring and control of microgrids,’’ *IEEE 26th International Symposium on Industrial Electronics (ISIE),* pp. 140-145, 2017,doi: 10.1109/ISIE.2017.8001237.

[112] M. Elkazaz, M. Sumner, S. Pholboon, and D. Thomas, ‘‘Optimization based Real-Time Home Energy Management in the Presence of Renewable Energy and Battery Energy Storage,” *International Conference on Smart Energy Systems and Technologies (SEST),* vol. 3, pp. 1-6, 2019, doi: 10.1109/SEST.2019.8849105.

[113] K. Parvin, M. A. Hannan, A. Q. Al-Shetwi, P. J. Ker, M. F. Roslan, and T. M. I. Mahlia, ‘‘Fuzzy Based Particle Swarm Optimization for Modeling Home Appliances Towards Energy Saving and Cost Reduction Under Demand Response Consideration,’’ *IEEE Access*, 2020, vol. 8, pp. 210784-210799, doi: 10.1109/ACCESS.2020.3039965.

[114] T. Molla, B. Khan, B. Moges, H. Alhelou, R. Zamani, and P. Siano, ‘‘Integrated optimization of smart home appliances with cost-effective energy management system,’’ *CSEE Journal of Power and Energy Systems*, vol. 5, pp. 249-258, 2019, doi: 10.17775/CSEEJPES.2019.00340.

[115] V. Hosseinnezhad, M. Shafie-Khah, P. Siano, and J. P. S. Catalão, ‘‘An Optimal Home Energy Management Paradigm With an Adaptive Neuro-Fuzzy Regulation,’’ *IEEE Access*, vol. 8, pp. 19614-19628, 2020, doi: 10.1109/ACCESS.2020.2968038.

[116] A. Sangswang and M. Konghirun, ‘‘Optimal Strategies in Home Energy Management System Integrating Solar Power, Energy Storage, and Vehicle-to-Grid for Grid Support and Energy Efficiency,’’ *IEEE Transactions on Industry Applications,* vol. 56, pp. 5716-5728, 2020, doi: 10.1109/TIA.2020.2991652.

[117] P. S. Kumar, R. P. S. Chandrasena, V. Ramu, G. N. Srinivas, and K. V. S. M. Babu, ‘‘Energy Management System for Small Scale Hybrid Wind Solar Battery Based Microgrid,’’ *IEEE Access*, vol. 8, pp. 8336-8345, 2020, doi: 10.1109/ACCESS.2020.2964052.

[118] R. S. Sreeleksmi, A. Ashok, and M. G. Nair, ‘‘A Fuzzy Logic Controller for Energy Management in a PV - Battery based Microgrid System,’’*IEEE International Conference on Technological Advancements in Power and Energy (TAP Energy),* 2017, pp. 1-6, doi: 10.1109/TAPENERGY.2017.8397282

[119] M. F. M. Yusof and A. Z. Ahmad, ‘‘Power energy management strategy of micro-grid system,’’ *IEEE International Conference on Automatic Control and Intelligent Systems*, 2016, pp. 107-112, doi: 10.1109/I2CACIS.2016.7885298.

[120] K. Manickavasagam, N. K. Thotakanama, and V. Puttaraj, ‘‘Intelligent energy management system for renewable energy driven ship,’’ *IET Electrical Systems in Transportation,* vol. 9, no. 1, pp. 24-34, Mar. 2019, doi:10.1049/iet-est.2018.5022.

[121] D. A. Aviles, J. Pascual, L. Marroyo, P. Sanchis, and F. Guinjoan, ‘‘Fuzzy Logic-Based Energy Management System Design for Residential Grid-Connected

Microgrids,'' *IEEE Transactions on Smart Grid*, vol. 9, no. 2, pp. 530-543, March 2018, doi: 10.1109/TSG.2016.2555245.

[122] D. A. Aviles, N. Espinosa, F. Guinjoan, L. Marroyo and P. Sanchis, ''Improved fuzzy controller design for battery energy management in a grid connected microgrid,'' *IECON 2014 - 40th Annual Conference of the IEEE Industrial Electronics Society*, USA, 2014, pp. 2128-2133, doi: 10.1109/IECON.2014.7048796.

[123] M. S. Ahmed, A. Mohamed, H. Shareef, R. Z. Homod, and J. A. Ali, ''Artificial neural network based controller for home energy management considering demand response events,'' *International Conference on Advances in Electrical, Electronic and Systems Engineering, Putrajaya*, Malaysia, 2016, pp. 506-509, doi: 10.1109/ICAEES.2016.7888097.

[124] L. Gigoni, A. Betti, E. Crisostomi, A. Franco, M. Tucci, F. Bizzarri, and D. Mucci, ''Day-ahead hourly forecasting of power generation from photovoltaic plants,'' *IEEE Transactions on Sustainable Energy*, vol. 9, no. 2, pp. 831-842, 2018, doi: 10.1109/TSTE.2017.2762435.

[125] R. Manojkumar, C. Kumar, S. Ganguly, and J. P. S. Catalão, ''Optimal Peak Shaving Control Using Dynamic Demand and Feed-In Limits for Grid-Connected PV Sources With Batteries,'' *IEEE Systems Journal*, vol. 15, pp. 5560-5570, 2021, doi: 10.1109/JSYST.2020.3045020.

[126] M. Abdalla, W. Min, and O. Mohammed, ''Two-Stage Energy Management Strategy of EV and PV Integrated Smart Home to Minimize Electricity Cost and Flatten Power Load Profile,'' *Energies*, pp. 6387, 2020, doi:10.3390/en13236387.

[127] U. R. Nair, and R. Costa-Castelló, ''A Model Predictive Control-Based Energy Management Scheme for Hybrid Storage System in Islanded Microgrids,'' *IEEE Acces*s, vol. 8, pp. 97809-97822, 2020, doi: 10.1109/ACCESS.2020.2996434.

[128] H. Muqeet, I. Sajjad, A. Ahmad, M. Iqbal, S. Ali, and J. Guerrero, ''Optimal Operation of Energy Storage System for a Prosumer Microgrid Considering Economical and Environmental Effects,'' *International Symposium on Recent Advances in Electrical Engineering*, vol. 4, pp. 1-6, 2019, doi: 10.1109/RAEE.2019.8887002.

[129] U. B. Tayab, F.Yang, M. El-Hendawi, and J. Lu, ''Energy management system for a grid-connected microgrid with photovoltaic and battery energy storage system,'' *in Australian & New Zealand Control Conference*, 2018, pp. 141-144, doi: 10.1109/ANZCC.2018.8606557.

[130] S. Golshannavaz, ''Cooperation of electric vehicle and energy storage in reactive power compensation: An optimal home energy management system considering PV presence,'' *Sustainable Cities and Society*, vol. 39, pp. 317-325, 2018, doi:https://doi.org/10.1016/j.scs.2018.02.018.

[131] O. Erdinc, N. G. Paterakis, T. D. P. Mendes, A. G. Bakirtzis, and J. P. S. Catalão, ''Smart household operation considering bi-directional EV and ESS utilization by

real-time pricing-based DR,'' *IEEE Trans. Smart Grid.*, vol. 6, no. 3, pp. 1281–1291, 2015, doi: 10.1109/TSG.2014.2352650.

[132] S. Aznavi, P. Fajri, A. Asrari, and F. Harirchi, ''Realistic and intelligent management of connected storage devices in future smart homes considering energy price tag,'' *IEEE Transactions on Industry Applications*, vol. 56, no. 2, pp. 1679-1689, 2020, doi: 10.1109/TIA.2019.2956718.

[133] G. Angenendt, S. Zurmühlen, R. Mir-Montazeri, D. Magnor, and D. U. Sauer, ''Enhancing battery lifetime in PV battery home storage system using forecast based operating strategies,'' *Energy Procedia,* vol. 99, pp. 80-88, 2016, doi: https://doi.org/10.1016/j.egypro.2016.10.100.

[134] Y. Chen, Y. Wu, C. Song, and Y. Chen, ''Design and Implementation of Energy Management System With Fuzzy Control for DC Microgrid Systems,'' *IEEE Transactions on Power Electronics,* ol. 28, no. 4, pp. 1563-1570, Apr. 2013, doi: 10.1109/TPEL.2012.2210446.

[135] V. A. Freire, L. V. R. d. Arruda, C. Bordons, and G. Teno, ''Home Energy Management for a AC/DC Microgrid Using Model Predictive Control,'' *International Conference on Smart Energy Systems and Technologies* (*SEST*), 9-11, 2019, pp. 1-6, doi: 10.1109/SEST.2019.8849077.

[136] F. Li, C. Cañizares, and Z. Lin, ''Energy Management System for DC Microgrids Considering Battery Degradation,'' *IEEE Power & Energy Society General Meeting (PESGM),* pp. 1-5, 2020, doi: 10.1109/PESGM41954.2020.9281580.

[137] C. Ju and P. Wang, ''Energy management system for microgrids including batteries with degradation costs,'' *IEEE International Conference on Power System Technology (POWERCON),* pp. 1-6, 2016, doi: 10.1109/POWERCON.2016.7754011.

[138] Institute of Public Policy Research (2016). *COMMUNITY AND LOCAL ENERGY CHALLENGES AND OPPORTUNITIE*S. Accessed: 5/8/2022. [Online]. Available: https://www.ippr.org/files/publications/pdf/community-energy_June2016.pdf.

[139] Piclo (2022). *Secondary trading in the Capacity Market: Introducing Piclo Exchange.* Accessed: 3/4/2022. [Online]. Available: https://www.piclo.energy/publications.

[140] C. Zhang, J. Wu, C. Long, and M. Cheng, ''Review of Existing Peer-to-Peer Energy Trading Projects,'' *Energy Procedia*, vol. 105, pp. 2563-2568, 2017, doi: https://doi.org/10.1016/j.egypro.2017.03.737.

[141] United Nations Cliamate Change (2022). *ME SOLshare: Peer-to-Peer Smart Village Grids | Bangladesh.* Accessed: 12/4/2022.. [Online]. Available: https://unfccc.int/climate-action/momentum-for-change/ict-solutions/solshare.

[142] PONTON (2022). *European Energy Trading Firms Test Peer-To-Peer Trad-ing Over The Blockchain.* Accessed: 15/4/2022. [Online]. Available: https://www.ponton.de/enerchain-p2p-trading-project/.

[143] N. Z. Aitzhan and D. Svetinovic, "Security and Privacy in Decentralized Energy Trading Through Multi-Signatures, Blockchain and Anonymous Messaging Streams," *IEEE Transactions on Dependable and Secure Computing*, vol. 15, no. 5, pp. 840-852, 2018, doi: 10.1109/TDSC.2016.2616861.

[144] R. Faia, J. Soares, T. Pinto, F. Lezama, Z. Vale, and J. M. Corchado, ‘‘Optimal Model for Local Energy Community Scheduling Considering Peer to Peer Electricity Transactions,’’ *IEEE Access*, vol. 9, pp. 12420-12430, 2021, doi: 10.1109/ACCESS.2021.3051004.

[145] V. Cherala, C. T. S, and P. K. Yemula, ‘‘Peer-to-Peer Energy Sharing Model for Interconnected Home Microgrids,’’ *IEEE International Conference on Power Systems Technology (POWERCON)*, pp. 1-6, 2020 ,doi: 10.1109/POWERCON48463.2020.9230580.

[146] Z. Zhang, R. Li and F. Li, ‘‘A Novel Peer-to-Peer Local Electricity Market for Joint Trading of Energy and Uncertainty,’’ *IEEE Transactions on Smart Grid*, vol. 11, no. 2, pp. 1205-1215, 2020, doi: 10.1109/TSG.2019.2933574.

[147] H. Muhsen, A. Allahham, A. Al-Halhouli, M. Al-Mahmodi, A. Alkhraibat, and M. Hamdan, ‘‘Business Model of Peer-to-Peer Energy Trading: A Review of Literature,’’*Sustainability*, 2022, vol. 14, pp.1616, doi: https://doi.org/10.3390/su14031616.

[148] A. Al-Sorour, M. Fazeli, M. Monfared, A. Fahmy, J. R. Searle, and R. P. Lewis, ‘‘Enhancing PV Self-Consumption Within an Energy Community Using MILP-Based P2P Trading,’’ *IEEE Access*, vol. 10, pp. 93760-93772, 2022, doi: 10.1109/ACCESS.2022.3202649.

[149] M. Elkazaz, M. Sumner, and D. Thomas, ‘‘A Hierarchical Centralized Community Energy Management System Using a Model Predictive Controller,’’ *International Conference on Smart Grids and Energy Systems (SGES)*, pp. 801-806, 2020, doi: 10.1109/SGES51519.2020.00148.

[150] M. S. H. Nizami, M. J. Hossain, K. Mahmud and J. Ravishankar, ‘‘Energy Cost Optimization and DER Scheduling for Unified Energy Management System of Residential Neighborhood,’’ *IEEE International Conference on Environment and Electrical Engineering and 2018 IEEE Industrial and Commercial Power Systems Europe* (*EEEIC / I&CPS* Europe), 2018, pp. 1-6, doi: 10.1109/EEEIC.2018.8493732.

[151] Y. Zhou, J. Wu, C. Long, M. Cheng, and C. Zhang, ‘‘Performance Evaluation of Peer-to-Peer Energy Sharing Models,’’ *Energy Procedia*, vol. 143, pp. 817-822, 2017, doi: https://doi.org/10.1016/j.egypro.2017.12.768.

[152] C. Lyu, Y. Jia, Z. Xu,‘‘Fully decentralized peer-to-peer energy sharing framework for smart buildings with local battery system and aggregated electric vehicles,’’ *Applied Energy*, vol. 299, pp. 1117243, 2021, doi: https://doi.org/10.1016/j.apenergy.2021.117243.

[153] C. Long, J. Wu, Y. Zhou, and N. Jenkins, ‘‘Peer-to-peer energy sharing through a two-stage aggregated battery control in a community Microgrid,’’ *Applied*

Energy, vol. 226, pp. 261-276, 2018, doi: https://doi.org/10.1016/j.apenergy.2018.05.097.

[154] K. Mahmud, M. S. H. Nizami, J. Ravishankar, M. J. Hossain, and P. Siano, ‘‘Multiple Home-to-Home Energy Transactions for Peak Load Shaving,’’ *IEEE Transactions on Industry Applications*, vol. 56, no. 2, pp. 1074-1085, 2020, doi: 10.1109/TIA.2020.2964593.

[155] S. Aznavi, P. Fajri, M. B. Shadmand and A. Khoshkbar-Sadigh, ‘‘Peer-to-Peer Operation Strategy of PV Equipped Office Buildings and Charging Stations Considering Electric Vehicle Energy Pricing,’’ *IEEE Transactions on Industry Applications*, vol. 56, no. 5, pp. 5848-5857, 2020, doi: 10.1109/TIA.2020.2990585.

[156] DYB (2018). *BYD BATTERY-BOX*. Accessed: 6/1/2021. [Online]. Available: https://www.originenergy.com.au/content/dam/origin/residential/solar/byd-battery-box-brochure-2018.pdf.

[157] BloombergNEF (2021). *Battery Pack Prices Fall to an Average of $132/kWh, But Rising Commodity Prices Start to Bite.* Accessed: 1/1/2022. [Online]. Available at: https://about.bnef.com/blog/battery-pack-prices-fall-to-an-average-of-132-kwh-but-rising-commodity-prices-start-to-bite/#_ftn1.

[158] Y. Zhang, Y. Xu, H. Yang, Z. Y. Dong, and R. Zhang, ‘‘Optimal Whole-Life-Cycle Planning of Battery Energy Storage for Multi-Functional Services in Power Systems,’’ *IEEE Transactions on Sustainable Energy*, vol. 11, no. 4, pp. 2077-2086, 2020, doi: 10.1109/TSTE.2019.2942066.

[159] Storing Renewable Energy (2016). *BYD Batteries.* Accessed: 16/2/ 2021. [Online]. Available: http://www.srenergy.co.uk/uploads/userfiles/file/BYD%20B-Box%20-%20UK.pdf.

[160] SSe (2020). *SSe Prices and Tariffs.* Accessed: 16/10/2019. [Online]. Available: https://products.sse.co.uk/our-prices/view-tariffs-and-prices?Postcode=cf102gp&FuelCategory=1&TariffStatus=1.

[161] J. Liu, W. Fang, X. Zhang, and C. Yang, ‘‘An Improved Photovoltaic Power Forecasting Model With the Assistance of Aerosol Index Data,’’ *IEEE Transactions on Sustainable Energy*, Energy, vol. 6, no. 2, pp. 434-442, 2015, doi: 10.1109/TSTE.2014.2381224.

[162] P. Shen, M. Ouyang, L. Lu, J. Li, and X. Feng, ‘‘The co-estimation of state of charge, state of health, and state of function for lithium-ion batteries in electric vehicles,’’ *IEEE Transactions on Vehicular Technology*, vol. 67, no. 1, pp. 92-103, 2018, doi: 10.1109/TVT.2017.2751613.

[163] Y. Song, M. Park, M. Seo, and S. W. Kim, ‘‘Improved SOC estimation of lithium-ion batteries with novel SOC-OCV curve estimation method using equivalent circuit model,’’ *in 4th International Conference on Smart and Sustainable Technologies (SpliTech)*, Jun. 2019, pp. 1-6, doi: 10.23919/SpliTech.2019.8783149.

[164] Z. Lao, B. Xia, W. Wang, W. Sun, Y. Lai, and M. Wang, ‘‘A novel method for lithium-ion battery online parameter identification based on variable forgetting factor recursive least squares,’’ *Energies*, vol. 11, no. 6, pp. 1358, 2018, doi:10.3390/en11061358.

[165] M. Li, C. Dong, Y. Mu, X. Dong, J. Cao, and H. Jia, ‘‘Parameter Estimation of Lithium Battery Thermal Model Based on Two-Stage Forgetting Factor Least Square Method,’’ in 2021 IEEE Energy Conversion Congress and Exposition (ECCE), pp. 1718-1723, 2021, doi: 10.1109/ECCE47101.2021.9595785.

[166] M. S. Chitnis, S. P. Pandit, and M. N. Shaikh, ‘‘Electric vehicle li-ion battery state of charge estimation using artificial neural network,’’ *in International Conference on Inventive Research in Computing Applications (ICIRCA)*, 2018, pp. 992-995, doi: 10.1109/ICIRCA.2018.8597234.

[167] M. Ismail, R. Dlyma, A. Elrakaybi, R. Ahmed, and S. Habibi, ‘‘Battery state of charge estimation using an artificial neural network,’’ *in IEEE Transportation Electrification Conference and Expo (ITEC)*, 2017, pp. 342-349, doi: 10.1109/ITEC.2017.7993295.

[168] M. Luzi, F. M. F. Mascioli, M. Paschero, and A. Rizzi, ‘‘A White-Box Equivalent Neural Network Circuit Model for SoC Estimation of Electrochemical Cells,’’I*EEE Transactions on Neural Networks and Learning Systems*, vol. 31, no. 2, pp. 371-382, 2020, doi: 10.1109/TNNLS.2019.2901062.

[169] J. Wang and Z. Zhang, ‘‘Lithium-ion Battery SOC Estimation Based on Weighted Adaptive Recursive Extended Kalman Filter Joint Algorithm,’’ *in 2020 IEEE 8th International Conference on Computer Science and Network Technology* (ICCSNT), pp. 11-15, 2020, doi: 10.1109/ICCSNT50940.2020.9304993.

[170] X. Han, M. Ouyang, L. Lu, and J. Li, ‘‘A comparative study of commercial lithium ion battery cycle life in electric vehicle: Capacity loss estimation,’’ *Journal of Power Sources*, vol. 268, pp. 658-669, 2014, doi: https://doi.org/10.1016/j.jpowsour.2014.06.111.

[171] LONDON DATASTORE (2022). *SmartMeter Energy Consumption Data in London Households*. Accessed: 2/3/2022. [Online]. Available: https://data.london.gov.uk/dataset/smartmeter-energy-use-data-in-london-households.

[172] Powervault (2022). *TECHNICAL SPECIFICATIONS*. Accessed: 2/2/2022. [Online]. Available: https://www.powervault.co.uk/technical/technical-specifications/.

[173] SP ENERGY NETWORKS (2021). *EXPORT LIMITATION*. Accessed: 24/11/2022. [Online]. Available: https://www.spenergynetworks.co.uk/pages/export_limitation.aspx.

[174] GREENCARS (2022). *GreenCars' Guide to Electric Car Batteries*. Accessed: 2/4/2022. [Online]. Available: https://www.greencars.com/guides/definitive-guide-to-electric-car-batteries-range.

[175] E. D. Kostopoulos, G. C. Spyropoulos, and J. K. Kaldellis, ‘‘Real-world study for the optimal charging of electric vehicles,’’ *Energy Reports*, vol. 6, pp. 418-426, 2020, doi: https://doi.org/10.1016/j.egyr.2019.12.008.

[176] EnergyUse CALCULATOR (2022). *Electricity usage of a Clothes Washer*. Accessed: 4/4/2022. [Online]. Available: https://energyusecalculator.com/electricity_clotheswasher.htm.

[177] EnergyUse CALCULATOR (2022). *Electricity usage of a Dishwasher*. Accessed: 4/4/2022. [Online]. Available: https://energyusecalculator.com/electricity_dishwasher.htm.

[178] Electric Vehicle Database (2022). *Nissan Leaf.* Accessed: 2/5/2022. [Online]. Available: https://ev-database.uk/car/1656/Nissan-Leaf.

[179] Federal Highway Administration (2022). *National Household Travel Survey*. Accessed: 2/3/2022. [Online]. Available: https://nhts.ornl.gov/.

[180] F. Teotia, P. Mathuria, and , R. Bhakar, ‘‘Peer-to-peer local electricity market platform pricing strategies for prosumers,’’ *IET Generation, Transmission & Distribution*, vol. 14, pp.4388-4397, 2022, doi: https://doi.org/10.1049/iet-gtd.2019.0578.

[181] R. Hamouda, M. Nassar, and M. Salama, ‘‘Blockchain-based sequential market-clearing platform for enabling energy trading in Interconnected Microgrids,’’ *International Journal of Electrical Power & Energy Systems,* vol. 144, pp. 108550, 2023, doi: https://doi.org/10.1016/j.ijepes.2022.108550.